Technische Universität München
TUM School of Medicine and Health

Impact of Progerin Expression on Adipose Tissue Loss in Hutchinson-Gilford Progeria Syndrome (HGPS)

Farah Najdi

Vollständiger Abdruck der von der TUM School of Medicine and Health der Technischen Universität München zur Erlangung einer

Doktorin der Naturwissenschaften (Dr. rer. nat.)

genehmigten Dissertation.

Vorsitz: Prof. Dr. Ellen Renner

Prüfer*innen der Dissertation:

1. Prof. Dr. Karima Djabali
2. Prof. Dr. Thomas Brück

Die Dissertation wurde am 22.05.2023 bei der Technischen Universität München eingereicht und durch die Fakultät für Medizin am 15.08.2023 angenommen.

Table of Contents

Abstract

Hutchinson-Gilford Progeria Syndrome (HGPS) is a rare genetic disorder causing premature aging in children. Affected individuals die at an average age of 14 years old due to cardiovascular diseases or stroke. Patients suffering from HGPS manifest several symptoms of normal aging including lipodystrophy or the loss of subcutaneous fat. Accumulation of progerin inside cells of HGPS patients has shown to cause premature senescence and inflammation. To determine whether this premature senescence is causing adipogenic depletion in HGPS patients, we induced the differentiation of skin-derived precursor stem cells (SKPs) from both healthy and HGPS fibroblast cultures into adipocytes. For each condition, two different cultures were used, low senescence cultures with 5% senescence and high senescence cultures with 30% senescence. Our results show that increased senescence in the original fibroblast culture reduced the SKP yield in both control and HGPS SKPs compared to the low senescence fibroblast cultures.

In addition, the differentiation capability of the SKPs was significantly lower when starting from 30% senescence cultures compared to the 5% senescence cultures in control and HGPS. Staining the differentiated adipocytes with Oil Red O (ORO), a specific neutral lipid marker, showed that the size of the lipid droplets was smaller in adipocytes obtained from old senescence SKPs compared to the lipid droplets obtained from low senescence SKPs in both control and disease state.

Assessing the level of senescence after 4 days of SKP culture showed that the HGPS SKPs accumulated senescence faster compared to control SKPs, when starting with fibroblast cultures of the same senescence percentage (either 5% or 15% senescence).

This was proven by the senescence-associated beta-galactosidase (SA-β-gal) assay and confirmed with the count of three different senescence markers: p21, $p16^{INK4a}$ and IL-8. The dissociated HGPS SKPs expressed a higher level of the previously mentioned markers compared to the dissociated control SKPs.

Treating the spheroids and the differentiated adipocytes with Baricitinib, a JAK-STAT inhibitor, ameliorated the adipogenic differentiation in HGPS SKPs. The overall expression of the lipid marker, Bodipy, was significantly higher in differentiated HGPS adipocytes treated with Baricitinib compared to their non-treated counterparts.

The expression of two well-characterized markers of adipogenesis: FABP4 (Fatty Acid Binding Protein 4) and PPARγ (Peroxisome proliferator-activated receptor gamma) proved that more cells were committed to the adipogenesis lineage in control compared to HGPS SKPs. PPARγ and FABP4 levels were significantly higher in control differentiated adipocytes compared to HGPS differentiated adipocytes respectively on day 7 and 14 of adipogenic differentiation.

We also proved by double staining that HGPS fibroblasts expressing high progerin signal were not capable of differentiating into adipocytes (shown by low or absence of Bodipy expression), and that these cells expressed high IL-8 signal indicating that they might be senescent.

Our data suggest that the premature senescence and chronic inflammation observed in HGPS cultures could be the reason behind the impaired adipogenesis observed in the patients.

Zusammenfassung

Das Hutchinson-Gilford Progeria Syndrom (HGPS) ist eine seltene genetische Störung, die bei Kindern zu vorzeitiger Alterung führt. Betroffene sterben im Durchschnitt im Alter von 14 Jahren an Herz-Kreislauf-Erkrankungen oder Schlaganfällen. Patienten, die an HGPS leiden, zeigen mehrere Symptome des normalen Alterns, einschließlich Lipodystrophie oder Verlust von subkutanem Fett. Es hat sich gezeigt, dass die Akkumulation von Progerin in den Zellen von HGPS-Patienten zu vorzeitiger Alterung und Entzündung führt. Um festzustellen, ob diese vorzeitige Seneszenz bei HGPS-Patienten zu einer adipogenen Depletion führt, haben wir die Differenzierung von aus der Haut stammenden Vorläuferstammzellen (SKPs) sowohl aus gesunden als auch aus HGPS-Fibroblastenkulturen in Adipozyten induziert. Für jede Bedingung wurden zwei verschiedene Kulturen verwendet, Kulturen mit niedriger Seneszenz mit 5 % Seneszenz und Kulturen mit hoher Seneszenz mit 30 % Seneszenz. Unsere Ergebnisse zeigen, dass eine erhöhte Seneszenz in der ursprünglichen Fibroblastenkultur die SKP-Ausbeute sowohl in Kontroll- als auch in HGPS-SKPs im Vergleich zu den Fibroblastenkulturen mit niedriger Seneszenz verringerte.

Darüber hinaus war die Differenzierungsfähigkeit der SKPs signifikant geringer, wenn von Kulturen mit 30 % Seneszenz ausgegangen wurde, verglichen mit den Kulturen mit 5 % Seneszenz in Kontrolle und HGPS. Die Färbung der differenzierten Adipozyten mit Oil Red O (ORO), einem spezifischen neutralen Lipidmarker, zeigte, dass die Größe der Lipidtröpfchen in Adipozyten, die von SKPs mit alter Seneszenz erhalten wurden, kleiner

war als in den Lipidtröpfchen, die von SKPs mit niedriger Seneszenz sowohl in der Kontrolle als auch in der Krankheit erhalten wurden Zustand.

Die Bewertung des Grads der Seneszenz nach 4 Tagen SKP-Kultur zeigte, dass die HGPS-SKPs die Seneszenz im Vergleich zu den Kontroll-SKPs schneller akkumulierten, wenn mit Fibroblastenkulturen des gleichen Seneszenzprozentsatzes (entweder 5 % oder 15 % Seneszenz) begonnen wurde. Dies wurde durch den senescence-associated beta-galactosidase (SA-β-gal) Assay nachgewiesen und durch die Zählung von drei verschiedenen Seneszenzmarkern bestätigt: p21, p16INK4a und IL-8. Die dissoziierten HGPS-SKPs exprimierten im Vergleich zu den dissoziierten Kontroll-SKPs ein höheres Niveau der zuvor erwähnten Marker.

Behandlung der Sphäroide und der differenzierten Adipozyten mit Baricitinib, einem JAK-STAT-Inhibitor, verbesserte die adipogene Differenzierung in HGPS-SKPs. Die Gesamtexpression des Lipidmarkers Bodipy war in differenzierten HGPS-Adipozyten, die mit Baricitinib behandelt wurden, signifikant höher als in ihren unbehandelten Gegenstücken.

Die Expression von zwei gut charakterisierten Markern der Adipogenese: FABP4 (Fatty Acid Binding Protein 4) und PPARγ (Peroxisom-Proliferator-aktivierter Rezeptor-Gamma) bewies, dass im Vergleich zu HGPS-SKPs mehr Zellen der Adipogenese-Linie unter Kontrolle waren. PPARγ- und FABP4-Spiegel waren signifikant höher in differenzierten Kontroll-Adipozyten im Vergleich zu HGPS-differenzierten Adipozyten an Tag 7 bzw. 14 der adipogenen Differenzierung.

Wir haben auch durch Doppelfärbung bewiesen, dass HGPS-Fibroblasten, die ein hohes Progerin-Signal exprimieren, nicht in der Lage waren, sich in Adipozyten zu differenzieren (gezeigt durch niedrige oder fehlende Bodipy-Expression), und dass diese Zellen ein hohes IL-8-Signal exprimierten, was darauf hinweist, dass sie seneszent sein könnten.

Unsere Daten legen nahe, dass die in HGPS-Kulturen beobachtete vorzeitige Seneszenz und chronische Entzündung der Grund für die bei den Patienten beobachtete beeinträchtigte Adipogenese sein könnte.

1. Introduction

1.1. Hutchinson-Gilford Progeria Syndrome

Hutchinson-Gilford Progeria Syndrome (HGPS) is a rare, autosomal dominant genetic disease, causing premature ageing in children. Affected children die at an average age of 14.5 mainly owing to myocardial infarction, premature atherosclerosis or stroke (Gordon, Brown, & Collins, 1993).

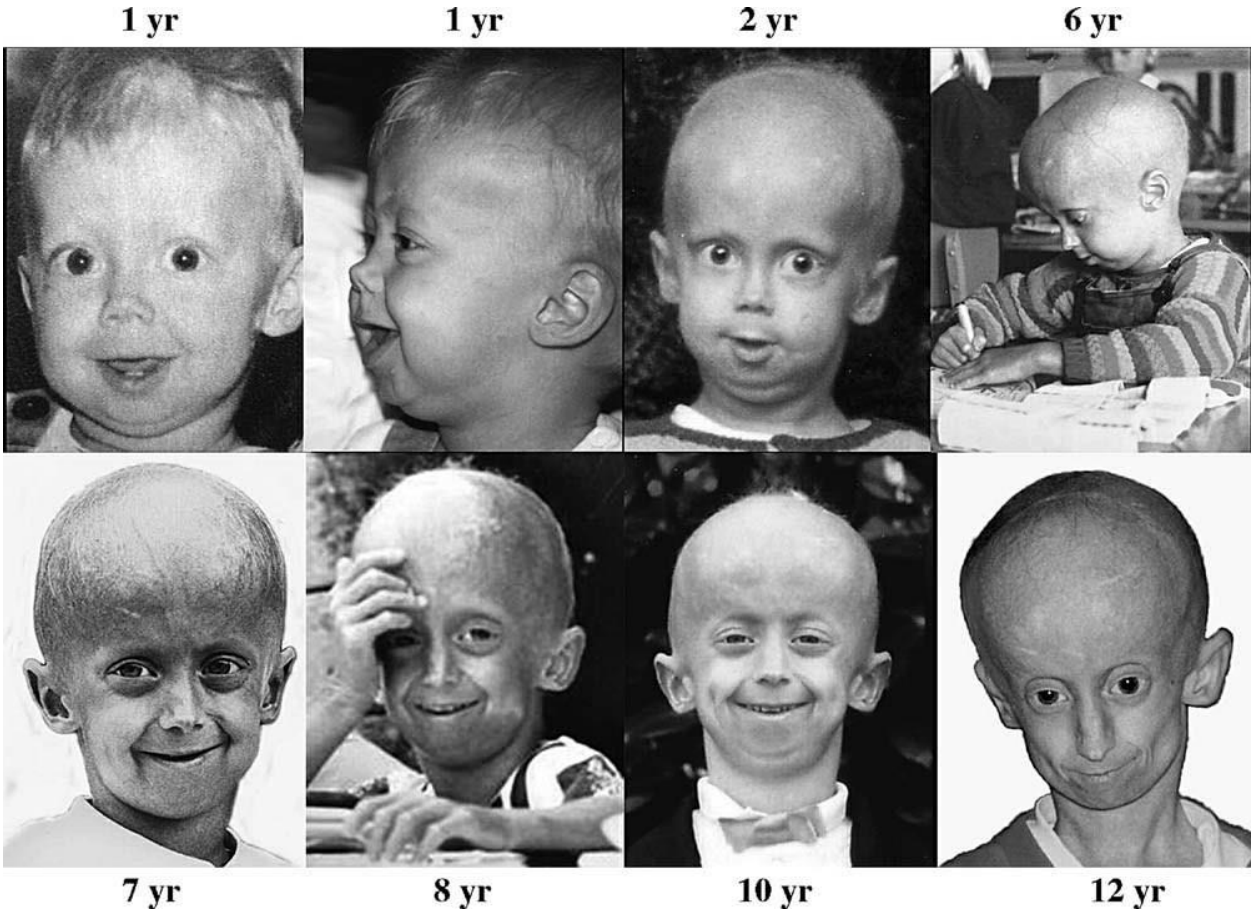

Figure 1. HGPS patient.

Patient suffering from Hutchinson-Gilford Progeria Syndrome from 1 year till 12 years of age. This figure was modified from Hennekam 2006.

1.1.1. Clinical Features

Progeria patients appear normal at birth and they start to show features of the disease starting in the first year of life (Sarkar & Shinton, 2001), these include profound growth retardation and failure to gain weight. Characteristic facial features consist of a sharped beaked nose, small mouth, alopecia and prominent veins especially in the scalp due to the loss of adipose tissue (Gordon et al., 1993). These patients also show other features that occur between the second and the fourth year of life, comprising: coxa valga, thin and high-pitched voice, loss of subcutaneous fat and joint stiffness (Gordon et al., 1993). The most important problem that these children suffer from is severe atherosclerosis, causing death due to myocardial infarction, heart failure or stroke (Merideth et al., 2008).

1.1.2. Genetic perturbation of HGPS

Despite that HGPS was first described in 1886 by Hutchinson, the genetic cause was not identified till 2003 (Eriksson et al., 2003). HGPS belongs to the family of laminopathies, in which 498 mutations in the *LMNA* gene (encoding lamin A and C proteins) are responsible for causing at least 15 known diseases (Gruenbaum, Margalit, Goldman, Shumaker, & Wilson, 2005). Several mutations in the *LMNA* gene are known to cause HGPS, these are divided into classic and non-classic genotype HGPS. In the classic genotype HGPS, which is the case in 90% of patients, a single nucleotide substitution (C-to-T) at position 1824 (exon 11) of *LMNA* triggers the disease (Gordon et al., 1993). In the non-classic genotype HGPS, affecting almost 10% of the patients, several other mutations for example, at positions 1968, 1822 and 1822 of *LMNA* can cause the disease (Gordon et al., 1993).

1.1.3. Normal Lamin A processing

The nuclear lamina is a network of multiple proteins lying inside the inner nuclear membrane. These proteins include mainly the lamins and the lamin-binding proteins. Lamins are type Ⅴ intermediate filament proteins that constitute the main component of the nuclear lamina. These lamins are the product of three different genes: *LMNA*, encoding lamin A and lamin C, *LMNB1* encoding lamin B1, and *LMNB2* encoding lamin B2 and B3 (Stuurman, Heins, & Aebi, 1998). Translation of the *LMNA* gene produces the prelamin A protein, which undergoes several post-translational modifications to become mature lamin A that is incorporated into the nuclear lamina. The prelamin A protein terminates with the amino acids CSIM (cysteine, serine, isoleucine, and methionine) at the C terminus. These amino acids, CSIM, comprises a CAAX motif (C refers to cysteine, A is an aliphatic amino acid and X is any amino acid usually methionine or leucine), which undergoes the first post-translational modification that is farnesylation (Beck, Hosick, & Sinensky, 1990). Farnesylation is the addition of a farnesyl group on the carboxyl-terminal cysteine, facilitating the translocation of the prelamin A to the nuclear lamina (Barrowman, Hamblet, George, & Michaelis, 2008). Following farnesylation, the terminal three amino acids (SIM) are then cleaved by a zinc metalloprotease, ZMPSTE24, and the newly exposed farnesylated cysteine undergoes carboxymethylation (by the Isoprenylcysteine carboxyl methyltransferase (ICMT) enzyme) (Boyartchuk, Ashby, & Rine, 1997; Sinensky et al., 1994). Subsequently, the zinc metalloprotease, ZMPSTE24, removes the last 15 amino acid residues of prelamin A including the farnesyl group. This final cleavage step will generate the mature lamin A of 72 kDa that will be incorporated into the nuclear lamina (Bergo et al., 2002; Dai et al., 1998; Hennekes & Nigg, 1994).

1.1.4. Lamin A mutation in HGPS

The name progeria is a Greek word that means "prematurely old". The protein responsible for the observed phenotype is called progerin. Progerin is an immature form of the lamin A protein, and its accumulation in the cell causes several toxic effects. Most cases of HGPS (almost 90% of the cases) are due to a silent mutation in the *LMNA* gene in exon 11 (H. Cao & Hegele, 2003; De Sandre-Giovannoli et al., 2003; Eriksson et al., 2003). This C to T substitution at position 1824 of *LMNA* (GGC>GGT) results in no change in the amino acid at the corresponding codon 608 (Gly608Gly) but instead activates a cryptic splice donor site, creating an mRNA with a 150 nucleotides deletion (Eriksson et al., 2003). This deletion will delete the second zinc metalloprotease, ZMPSTE24, cleavage site, consequently, preventing the removal of the farnesyl group at the C terminus of the prelamin A. The resulting mutant protein of prelamin A is therefore permanently farnesylated and is called progerin (Capell et al., 2005; Glynn & Glover, 2005; Mallampalli, Huyer, Bendale, Gelb, & Michaelis, 2005; Toth et al., 2005; S. H. Yang et al., 2005). The protein progerin becomes irreversibly anchored into the nuclear lamina preventing normal lamina function. This leads to several functional alterations, including a disruptive heterochromatin structure, in addition to the formation of nuclear blebs and nuclear pore clustering (Csoka et al., 2004; Goldman et al., 2004; Reddel & Weiss, 2004; Scaffidi & Misteli, 2005).

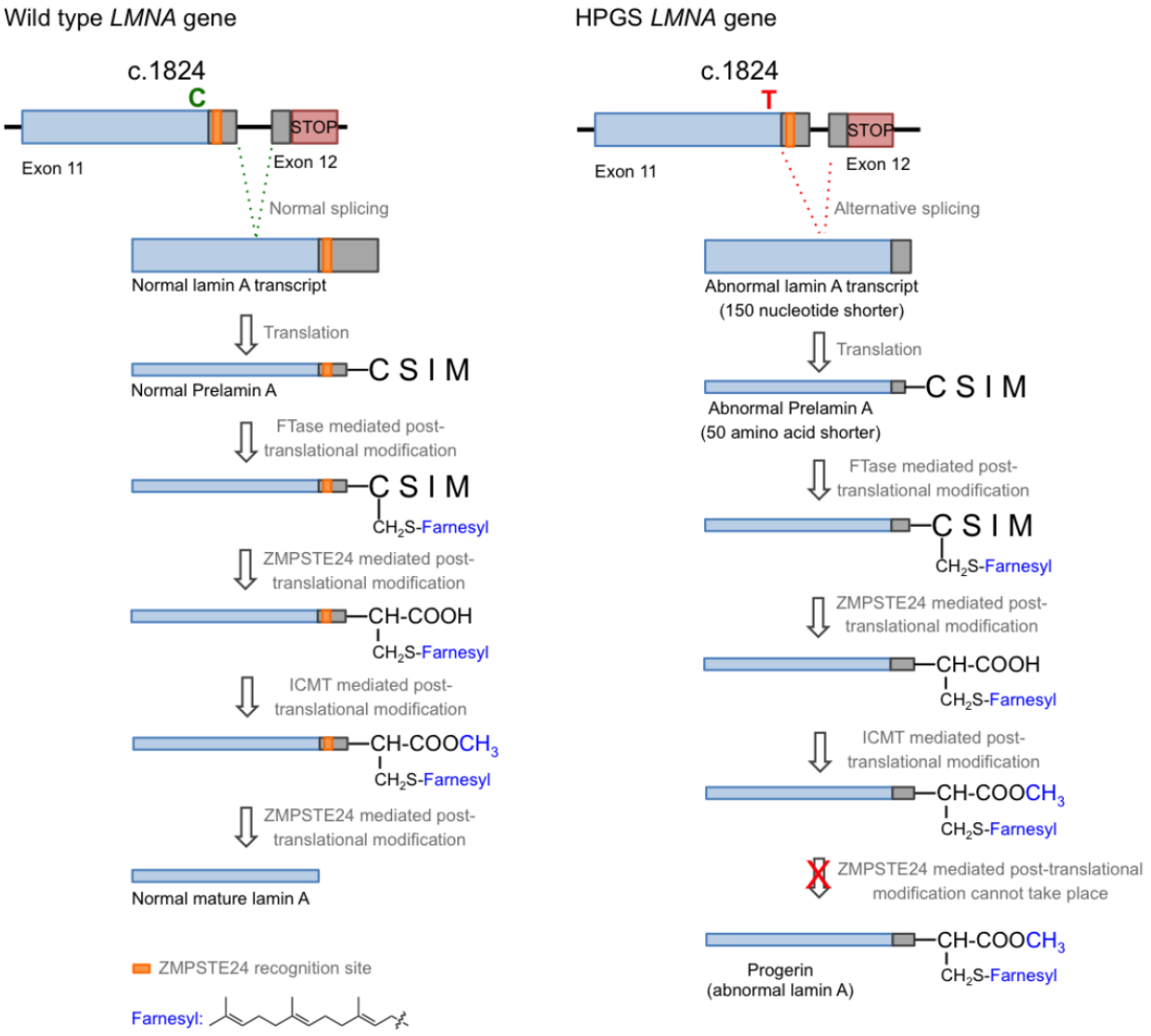

Figure 2. Post-translational processing of lamin A and progerin.

This figure was modified from Macicior et al. 2021.

1.1.5. Current treatment strategies for HGPS

Unfortunately, to date no cure has been found to treat HGPS patients. The available treatments act on improving the clinical condition of the patients and reducing the complications caused by the disease. Nevertheless, several treatment techniques *in vitro* and *in vivo* have been developed with the goal of finding a proper cure. Therefore, two

types of treatment strategies are determined: treatment of manifestation caused by the disease and pharmacological treatment of HGPS.

- Treatment of manifestations

HGPS patients are given a high-caloric diet with vitamin supplementation in order to assure proper nutrition (Gordon, 2019; Gordon et al., 1993). Physical activity and body bracing are recommended to manage hip dislocation, which is very common in HGPS patients due to coxa valga. Electrocardiogram (ECG) is performed annually or semi-annually for the diagnosis of atherosclerosis of the coronary artery. The patients are also treated with a low dose of aspirin (2-3 mg/kg body weight) to reduce the chance of cardiovascular complications and stroke (Gordon, 2019).

- Pharmacological treatment of HGPS

Several treatment strategies have been proposed to treat HGPS. Different areas have been targeted in developing therapeutical interventions to treat the disease: 1) Preventing post-translational modification of progerin (Farnesylation or methylation), 2) Increasing progerin clearance, 3) Amelioration of progerin downstream deleterious effects, 4) Inhibition of the aberrant splicing and 5) Correction of the mutation causing the disease.

1) Preventing post-translational modification of progerin

In HGPS, the deletion of the ZMPSTE24 cleavage site inhibits the cleavage of the farnesylated carboxy terminus from the prelamin A protein. This leads to the formation of an immature form of farnesylated prelamin A referred to as progerin. Consequently, progerin remains permanently anchored to the inner nuclear membrane resulting in

disruption of the nuclear scaffold (Delbarre et al., 2006). Based on these steps, scientists predicted that the use of farnesyltransferase inhibitor (FTI) drugs will reduce progerin production and eventually their toxicity. FTI are small molecules, that were initially used in cancer treatment. They bind to the farnesyltransferase CAAX binding site preventing prelamin A farnesylation (Basso, Kirschmeier, & Bishop, 2006). On the cellular level, treatment with FTI restored nuclear morphology (Capell et al., 2005; Constantinescu, Csoka, Navara, & Schatten, 2010), ameliorated DNA DSBs (double strand breaks) repair (Marji et al., 2010) and improved self-renewal capability in stem cells expressing progerin (Pacheco et al., 2014). Treating HGPS mice models with FTI also showed improvement in their phenotypes; the mice's life span was prolonged, their weight increased and cardiovascular defects were prevented (Capell et al., 2008; S. H. Yang, Andres, Spielmann, Young, & Fong, 2008; S. H. Yang et al., 2006).

Another post-translational modification blockades used are the isoprenylcysteine carboxyl methyltransferase (ICMT) inhibitors. ICMT is the addition of a methyl group at the CAAX motif of the prelamin A in a process called carboxymethylation. HGPS fibroblasts treated with N-acetyl-S-farnesyl-cysteine (AFC), an ICMT inhibitor, showed an increase in cellular proliferation and delayed senescence (Ibrahim et al., 2013). Moreover, inhibiting ICMT activity by the use of lentiviral short hairpin RNAs (shICMT) increased both life span and body weight, ameliorated grip strengths and prevented bone fracture in progeroid mice (Ibrahim et al., 2013).

2) Increasing progerin clearance

Another treatment strategy is to increase progerin clearance by activating autophagy. Several drugs have been used for this cause like rapamycin, sulforaphane and retinoids. Autophagy is a conserved cellular process that degrades dysfunctional components. It maintains cellular homeostasis and plays an important role during development, disease and aging (Hansen, Rubinsztein, & Walker, 2018). Autophagy is mainly regulated by the mTOR pathway (mammalian target of rapamycin) (Kim & Guan, 2015). The activation of the mTOR pathway will lead to the inhibition of autophagy, and inhibiting this pathway with pharmacological interventions will eventually lead to the activation of autophagy (Kim & Guan, 2015). Rapamycin is a specific inhibitor of mTOR that is usually used to prevent organ transplant rejection (Chueh & Kahan, 2005). The use of rapamycin to increase progerin clearance by activating autophagy has shown to improve the nuclear shape structure and delayed senescence in fibroblasts from HGPS patients (K. Cao et al., 2011; Graziotto, Cao, Collins, & Krainc, 2012). Besides autophagy, mTOR is known to regulate several important cellular functions including transcription, cellular growth and immune response. To this cause, due to the importance of the mTOR pathway in leading a normal cellular function, caution should be taken when rapamycin is tested directly in HGPS patients. Furthermore, rapamycin has shown its ability to prevent adipogenesis (Cho, Park, Lee, Lee, & Kim, 2004; Yeh, Bierer, & McKnight, 1995). Therefore, extra care should be taken when considering its use in HGPS children who already suffer from lipodystrophy and generalized lipoatrophy.

Sulforaphane (SFN) is an antioxidant that is also used to increase progerin clearance. SFN is found in cruciferous vegetables like broccoli and cauliflower, and has shown to ameliorate the cellular hallmark observed in HGPS patients *in vitro* (Gabriel, Roedl,

Gordon, & Djabali, 2015). Combinational treatment with SFN and FTI on HGPS fibroblasts showed promising results; they reduced ROS production, decreased DNA damage and ameliorated cellular homeostasis (Gabriel, Shafry, Gordon, & Djabali, 2017).

Retinoids like ATRA (all-trans retinoic acid) were also tested on HGPS fibroblasts since the LMNA promoter contains retinoic acid responsive elements and they also showed capability to induce autophagy in a cell (Rajawat, Hilioti, & Bossis, 2010, 2011). Treatment of HGPS fibroblasts with retinoids alone (Kubben, Brimacombe, Donegan, Li, & Misteli, 2016) or in combination with rapamycin (Pellegrini et al., 2015) showed a synergistic effect of progerin clearance and ameliorated the HGPS phenotype observed *in vitro*.

3) Amelioration of progerin downstream deleterious effects

Several therapeutical interventions are based on reducing the downstream toxic effects of progerin accumulation. These include: reducing ROS generation and mitochondrial dysfunction (Richards, Muter, Ritchie, Lattanzi, & Hutchison, 2011) and reducing cellular senescence and the hyperactivation of the NF-κB pathway (Osorio et al., 2012; Tilstra, Clauson, Niedernhofer, & Robbins, 2011).

Mitochondrial dysfunction and increased oxidative stress are considered markers of HGPS. The use of antioxidants like N-acetyl cysteine (NAC), ROS scavenger, reduced the levels of ROS generation and improved the growth rate of HGPS fibroblasts *in vitro* (Kubben, Zhang, et al., 2016; Richards et al., 2011). Second, rho-associated protein kinase (ROCK) increased mitochondrial ROS production by modulating the interaction between cytochrome c and Rac1b (Kang et al., 2017). Treating HGPS fibroblasts with Y-

27632, a ROCK inhibitor, has shown to ameliorate nuclear abnormalities, improve mitochondrial functions and reduce DNA-DSB (Kang et al., 2017).

Another important therapeutical intervention in ameliorating progerin downstream effect is to modulate the inflammatory pathways. It has been shown that the NF-κB pathway is implicated in aging (Adler et al., 2007; Tilstra et al., 2011). Blocking this pathway using a non-steroidal anti-inflammatory drug, sodium salicylate for example, increased the life span and reduced progeroid features in a mouse model of HGPS (Osorio et al., 2012). The JAK-STAT signaling pathway is also implicated in inflammation and was found to be overactivated in HGPS fibroblasts (C. Liu, Arnold, Henriques, & Djabali, 2019). Inhibiting this overactivation with a JAK 1/2 inhibitor, Baricitinib, showed several improvements in the phenotype of HGPS fibroblasts. It reduced senescence, ameliorated cellular homeostasis, activated autophagy and reduced ROS generation while elevating the ATP levels (C. Liu et al., 2019).

4) Inhibition of the aberrant splicing

HGPS is mainly caused by a mutation in exon 11 in the *LMNA* creating a cryptic splicing site resulting in the formation of progerin, a truncated form of prelamin A. Researchers showed that this aberrant splicing is favored by the RNA-binding protein SRSF-1 (Serine/Arginine-Rich Splicing Factor 1) (Lopez-Mejia et al., 2011). The use of an antidiabetic drug, metformin, that decreased SRSF-1 expression, diminished the pathological defects of human HGPS fibroblasts and $Lmna^{G609G/G609G}$ mouse fibroblasts (Egesipe et al., 2016; Shin et al., 2017). Treatment of mesenchymal stem cells obtained from HGPS-induced pluripotent stem cells (HGPS-iPSCs-MSCs) reduced progerin

expression, ameliorated nuclear shape abnormalities and improved osteoblastic differentiation in these cells (Egesipe et al., 2016).

Another drug that was shown to downregulate SRSF-1 is MG132, an autophagy-activating drug (Harhouri et al., 2017). Administration of MG132 via intramuscular injection improved cellular viability and decreased progerin formation in HGPS fibroblasts (Harhouri et al., 2017).

5) Correction of the mutation causing the disease

The fact that HGPS is caused by a single-point mutation makes it a suitable disease to be treated by genetic modification. Therefore, the genome editing system CRISPR/Cas (Clustered Regularly Interspaced Short Palindromic Repeats/Cas protein) gained so much attention as a novel treatment approach for HGPS (Doudna & Charpentier, 2014; Hsu, Lander, & Zhang, 2014; Sander & Joung, 2014). CRISPR/Cas allows genome editing at a specific location and the alterations performed are permanent. The use of the CRISPR/Cas9 system with the adeno-associated virus-derived vector as a delivery model, increased the weight and life span of HGPS mouse models, reduced progerin levels and ameliorated the progeria phenotype in these mice (Beyret et al., 2019). Although this genome editing approach has many advantages, many factors can still affect its specificity and efficacy. CRISPR/Cas can generate mutation in undesired sites in the genome ("Keep off-target effects in focus," 2018), known as off-target effects. Another reason is the presence of cell-mediated immunity against the most used Cas9 orthologs (obtained from *Staphylococcus aureus* and *Streptococcus pyogenes*)

(Charlesworth et al., 2019), which can eventually cause a severe immune response in the treated patients.

1.2. Adipogenesis

The adipose tissue is a complex organ that plays an important role in energy storage (Galic, Oakhill, & Steinberg, 2010). It is composed of several types of cells: adipocytes, preadipocytes, immune cells, nerves and endothelial cells (Cinti, 2005). The discovery of leptin in the year 1994, proved that the adipose tissue is not only implicated in energy storage and mechanical support, it carries out many endocrine functions and coordinated energy homeostasis (Galic et al., 2010; Lau, Dhillon, Yan, Szmitko, & Verma, 2005). It was also proven that the adipose tissue secrets different proteins that are implicated in the regulation of several functions; including blood pressure, angiogenesis, reproduction, immune response and energy balance (Agarwal & Garg, 2006; Cristancho & Lazar, 2011; Lau et al., 2005; Lowe, O'Rahilly, & Rochford, 2011). There are two main types of adipose tissue, white (WAT) and brown (BAT) adipose tissue (Cinti, 2005). The brown adipose tissue is responsible for thermogenesis (Frontini & Cinti, 2010), whereas the white adipose tissue is an endocrine organ that coordinates and regulates different functions such as lipid metabolism and insulin sensitivity (Cinti, 2005). These two types of adipocytes differentiate from mesenchymal stem cells (MSCs) following a process called adipogenesis (Gesta, Tseng, & Kahn, 2007). Adipogenesis is composed of two main stages: commitment and terminal differentiation (Gesta et al., 2007). The commitment stage involves the conversion of a pluripotent stem cell to a pre-adipocyte. The second phase which is the terminal differentiation phase involves the differentiation of the pre-adipocytes into mature adipocytes (Rosen & MacDougald, 2006). Several signaling

pathways and factors are implicated in the adipogenesis process, but two main factors gained so much attention since they are crucial to induce adipocyte differentiation; these are: the nuclear receptor PPARγ (Peroxisome proliferator- activated receptor gamma) and the members of the C/EBP family (MacDougald & Mandrup, 2002; Rosen, Walkey, Puigserver, & Spiegelman, 2000). PPARγ is known to be the master regulator of adipogenesis and without its presence, the differentiation into adipose could not take place (Tontonoz, Hu, & Spiegelman, 1994). It is a member of the nuclear receptor family and it is composed of two isoforms: PPARγ1 and PPARγ2 (Rosen & MacDougald, 2006). PPARγ2 is exclusively expressed in adipocytes, whereas PPARγ1 could be expressed in other cell types like macrophages for example (Rosen & MacDougald, 2006). PPARγ activates several downstream effects to induce adipogenesis, but most importantly, it is responsible for the activation of the transcription factor C/EBPα (Wu et al., 1999).

Several members of the C/EBP family are implicated in adipogenesis and are expressed in adipocytes. These include: C/EBPα, C/EBPβ and C/EBPδ (Rosen & MacDougald, 2006). In the early stages, the induction of C/EBPβ and C/EBPδ activates C/EBPα, which in turn, directly activates many adipogenic genes (Ghaben & Scherer, 2019). C/EBPα synergize with PPARγ to activate the adipogenesis program and induce a downstream cascade leading to the transcription of genes implicated in mature adipocytes such as AP2, adiponectin and the different set of genes activating the expression of the insulin receptor (Lefterova et al., 2008).

- Molecular mechanism of adipogenesis

The differentiation into adipocytes is a two-step process starting with the commitment phase in which a pluripotent cell is committed into a pre-adipocyte, followed by the differentiation phase, during which the pre-adipocyte accumulates lipids and becomes a mature adipocyte (Rosen & MacDougald, 2006).

In the commitment phase, studies have proven the important role of bone morphogenetic protein 2 (BMP2) and bone morphogenetic protein 4 (BMP4) in driving adipogenic differentiation *in vitro* (Bowers, Kim, Otto, & Lane, 2006; Huang et al., 2009; Wang, Israel, Kelly, & Luxenberg, 1993). These BMPs indirectly activates the transcription factor SMAD4 by activating its heterodimeric partners SMAD1, SMAD5 and SMAD8 (Huang et al., 2009). SMAD4 induces terminal differentiation by activating PPARγ. The activation of the master regulator of adipogenesis PPARγ stimulates C/EBPα (Wu et al., 1999). C/EBPα, in its turn, can also activate PPARγ, creating a positive feedback loop (Lin & Lane, 1994; Rosen et al., 2002; Tontonoz, Hu, & Spiegelman, 1994) allowing the induction of genes implicated in the terminal differentiation process.

1.2.1. Lipodystrophy

Lipodystrophies are a group of disorders characterized by complete or partial lack of adipose tissue. Lipodystrophies caused by genetic mutations are divided into two types: familial partial lipodystrophies (FPLD) and congenital generalized lipodystrophies (CGL) (Garg & Agarwal, 2009; Hegele, Joy, Al-Attar, & Rutt, 2007).

- Manifestation of lipodystrophy in HGPS patients

HGPS patients suffer from lipodystrophy that can start at 6 months of age and could take 3-4 years to become apparent (Hennekam, 2006). Lipodystrophy begins in the limbs, spreads to the thorax and neurocranium and finally starts to become visible in the face with the disappearance of the buccal and pubic fat pads (DeBusk, 1972; Hennekam, 2006). The loss of subcutaneous fat causing the thinning of the skin makes the blood vessels more visible especially on the scalp and around the nasal bridge, making it a unique phenotype of the children (Hennekam, 2006; Ullrich & Gordon, 2015). In addition, HGPS patients lose their body fat and fail to thrive although the energy intake they consume is sufficient (Merideth et al., 2008). The consequences of lipodystrophy in these patients will cause foot pain due to the lack of subcutaneous fat found under the calcaneus.

The fact that patients with lipodystrophy suffer from metabolic diseases shows the importance of functional adipose tissue on humans' health. As previously described in the section above (section 1.2), the adipose tissue is not only responsible for storing excess fat (Robbins & Savage, 2015), but it is also an endocrine organ that regulates several functions affecting insulin sensitivity, inflammation, angiogenesis and appetite (Agarwal & Garg, 2006; Cristancho & Lazar, 2011; Lowe et al., 2011).

Normally, fat accumulates in the adipose tissue in the form of triglyceride (Robbins & Savage, 2015). In the absence of adipose tissue, such as in the case of patients with lipodystrophy, fat accumulates in visceral depots and non-adipose sites such as the liver, skeletal muscle and pancreas (Unger, 2003). This ectopic storage of lipid in these visceral depots will cause metabolic complications and lipotoxicity, leading to insulin resistance, fatty liver and increased cardiovascular risks (Samuel & Shulman, 2012; Savage,

Petersen, & Shulman, 2007; Virtue & Vidal-Puig, 2010). In addition, lack of adipose tissue will decrease the level of leptin in HGPS patients (Gordon et al., 2018), which is significant since leptin was shown to play an important role in immunity, energy expenditure and cardiovascular disease (Koh, Park, & Quon, 2008; Piemonti et al., 2003).

- Causes of lipodystrophy in HGPS patients

The first identified genetic causes of familial partial lipodystrophies (FPLD) were mutations in the *LMNA* gene (H. Cao & Hegele, 2000; Hegele, Anderson, Wang, Jones, & Cao, 2000; Hegele, Cao, Anderson, & Hramiak, 2000; Shackleton et al., 2000). Research has been conducted to understand how mutation in the *LMNA* gene affects lipid metabolism and adipocyte differentiation. In fact, inducing progerin expression in pre-adipocytes and adipocytes in mice models contributed to tissue depletion and increased inflammation and senescence (Revechon et al., 2017). In addition, differentiated HGPS adipocytes obtained from induced pluripotent stem cells (HGPS-iPSCs) (reprogrammed from HGPS fibroblasts) showed impaired lipid storage capability at late differentiation stage (Xiong, LaDana, Wu, & Cao, 2013). In this study, they indicate that progerin seemed to inhibit the expression of two important regulators of adipogenesis: PPARγ and CEBP/α (Xiong et al., 2013).

1.3. Stem Cells

Stem cells, by definition, are cells capable of either dividing into new stem cells or differentiating into various cellular lineage (Fuchs & Segre, 2000). Stem cells can be divided into three main groups: totipotent, pluripotent and multipotent stem cells. Totipotent stem cells are the type of stem cells that are present during early

embryogenesis. They can give rise to all human cell types and extra-embryonic tissues such as the placenta (Mitalipov & Wolf, 2009). Pluripotent stem cells are present during late embryogenesis and can differentiate into all human cell types except the extra-embryonic tissue.

The multipotent stem cells, are the type of stem cells present during adulthood, and they can only differentiate into several specialized stem cells found in a specific organ or tissue. They are found at different body sites like the bone marrow, the adipose tissue, the brain and the skin and their role is to compensate lost cells (Crane, Jeffery, & Morrison, 2017; S. Liu, Dontu, & Wicha, 2005; Rietze & Reynolds, 2006; Schneider, Unger, van Griensven, & Balmayor, 2017). In this study, we will focus on multipotent stem cells found in the skin known as skin-derived precursor cells or SKPs (Fernandes et al., 2004; Toma, McKenzie, Bagli, & Miller, 2005).

1.3.1. Skin-Derived Precursor Cells (SKPs)

SKPs are a type of multipotent stem cells found in the dermis during adulthood (Toma et al., 2001). They were first described by Toma et al., and they grow as floating spheres when cultured in medium containing basis fibroblast growth factor (bFGF) and epidermal growth factor (EGF) (Toma et al., 2001). These SKPs express stem cells markers (Avilion et al., 2003; Mitsui et al., 2003; Pesce & Scholer, 2001) and show the capability to differentiate into several types of cells including neurons, glial cells, smooth muscle cells and adipocytes (Toma et al., 2001). Recent studies showed the possibility of these SKPs to differentiate into Schwann cells (Walsh, Biernaskie, Midha, & Kallos, 2016) and neurons when cultured in a neurobasal medium supplemented with neurotrophic factors

(Toma et al., 2005). The differentiated cells showed neuron-like morphology and expressed neuronal markers like βIII-tubulin (Toma et al., 2005). This neurogenesis capacity is particularly important, allowing the SKPs to be used in axon/nerve regeneration research (Kumar et al., 2016; Mozafari et al., 2015; Vasudeva, Abd-El-Barr, & Chi, 2015) and in cell therapy for neurological diseases and injuries (Willis & Fox, 2016; L. Yang et al., 2015).

In addition, SKPs showed the ability to differentiate into endodermal cells. In the presence of hepatogenic factors, SKPs successfully differentiated into hepatocyte-like cells (De Kock, Vanhaecke, Biernaskie, Rogiers, & Snykers, 2009). They also serve as a promising tool for diabetes research after showing the capability of differentiating into glucose-responsive, insulin producing cells (Mehrabi et al., 2015).

This plasticity held by the SKPs and the fact that they are present during adulthood made them a very attractive tool for disease modeling and therapeutical research.

1.1.3.1. Isolation of the SKPs

Two main types of SKP isolation were described in the literature, isolating the SKPs from fresh skin biopsies (Toma et al., 2001) or dermal primary fibroblast cultures by using different stressors (Budel & Djabali, 2017; Wenzel et al., 2012) or without any stressor (Hill et al., 2012).

- Isolation of SKPs from skin biopsies

The classical isolation technique of the SKPs is performed by collecting them from the dermis of skin biopsies. The dermis is cut into small pieces (2-3 mm^3) and digested with

trypsin. The dissociated dermis is then cultured in SKP media containing DMEM supplemented with epidermal growth factor (EGF), fibroblast growth factor (bFGF) and B-27. The cell suspension was cultured in T-25 flasks and mature spheroids were obtained after 3-4 weeks (Toma et al., 2001). This technique requires obtaining fresh skin biopsies every time the collection of the SKPs needs to be performed. This decreases the accessibility and availability of these SKPs, especially in HGPS children due to the rarity of the disease.

- Isolation of SKPs from dermal primary fibroblast cultures

In 2012, Wenzel et al showed the possibility to isolate SKPs from pre-established dermal fibroblast cultures (Wenzel et al., 2012). In this technique, trypsin was used as a cellular stressor to isolate the SKPs found in the fibroblast culture. The main idea behind this isolation method is that the cells with stemness potential like the SKPs will resist the stress conducted by trypsin and they will survive, whereas normal cells would not. Following the isolation with trypsin, the collected SKPs will further be cultured for 21 days in SKP medium containing B-27 and growth factors such as EGF and FGF (Wenzel et al., 2012). The use of primary fibroblast cultures as a source for SKPs holds many advantages since these fibroblasts can be purchased from different cell banks such as Coriell or ATCC, their growth and expansion are performed without the use of expensive growth factors and finally they can be stored at -80°C for a very long period.

Although this technique described by Wenzel et al. holds many advantages it is still subject to limitations such as the low yield obtained and long-term cultures (21 days).

To optimize this technique, Leithe et al. used another kind of stressor, acidic buffer, to isolate the SKPs (Budel & Djabali, 2017). The protocol consists of using a low pH HBSS buffer with a pH 5.7. The collected primary fibroblast cells were left in the HBSS buffer (pH 5.7) for 30 min. After treatment, the cells were cultured in SKP media for 5 days. On day 5 of culture, mature spheroids were obtained and were ready either for analysis or the use in following experiences.

Leithe et al. performed the pH isolation technique (named pH-SKP protocol) in parallel with the trypsin isolation technique (established by Wenzel et al. (Wenzel et al., 2012)) and the no-stress technique (described in the literature by Hill et al. (Hill et al., 2012)) in order to collect the SKPs. They compared the total yield of the spheroids from the different conditions. Acidic stress showed to produce the highest spheroids yield on day 3, 5 and 7 of SKP culture compared to the trypsin and no-stress methods. In addition, spheroids obtained from the pH-SKP protocol expressed multipotent stem cell markers such as Nestin (Lendahl, Zimmerman, & McKay, 1990), CD9 (International Stem Cell et al., 2007) and NG2 (Legg, Jensen, Broad, Leigh, & Watt, 2003). Therefore, in this study, we used the pH-SKP protocol in order to collect the SKPs form fibroblast cultures.

1.4. Senescence

Cellular senescence is an irreversible state of cell cycle arrest occurring in response to a number of damaging stimuli in particular oncogenic stress (Munoz-Espin & Serrano, 2014). Senescence shows benefits to the organism, acting as a safeguard against tumorigenesis (Sharpless & Sherr, 2015). However, the excessive accumulation of senescent cells in a tissue will create a pro-inflammatory milieu and decrease the regenerative capacities of the cells (Lecot, Alimirah, Desprez, Campisi, & Wiley, 2016;

Sharpless & Sherr, 2015). Several stimuli are capable of inducing senescence *in vitro*. These include: DNA damage-induced senescence (Munoz-Espin & Serrano, 2014), oncogene-induced senescence (OIS) (Munoz-Espin & Serrano, 2014; Sharpless & Sherr, 2015), oxidative stress-induced senescence (Hernandez-Segura et al., 2017), chemotherapy-induced senescence (Petrova, Velichko, Razin, & Kantidze, 2016), mitochondrial dysfunction-associated senescence (MiDAS) (Wiley et al., 2016), epigenetically induced senescence (Petrova et al., 2016) and paracrine senescence (Acosta et al., 2013). Two main tumor suppressor pathways are known to induce and to maintain senescence, the p53/p21 and p16INK4a/pRB pathways (Campisi, 2013).

Several techniques are used nowadays to identify senescence in a cell. In addition to permanent growth arrest, many different features and markers are used to detect senescence. Unfortunately, due to the heterogeneity of senescent cells and to the fact that not all senescent cells express all senescence markers, a combination of several techniques is usually applied to prove the senescence state (Hernandez-Segura, Nehme, & Demaria, 2018).

An important hallmark of senescence *in vitro* (and not *in vivo*) is the morphology of senescent cells. Senescent cells show an enlarged cell body, they become flat and vascularized. These features can be evaluated using bright field microscopy (Sharpless & Sherr, 2015). As mentioned above, this shape of the cell alone cannot be used to prove the senescent state. Several markers are used to identify and prove the presence of senescence in cultured cells.

The most commonly used marker to detect senescence is the staining for senescence-associated β-galactosidase (SA-βgal) (Dimri et al., 1995). Senescent cells are characterized by an increase in the lysosomal content and as a result by an increase in the lysosomal enzyme senescence-associated β-galactosidase (SA-βgal). This upregulated SA-βgal activity can be measured in senescent cells at pH 6.0. (Kurz, Decary, Hong, & Erusalimsky, 2000; Lee et al., 2006). Another type of assay includes measuring the levels of cyclin dependent kinase inhibitors (CDKIs), p16 and p21 (Sharpless & Sherr, 2015; Wiley et al., 2017). Generally, the levels of p16 and p21 are low or undetectable in healthy cells and are upregulated in senescent cells (Beausejour et al., 2003; McConnell, Starborg, Brookes, & Peters, 1998). Furthermore, senescent cells induce a pro-inflammatory response known as the senescence-associated secretory phenotype (SASP) (Campisi, 2013; Evan & d'Adda di Fagagna, 2009; Kuilman & Peeper, 2009). The SASP includes the secretions of cytokines, chemokines and proteases (Acosta et al., 2008; Coppe et al., 2008; Kuilman et al., 2008). Secreted cytokines such as IL-6, IL-8 and IL-1a are used as senescence markers (Coppe et al., 2008; Sharpless & Sherr, 2015) detected either by immunostaining or ELISA (Zhu et al., 2015).

1.5. Aim of this study

The adipose tissue is a highly active metabolic organ playing several important roles in our body (Wozniak, Gee, Wachtel, & Frezza, 2009). The partial or total loss of adipose tissue, known as lipodystrophy, leads to abnormal lipid accumulation and increased cardiovascular risk. Cardiovascular complications and stroke are known to be the main causes of death in HGPS patients, who also suffer from lipodystrophy. The absence of

fat in these patients is not only implicated in hindering proper metabolic function, but also causes physical pain to the children.

In order to study lipodystrophy in these patients, one possibility would be to collect adipocytes directly from them. This possibility is not favorable, since the patients already suffer from low or absence of adipose cells, not to mention the stress that the procedure will cause to the children.

Recently, stem cells, especially adult stem cells, are considered a very promising tool for medical treatments and therapies. Unlike the use of embryonic stem cells, the use of adult stem cells does not hold any ethic and legal burdens. Skin derived precursor stem cells or SKPs are a type of adult stem cells that reside within the dermis. They lately gained so much attention due to their many advantages: they are multipotent, present during adulthood and they can be isolated from skin biopsies independently from the subject's age, site of biopsy or disease. However, the use of these SKPs has an important limitation, isolating them has to be done from fresh skin biopsies. Which definitely decreases their availability and accessibility. Previous studies performed in our lab showed that SKPs can be isolated starting from fibroblast cultures of healthy individuals (Budel & Djabali, 2017). The technique consists of using a low pH HBSS buffer on the fibroblast cultures, followed by culturing the spheroids in SKP media containing growth factors such as epidermal growth factor (EGF) and fibroblast growth factor (FGF) for a period of 5 days. The collected SKPs expressed stem cells markers (Nestin, CD9 and vimentin) and showed the ability to differentiate into several types of cells including smooth muscle cells, fibroblasts and adipocytes (Budel & Djabali, 2017).

Since the isolation of SKPs from fibroblast cultures was only tested on cultures obtained from healthy individuals (Budel & Djabali, 2017), the first aim of the thesis was to investigate the possibility of isolating SKPs from fibroblast cultures obtained from HGPS patients. For this, the pH-SKP protocol was performed on two different HGPS cell lines and the collection of SKPs was followed.

Second, we wanted to check the differentiation capacities of the isolated HGPS SKPs and compare it to the differentiation potential of control SKPs. In this way we can create a disease model allowing us to study adipogenesis in HGPS children without the need to obtain fresh skin biopsies from the patients. The collected HGPS SKPs were dissociated and led to adhere in adipocyte differentiation media for 21 days. The total differentiation area and the size of lipid droplets were quantified after staining with Oil Red O and Bodipy.

The third aim we wanted to achieve in this work is to understand the role of senescence in SKP collection and differentiation in both control and HGPS. Senescence and the senescence-associated secretory phenotypes (SASPs) are known to reduce the differentiation potential of the stem cells. Hence, we wanted to investigate if the premature senescence observed in HGPS fibroblasts (C. Liu et al., 2019) and the chronic inflammation that it will create will have a role in the decreased adipogenic differentiation capabilities observed in HGPS patients. Towards this goal, the cultures were divided based on their senescence percentage and the differentiation potentials from both young and old senescence cultures were recorded.

2. Materials and Methods

2.1. Materials

2.1.1. Cell lines

Table 1. Cell lines used in this study.

Cell line	Organism of origin	Provenance
GMO1651c	Human, 13-year-old female HGPS patient	Coriell Institute for Medical Research (Camden, NJ, USA)
GMO5565	Human, 3-year-old male HGPS patient	Coriell Institute for Medical Research (Camden, NJ, USA)
GMO5567A	Human, 12-year-old male HGPS patient	Coriell Institute for Medical Research (Camden, NJ, USA)
3T3-L1 preadipocytes	Mouse	ATCC® CL-173™
HGADFN003	Human, 2-year-old male HGPS patient	Progeria Research Foundation Cell and Tissue Bank
HGADFN127	Human, 3-year-old female HGPS patient	Progeria Research Foundation Cell and Tissue Bank

2.1.2. Reagents

Table 2. List of reagents used in this study.

Reagent	Manufacturer	Reference number

2-propanol	Sigma-Aldrich	190764
3-Isobutyl-1-methylxanthin (IBMX)	Sigma	I7018
4,4-Difluoro-1,3,5,7,8-Pentamethyl-4-Bora-3a,4a-Diaza-s-Indacene (Bodipy 493/503)	Invitrogen	D3922
5-bromo4-chloro-3-indolyl P3-D-galactoside (X-gal)	Sigma-Aldrich	3117073001
Baricitinib	Absource Diagnostics	LY3009104, INCB028050
B27 Supplement (50x)	ThermoFisher-Gibco	17504-044
Citric Acid	Merck	8.18707.1000
DAPI Vectashield mounting medium	Vector Inc., Burlingame, CA, USA	VEC-H-1200
Dexamethasone	Sigma	D4902
Dimethyl sulfoxide (DMSO)	Sigma	D2650
Dulbecco's Modified Eagle Medium (DMEM) GlutaMax, High glucose, 4.5 g/l D-Glucose, Pyruvate	Gibco	31966-021
Dulbecco's Modified Eagle Medium (DMEM) GlutaMax, Low glucose, 1 g/l D-Glucose, Pyruvate	Gibco	21885-025
Dulbecco's phosphate-buffered saline (PBS)	Sigma	D8537
Epidermal Growth Factor (EGF)	ThermoFisher-Gibco	PHG0311
Ethanol absolute/pure (EtOH)	VWR	20821.321
Fetal Bovine Serum (FBS)	Gibco	10270–106

Fibroblast Growth Factor basic (bFGF)	ThermoFisher-Gibco	PHG0021
Formaldehyde 37%	Merck	104003
Fungizone/Amphotericin B	ThermoFisher-Gibco	15290-018
Gelatin	Sigma	G-7765
Gentamicin (10 mg/ml)	Gibco	15710049
Glutaraldehyde	Sigma-Aldrich	G5882
Ham's F-12 Nutrient Mix	Gibco	21765-029
Hanks' Balanced Salt Solution (HBSS)	ThermoFisher-Gibco	14175-053
Incuwater Clean	PanReac Applichem	A5219
Indomethacin	Sigma	I7378
Insulin	Sigma	I2643
L-Ascorbic Acid 2-phosphate	Sigma	A8960
L-Glutamine 200 mM (100X)	Gibco	25030-024
Magnesium Chloride (MgCl2)	Sigma-Aldrich	M-1028
MilliQ (Biocel A10)	Merck/Millipore	
NaCl	Sigma-Aldrich	310166
Oil Red O	Sigma-Aldrich	O0625
Paraformaldehyde (PFA)	Sigma-Aldrich	P-6148
Penicillin-Streptomycin (5000 U/ml)	Gibco	15140-122
Potassium Ferricyanide	Merck	104973
Potassium Ferrocyanide	Sigma-Aldrich	P9387
Sodium Hydroxyde (NaOH)	Roth	T135.1

Sodium Phosphate	Sigma-Aldrich	S-5136
Triton X-100	Sigma	T9284
Trypsine 0.25 % EDTA	Gibco	25200-056
Tween 20	Sigma	SLBR620IV

2.1.3. Antibodies

Table 3. List of antibodies and dilutions used in this study.

Primary antibodies						
Name/Target	Species	Dilution	Incubation time	Fixation	Supplier	Catalog. Number
anti-p16INK4A	Mouse	1/250	overnight at 4°C	MeOH	Sigma Aldrich	P0968
anti-p21	Rabbit	1/250	overnight at 4°C	2% PFA	Invitrogen	MA5-14949
anti-IL-8 (CXCL8)	Mouse	1/400	3h at RT	2% PFA	Invitrogen	M801
anti-progerin S9	Rabbit	1 to 1	overnight at 4°C	2% PFA	Lab Djabali	–
anti-PPARγ (E8)	Mouse	1/100	2h at RT	2% PFA	Santa Cruz Biotechnology	sc-7273

anti-FABP4	Rabbit	1/100	2h at RT	2% PFA	Sigma Aldrich	HPA002188
anti-Lamin A	Mouse	1/2000	2h at RT	2% PFA	Santa Cruz Biotechnology	sc-376248
Secondary antibodies						
Name/ Target	Species	Dilution	Incubation time	Fixation	Supplier	Catalog Number
α-mouse IgG Alexa Fluor 488	Donkey	1/1000	1h	_	LifeTech-nologies	A21202
α-mouse IgG Alexa Fluor 555	Donkey	1/1000	1h	_	LifeTech-nologies	A31570
α-rabbit IgG Alexa Fluor 488	Donkey	1/1000	1h	_	LifeTech-nologies	A21206
α-rabbit IgG Alexa Fluor 555	Donkey	1/1000	1h	_	LifeTech-nologies	A31572

2.1.4. Consumables

Table 4. List of consumables used in this study.

Consumable	Manufacturer
Coverslips Ø 12 mm	VWR
Freezing tubes	VWR
Microscope slides	Thermofisher Scientific
Parafilm M	Sigma
Petri dishes (adhesive bottom): 3 cm, 10 cm	Fisher Scientific-Falcon
Petri dishes (adhesive bottom) 10 cm	Sarstedt
Polypropylene conical tubes: 15 ml	Neolab
Polypropylene conical tubes: 50 ml	Sarstedt
Tip one pipet tips: 10 µl, 20 µl, 200 µl, 1000 µl	Starlab
Serological pipettes: 2 ml, 5 ml, 10 ml, 25 ml	Sarstedt
T25 non-treated flasks	Fisher Scientific-Falcon
6, 12, 24 well plates	Sarstedt
Syringe Filters (0.2 µm)	Sartorius
Syringes: 1 mL, 5mL, 10 mL, 20 mL, 50 mL	BD Discardit
Microtubes: 1.5 mL, 2 mL	Sarstedt

2.1.5. Devices

Table 5. List of the devices used in this study.

Name of the device	Manufacturer

Axio Imager D2 fluorescence microscope with AxioCam MRm with objectives: 10x, 20x, 40x, 40x oil, 63x oil	Zeiss
Axiovert 40 CFL bright field microscope with objectives: 5x, 10x, 20x	Zeiss
BioFuge Fresco	Heraeus
Bio-Rad Power Pack Basic and Universal	Bio-Rad
CASY® 1 Cell Counter	Roche
Centrifuge 5804R	Eppendorf
Eppendorf Research Pipettes: 0.1-2.5 µl, 0.5-10 µl, 2-20 µl, 10-100 µl, 100-1000 µl	Eppendorf
Incubator CB 220	Binder
Fridge 4°C	Thermo Scientific
Freezer -20°C	Thermo Scientific
Freezer -80°C	Thermo Scientific
Laminar Flow	Thermo Scientific
Leica TCS SP5	Leica Microsystems
MilliQ Biocel A10	Merck/Millipore
MiniSpin	Eppendorf
Mini Protean Cell	Bio-Rad
MS2 Minishaker Vortexer	IKA
Multifuge 3 S-R Centrifuge	Thermo Scientific
Pipetus-Pipetboy	Hirschmann Laborgeräte
Quintex LA230S Precision Balance	Sartorius
CP4202S Precision Balance	Sartorius
Thermomixer comfort	Eppendorf

TransBlot SD SemiDry TransferCell	Bio-Rad
VacuSafe comfort pump	IBS Integra Bioscience
Varioclav 75S	Thermo Scientific
Incubator without CO2	Binder

2.1.6. Softwares

Table 6. Softwares used in this study.

Name of the Software	Manufacturer/Developer
AxioVision SE 64 Rel.4.9	Zeiss
ImageJ	Wayne Rasband, NIH
ImageLab 5.2.1	Bio-Rad
MS Office 2016	Microsoft
Photoshop CC 2016	Adobe
Prism version 6.01	GraphPad

2.2. Methods

2.2.1. Cell culture

All cell culture work was performed in a biosafety cabinet under sterile conditions.

2.2.1.1. Fibroblast culture

2.2.1.1.1. Cell lines and incubating conditions

In this study three different types of cell lines were used. For the control groups, human primary dermal fibroblast cell lines obtained from healthy individuals were used: GMO5565 (3-year-old male), GMO1651 (13-year-old female) and GMO5567A (12-year-old male). These cells were purchased from the Coriell Institute for Medical Research (Camden, NJ, USA). For the HGPS cell lines, two different HGPS primary dermal fibroblast cell lines were used: HGADFN003 (2-year-old male) and HGADFN127 (3-year-old female). The last type of cell lines is 3T3-L1 murine fibroblast-like preadipocytes (ATCC® CL-173™), obtained from ATCC (Manassas, VA, USA). These cell lines were cultured in 10 cm Petri dishes with adhesive bottom. Each 10 cm dish was fed with 8 mL fibroblast culture medium (See Table 7), and the medium was refreshed every second day. Cells were cultured in a humidified incubator at 37°C with 5% CO_2.

Table 7. Composition of fibroblast culture medium (for 500 mL).

Reagent	Percentage	Volume
Dulbecco's modified Eagle's medium (DMEM; 4.5 g/L glucose)	87,5 %	437,5 ml
Fetal bovine serum (FBS)	15%	75 ml
L-glutamine	1%	5 ml
Penicillin/streptomycin	1%	5 ml
Gentamycin	0,5%	2,5 ml

2.2.1.1.2. Passaging cells

After reaching 80% of cellular confluency, each dish was splited to 4 new dishes. First, the cells were washed with 6-8 mL PBS to remove all traces of FBS that could inhibit the activity of trypsin. The PBS was aspirated and replaced with 1 mL trypsin-EDTA. The cells were incubated with the trypsin for 5-7 min in the incubator at 37 °C. The dishes were then checked under a microscope to make sure that the cells have detached, this was recognized by the appearance of round floating cells. Once all the cells have detached, the trypsin activity was stopped by adding 7 mL of the fibroblast culture medium (Table 7), leading to a final volume of 8 mL in the dish. The cells were resuspended by pipetting up and down several times and transferred equally into new dishes. Each dish received 2 mL of the cell suspension and 6 mL culture medium (Table 7). The new dishes were gently agitated, ensuring homogenous distribution of the cells, then cultured in a humidified incubator at 37°C with 5% CO_2. After reaching confluency, the cells were either splitted again following the same method that was just described, used for experiments or frozen at -80°C to make stocks.

2.2.1.1.3. Freezing and thawing cells

In order to make stocks, the cells were frozen in cryo tubes and kept at -80°C. First the cells were collected as described in the paragraph: Passaging cells. Then the cells were centrifuged at 1200 rpm for 5 min, and the supernatant was removed using a pump. The obtained pellet was resuspended with 4 mL of freezing media. The freezing media is composed of FBS supplemented with 10% DMSO. From each dish, with a cell confluency

of 80%, 4 freezing tubes were made. The cryo tubes were quickly transferred to the -80°C to prevent any cellular stress or death.

For the thawing, each cryo tube containing 1 mL of cell suspension was placed in a water bath (at 37°C) until the content is completely liquid. The suspension was then transferred into a 10 cm dish containing 7 mL of fibroblast culture medium (Table 7). The dish was shacked gently to ensure homogeneous distribution of the cells. The dish was later placed in a humidified incubator at 37°C with 5% CO_2.

2.2.1.1.4. Senescence-Associated Beta-Galactosidase (SA-β-Gal) assay

Senescence was assessed using the protocol from Dimri et al. (Dimri et al., 1995). The senescence test was assessed every second passage to keep track of the senescence index of our cultures. The preparation of the senescence dish was performed as following: while passaging the confluent cells, 200 µL were taken from the 8 mL cell suspension and transferred to a 3.5 cm dish. Additional 2 mL culture medium were added to the 3.5 cm dish and the dish was gently shacked to assure homogenous distribution of the cells. In order to perform the assay, the fibroblasts were then kept in the incubator for 2-3 days until reaching 60-70% confluency. The composition of the fixing and staining buffer used are mentioned in Table 8 and 9.

First, the fibroblasts were washed with PBS and fixed for 5 min with the fixing buffer (Table 8) containing 0.2%glutaraldehyde and 2% formaldehyde. Cells were then washed twice with PBS (5 min for each wash) and incubated overnight at 37 °C in the SA-β-Gal staining solution in an incubator at 37°C with no CO_2 (Table 9). Blue stained cells were considered as positive, and on average, 1000 cells were counted from each sample.

Table 8. Preparation of the fixing buffer for one dish to be stained with the Senescence-Associated Beta-Galactosidase Assay.

Reagent	Stock concentration	Volume for 1 dish (µl)
Glutaraldehyde	25% solution in H2O	8
Formaldehyde	37%	50
PBS	1X	940

Table 9. Preparation of the staining buffer for staining one dish with the Senescence-Associated Beta-Galactosidase Assay.

Reagent	Preparation	Stock concentration	Volume for 1 dish (µl)
Citrate acid	3,84 g citrate acid in 200 mL MilliQ water	0,1 M	—
Sodium phosphate	5,67 g sodium phosphate in 200 mL MilliQ water	0,2 M	—
Citrate/sodium phosphate, pH 6.0	Mix 36.50 ml of 0.2 M citrate acid with 63.50 ml of 0,2 M sodium phosphate to adjust to pH 6.0	40 mM Citrate	840
5mM Potassium Ferricyanide (III)	3.3 g Potassium Ferricyanide in 50 mL MilliQ water	200 mM	25
5mM Potassium Ferrocyanide (II)	4.2 g Potassium Ferrocyanide in 50 mL MilliQ water	200 mM	25
2 mM MgCl2	10 mL MgCl2 (1.0 M Solution) in 50 ml MilliQ water	200 mM	10

150mM NaCl	17.5 g NaCl in 100 ml MilliQ water	3 M	50
0,5mg/ml X-gal	10 mg X-gal in 1 ml DMSO	10 mg/1ml	50

2.2.1.2. Low-pH SKP isolation and culture

Primary fibroblast cultures (80% confluent) were collected by trypsin-EDTA and pelleted at 1200 rpm for 5 min at room temperature (RT), and washed once with phosphate-buffered saline (PBS) buffer. One million cells were resuspended in 500 µL of pH-adjusted Hank's balanced salt solution (HBSS) buffer. The pH of the HBSS buffer was adjusted to 5.7 using HCL. Cells suspended in HBSS buffer with pH 5.7 were incubated for 25 min at 37 °C and agitated every 5 min. The cell suspensions were centrifuged for 5 min at 1200 rpm at RT. Next, each pellet was suspended in 6 mL of SKP media (Toma et al., 2005) mentioned in Table 10, and the suspension was equally divided into two T25 non-tissue-culture-treated flasks. The cultures were supplemented every other day with 10 x SKP media (SKP media with 10x concentrated EGF, bFGF, and B27) (Table 11) diluted to a final concentration of 1x in culture media and agitated daily by pipetting up and down to prevent the adherence of the spheroids to the plastic flask.

Table 10. Composition of the 1X SKP medium (for 10 mL), based on Toma et al. (2005).

Reagent (with original concentration)	End concentration	Volume (µl)
DMEM (1 g/L glucose)	—	7255.5
F12	—	2418.5

EGF (0.1 mg/mL)	20 ng/mL	2
bFGF (0.1 mg/mL)	40 ng/mL	4
B27	2% v/v	200
Fungizone (250 µg/mL)	0.5 µg/mL	20
Pen/Strep (10,000 U/10,000 µg/mL)	100 U/100 µg/mL	100

Table 11. Composition of the 10X SKP medium (for 10 mL), based on Toma et al. (2005).

Reagent (with original concentration)	End concentration	Volume (µl)
DMEM (1 g/L glucose)	—	5865
F12	—	1955
EGF (0.1 mg/mL)	200 ng/mL	20
bFGF (0.1 mg/mL)	400 ng/mL	40
B27	20% v/v	2000
Fungizone (250 µg/mL)	0.5 µg/mL	20
Pen/Strep (10,000 U/10,000 µg/mL)	100 U/100 µg/mL	100

Preparation of the reagents used in the SKP medium:

- Master Stock of EGF (1 mg/mL)

The EGF (Epidermal Growth Factor) 100 µg powder vial was purchased from ThermoFisher-Gibco, PHG0311 and it was stored at 2-8° C. The vial was placed in a 50 mL tube and centrifuged at high speed to make sure that all the powder was collected at

the bottom. Next, the vial was opened under a sterile biosafety cabinet and 100 µL of sterile PBS was added to obtain a final concentration of 1 mg/mL. The mix was gently pipetted up and down to ensure that all the powder was completely dissolved in PBS. The solution was aliquoted in 10 µL portions and stored at -20° C.

- Working Stock of EGF (0.1 mg/mL)

For the working stock, 10 µL of the EGF master stock (1 mg/mL) was added to 90 µL of DMEM low glucose media (Gibco, 21885-025) to obtain a final concentration of 0.1 mg/mL. The solution was pipetted up and down to make sure that the content is completely mixed. Aliquots of 10 µL were prepared and stored and -20° C to prevent repeated freeze-thaw cycles.

- Master Stock of FGF (0.5 mg/mL)

The FGF (Fibroblasts Growth Factor) 100 µg vial was purchased from ThermoFisher-Gibco, PHG0021 and it was stored at 2-8°C. Same as the EGF vial, the FGF vial was placed in a 50 mL tube and centrifuged at the highest centrifugation speed to make sure that the powder is completely collected at the bottom of the tube. The vial was opened in a sterile biosafety cabinet and 200 µL of sterile demineralized double distilled water for a final concentration of 0.5 mg/mL. The solution was pipetted up and down to make sure that the powder was completely dissolved. The solution was aliquoted in 20 µL portions and stored at -20° C.

- Working Solution of FGF (0.1 mg/mL)

For the working solution, 20 µL of the FGF master solution (1 mg/mL) was added to 80 µL of DMEM low glucose media (Gibco, 21885-025) to obtain a final concentration of 0.1 mg/mL. The solution was pipetted up and down to make sure that the content is completely mixed. Aliquots of 20 µL were prepared and stored and -20° C to prevent repeated freeze-thaw cycles.

Table 12. Summary of the preparation of the growth factor stocks for the SKP medium.

Factor	Stock	Master stock preparation	Aliquots master stock	Working stock preparation	Aliquots working stock
EGF	100 µg lyophilized powder (stored at 2-8°C)	100 µg powder +100 µL sterile PBS (final concentration: 1 mg / mL)	10 µl (Stored at -20°C)	10 µL of master stock + 90 µL low glucose DMEM (0.1 mg/mL)	10 µl (Stored at -20°C)
FGF	100 µg lyophilized powder (stored at 2-8°C)	100 µg powder + 200 µL sterile demineralized water (final concentration: 0.5 mg / mL)	20 µl (Stored at -20°C)	20 µL of master stock + 80 µL of low glucose DMEM (0.1 mg/mL)	20 µl (stored at -20°C)

- B-27™ Supplement (50X), serum free

B27 supplement (50X) was purchased from ThermoFisher-Gibco as 10 mL vial at -20° C. The solution was thawed and aliquoted in 1 mL portions and stored at -20° C to prevent the freeze-thaw cycles.

2.2.1.3. Differentiation into adipocytes

2.2.1.3.1 Differentiation of SKPs into adipocytes

SKPs at day 4 were collected and washed twice with PBS. In case of adherence, the spheroids were incubated in adherence medium (Table 13) for 24 h, then switched to adipocyte differentiation medium (ADM) (Table 15). For trypsinization, the spheroids were dissociated with trypsin-EDTA and then seeded onto 0.2% gelatin-coated cover slips in a 24-well plate. In the control SKP group, 8 x 10^4 dissociated SKPs were seeded per well, whereas in the HGPS SKP group, 10^5 dissociated SKPs were seeded per well. The cells were cultured in the ADM according to the table 15, and the media was refreshed every 2–3 days. Baricitinib, 1 µM, was added to the SKP medium and ADM.

Table 13. Composition of the SKP adherence media (for 10 mL).

Reagent (with original concentration)	End concentration	Volume (µl)
DMEM (1 g/L glucose)	—	6880.5
F12	—	2293.5
EGF (0.1 mg/mL)	20 ng/mL	2
bFGF (0.1 mg/mL)	40 ng/mL	4
B27 (50X)	2% v/v	200
Fungizone (250 µg/mL)	0.5 µg/mL	20
Pen/Strep (10,000 U/10,000 µg/mL)	100 U/100 µg/mL	100
FBS	5% v/v	500

Table 14. Adipocyte differentiation medium (ADM) without the differentiation factors.

Material (with original concentration)	End concentration	Volume (ml)
DMEM (4.5 g/L glucose)	—	500
F12	—	167
FBS	10% v/v	66,7
Pen/Strep (10,000 U/10,000 µg/mL)	100 U/100 µg/ml	6,67

Table 15. Adipocyte differentiation medium (ADM) (50 mL).

Material (with original concentration)	End concentration	Volume (µl)
ADM without the factors (see Table 14)	—	48137,5
Insulin (1.0 mg/mL)	10 µg/ml	500
3-isobutyl-1-methylxanthine (IMBX) (50 mM)	0.5 mM	500
L-Ascorbic acid (10 mM)	100 µM	500
Dexamethasone (25 µM)	0.1 µM	200
Indomethacin (40 mM)	50 µM	100
Fungizone (250 µg/mL)	0.5 µg/ml	62,5

Preparation of the reagents used in the ADM:

- IBMX (3-isobutyl-1-methylxanthine) Stock Solution (50 mM)

In order to prepare 10 mL of IBMX with a concentration of 50 mM, 111.1 mg of IBMX powder was dissolved in 2 mL of 99% cell-grade ethanol under a chemical fume hood. Force pipetting was performed to make sure that the powder was completely dissolved. The solution was filtered using a 0.22 µm filter for sterilization. Aliquots of 500 µL were made and stored at -20° C.

- Insulin Stock Solution (1 mg/mL)

To prepare 5 mL of insulin stock solution with a concentration of 1 mg/mL, 5 mg of powder insulin were dissolved in 5 mL of HCL (0.01 M) under a chemical fume hood. Force pipetting was performed to ensure the dissolvement of the insulin in the HCL solution. The solution was filtered using a 0.22 µm filter for sterilization. Aliquots of 500 µL were made and stored at -20° C.

- Dexamethasone Stock Solution (25 µM)

To prepare 50 mL of dexamethasone with a concentration of 250 µM, 5 mg of dexamethasone was dissolved on 50 mL of 99% cell-grade ethanol under a chemical fume hood. Force pipetting was performed to make sure that the powder was completely dissolved. The solution was filtered using a 0.22 µm filter for sterilization. This stock was aliquoted and stored at -20° C. In order to obtain the working solution of 25 µM, the stock was further diluted 1:10 in sterile PBS and was also kept at -20° C.

- Indomethacin Stock Solution (40 mM)

For the preparation of 2 mL of Indomethacin stock solution of 40 mM, 28.62 mg of Indomethacin was weighed under a chemical fume hood and dissolved in 2 mL of 100%

DMSO. Force pipetting was performed to make sure that the powder was completely dissolved. The solution was filtered using a 0.22 µm filter for sterilization. Aliquots of 300 µL or 500 µL were made and stored either at -20 ° C for no longer than 6 months or at -80° C for long-term.

2.2.1.3.2 Differentiation of 3T3-L1 into adipocytes

The 3T3-L1 preadipocytes were cultured at 37 °C in 5% CO2-enriched air in DMEM, supplemented with 15% FBS, 1% L-glutamine, 1% penicillin/streptomycin, and 0.5% gentamycin (Table 7). Cells were seeded in 6-well plates on glass cover slips at a density of 2 x 10^5 cells per well. After reaching confluency, differentiation was induced by replacing the medium with ADM (Table 15). After 72 h, the medium was replaced with DMEM supplemented with 10% FBS, 10 µg/mL insulin, and 100 U/100 µg/mL penicillin/ streptomycin (ADM II) for 4 days, with one medium change during this period. On day 7, the medium was replaced with DMEM supplemented with 10% FBS and 100 U/100 µg/mL penicillin/streptomycin (basal medium). This medium was refreshed every second day until day 14 of differentiation. At days 3,7 and 14 of differentiation, the cells were fixed and stained with markers for lipid droplets (Oil Red O, Bodipy) or immunofluorescence.

Table 16. Composition of adipocyte differentiation medium II (ADM II) (for 50 mL).

Material	Volume (ml)
DMEM 4.5 g/L glucose	44
FBS	5
Insulin	0,5

Penicillin/streptomycin	0,5

Table 17. Composition of basal medium (BM) (for 50 mL).

Material	Volume (ml)
DMEM 4.5 g/L glucose	44.5
FBS	5
Penicillin/streptomycin	0,5

2.2.2. Immunocytochemistry

Cells were grown on glass cover slips and fixed either with ice-cold methanol or 2% PFA. For methanol fixation, the cells were fixed for 10 min at -20 °C, whereas for PFA fixation, the cells were fixed for 10 min at RT. Next step was permeabilizing the cells, and this was performed only in case of PFA fixation. After fixation with methanol, no permeabilization was needed. Following PFA fixation, the cells were permeabilized with 0.2% Triton X-100 in PBS for 10 min at RT and washed two times with PBS. Following fixation, the cells were blocked for 30 min with 10% FBS in PBS. The primary antibodies were diluted in the blocking buffer at the concentrations and incubation periods mentioned for each antibody (Table 3). Antibodies incubated for a few hours were left at RT, whereas antibodies incubated overnight were placed in a cold room at 4 °C. Next, the cells were rinsed three times with PBS, before the secondary antibodies diluted in the blocking buffer were added for 1 h at RT. Following incubation with the secondary antibody, cells were washed 3 times with PBS. Cells were counterstained with DAPI Vectashield mounting medium. Images were acquired using an Axio Imager D2 fluorescence microscope.

2.2.3. Staining lipid droplets

Two different lipid staining dyes were used: one colorimetric dye, Oil Red O (ORO) and another fluorescent dye, Bodipy.

2.2.3.1. Oil Red O (ORO) staining

ORO stock solution was prepared by dissolving 150 mg of ORO powder in 50 mL 99% 2-propanol. The working solution was prepared by mixing 3 parts of the ORO stock solution with 2 parts of demineralized water. Afterwards, it was then incubated for 10 min at room temperature and then filtered two times using Whatman filter paper to prevent the presence of undissolved Oil Red O powder. To perform the ORO staining, the differentiated adipocytes were first fixed with 4% PFA for 30 min at room temperature. Cells were then incubated for 5 min in 60% isopropanol, then in the previously prepared filtered ORO solution also for 5 min. Finally, the cells were rinsed 2 times with tap water and were ready for microscopy analysis. The stained cells were left in demineralized water and stored at 4 °C.

2.2.3.2. Bodipy 493/503 straining

Differentiated adipocytes obtained from control and HGPS SKPs were washed twice with PBS 1X. The differentiated cells were then treated with 2 µM Bodipy dissolved in PBS for 15 min at 37 °C. The slides were washed twice with PBS 1X and fixed with 4% PFA for 20 min at room temperature. Care must be taking when aspirating the solutions to prevent any cell detachment. Following PFA fixation, the cells were washed 3 times with PBS 1X

and counterstained with DAPI. This described protocol was performed in case staining only with Bodipy and DAPI was needed.

For double staining of immunofluorescence imaging with Bodipy, 2 µM Bodipy were added with the secondary antibody during immunocytochemistry in blocking buffer for 1 h at RT.

2.2.4. Image analysis

All the images were analyzed and the brightness/ contrast was adjusted using Fiji (Schindelin et al., 2012). The images and panels were all imported into Adobe Photoshop for illustration.

2.2.5. Statistical Evaluation and Graphics

The results of the experiments are presented as mean ± SD. The results were compared using either Student's t-test or two-way ANOVA. All the performed experiments were repeated at least three times as indicated in the figure legends. *p* values under 0.05 were considered significant and the following symbols were used: ns, not significant, $p > 0.05$, * $p \leq 0.05$, ** $p \leq 0.01$, and *** $p \leq 0.001$. The software GraphPad Prism version 6.01 (GraphPad, San Diego, CA, USA) was used to perform all the calculations and to draw the graphs.

3. Results

3.1. Characterization of HGPS SKPs

Studies performed on SKPs by Leithe et al. showed that these precursor cells could be isolated from normal skin fibroblast cultures (Budel & Djabali, 2017). For this isolation, three different treatments were used: low pH SKP isolation, trypsin SKP isolation and no stress SKP isolation. According to the obtained results, the pH SKP isolation protocol showed the highest SKP yield and growth, therefore, we decided to use the pH SKP isolation technique in all our further experiments (Budel & Djabali, 2017).

These previous studies by Leithe et al. showed that the isolation of the SKPs is possible using fibroblast cultures obtained from healthy individuals. In the first part, we wanted to test if the SKPs can also be isolated from fibroblast cultures obtained from HGPS patients. The pH-SKP isolation protocol consisted on collecting the 80-90% confluent fibroblasts and centrifuge them to obtain the cell pellet. The pH stress induction was performed by adding HBSS buffer with a pH 5.7 at 37°C for 30 min. Finally, the pellet was washed twice with PBS and cultured in SKP culture medium containing DMEM low glucose (1g/L), B27, and growth factors such as EGF and FGF. After 4 days, the SKP spheroids were ready to be analyzed or used for further experiments (Image 3a).

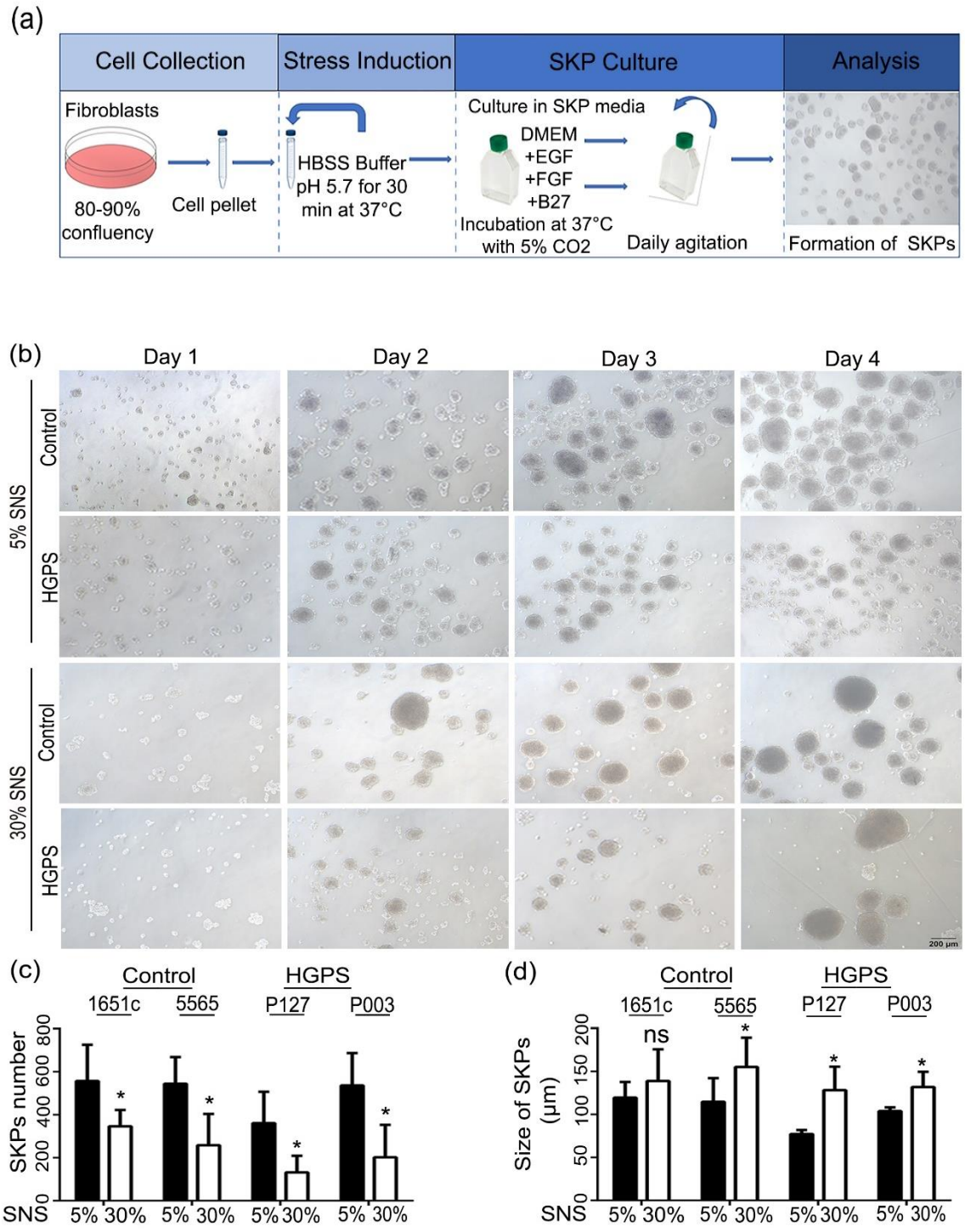

Figure 3. Isolation of SKPs from control and HGPS fibroblasts.

(**a**) Panel showing the protocol for SKP isolation. Briefly, fibroblasts were pelleted and treated with HBSS buffer (pH 5.7) for 30 min at 37 °C. Cells were cultured in SKP media containing DMEM

low glucose, EGF, FGF, and B27. The flasks were agitated daily, and the spheroids were harvested at day 4 for analysis. (**b**) SKPs formation from both control (GMO1651c, GMO5565) and HGPS (HGADFN127, HGADFN003) fibroblasts with 5% and 30% senescence (SNS). (**c, d**) Quantification of the number and the diameter of the spheroids from control and HGPS fibroblast cultures with 5% and 30% SNS at day 4. Values are presented as mean ± SD (n=3), * $p < 0.05$, ** $p < 0.01$, *** $p < 0.001$, (c, d) unpaired t-test. HBSS: Hanks Balanced Salt Solution, DMEM: Dulbecco′s modified Eagle medium, EGF: epidermal growth factor, FGF: fibroblast growth factor, SKPs: skin-derived precursor cells, SNS: senescence.

Senescence and the secretion of the senescence-associated secretory phenotypes (SASPs) are known to be implicated in stem cell depletion and the loss of stem cells regenerative capacity (Freund, Orjalo, Desprez, & Campisi, 2010). On the other hand, HGPS fibroblasts were shown to enter into senescence faster compared to their control counterparts (C. Liu et al., 2019). To study the effect of senescence on the collection of SKPs from control and HGPS fibroblasts, we divided our cultures based on their senescence percentage. Cultures with around 5% senescence were considered young, whereas cultures with around 30% senescence were considered old. In this experiment we used two different control cell lines: GMO1651c and GMO5565 and two different HGPS cell lines: HGADFN127 and HGADFN003. The formation of the spheroids was recorded every day during the 4 days of SKP culture (Image 3b). At day 4, the number of the spheroids in each flask was counted and the average diameter of the spheroids was calculated (Image 3c, d).

Isolating the SKPs from young cultures (around 5% SNS) from both control or HGPS fibroblasts showed an increased yield in comparison with the number of SKPs obtained when starting from old fibroblast cultures (around 30% SNS) (Image 3c). For the

GMO1651c the average yield was 557 spheroids per flask compared to 347 spheroids when starting from old cultures, the second control cell line, GMO5565, showed an average yield of 544 spheroids per flask compared to 258 spheroids when starting from 30% senescence cultures (Image 3c). The yield of the HGPS spheroids also showed a decrease in number when working with old fibroblast cultures. For the HGADFN127 cell line we could isolate an average of 361 spheroids from young fibroblast cultures compared to 132 spheroids from the old cultures. From the second HGPS cell line HGADFN003, 536 spheroids were obtained from 5% senescence cultures compared to 202 from the 30% senescence cultures (Image 3c).

Concerning the size of the spheroids, SKPs isolated from old fibroblast cultures appeared to be larger compared to those isolated from young fibroblast cultures (Image 3b, d). The average size of the spheroids when starting from young cultures was 120 µm and 115 µm for GMO1651c and GMO5565 respectively (Image 3d). This value increased to 139 µm and 155 µm when starting from old cultures for GMO1651c and GMO5565 respectively (Image 3d). For the HGPS SKPs the average size of the spheroids was smaller compared to their control counterparts when starting from young fibroblast cultures with 77 µm for HGADFN127 and 104 µm for HGADFN003 (Image 3d). This value increased to 128 µm for HGADFN127 and 132 µm for HGADFN003 when starting with old fibroblast cultures (Image 3d).

Altogether, these data indicate that just like control fibroblasts, it is possible to isolate SKPs starting from HGPS fibroblasts. The number of the obtained SKPs was inversely correlated with the percentage of senescence of the starting fibroblast culture of both control and HGPS cell lines.

3.2. Adipogenic differentiation of SKP spheroids

Stem cells obtained from HGPS patients showed impaired adipogenesis capability and severe lipid storage defects (Xiong et al., 2013). In order to detect if this defect is related to the presence of a high number of senescent cells in the cultures, we induced the differentiation of our pH-SKPs derived from both control or HGPS fibroblasts into adipocytes. To achieve this goal, we used the previously described protocol by Leithe et al (Budel & Djabali, 2017). The protocol consists on collecting the spheroids at day 4 of SKP culture and let them adhere on a gelatin coated cover slips in a 24 well plate (Image 4a). For the first 24 hours, the spheroids were cultured in SKP adherence media (Table 13) then switched to adipocyte differentiation media (Table 15) for 21 days with media changes every second day (Image 4a).

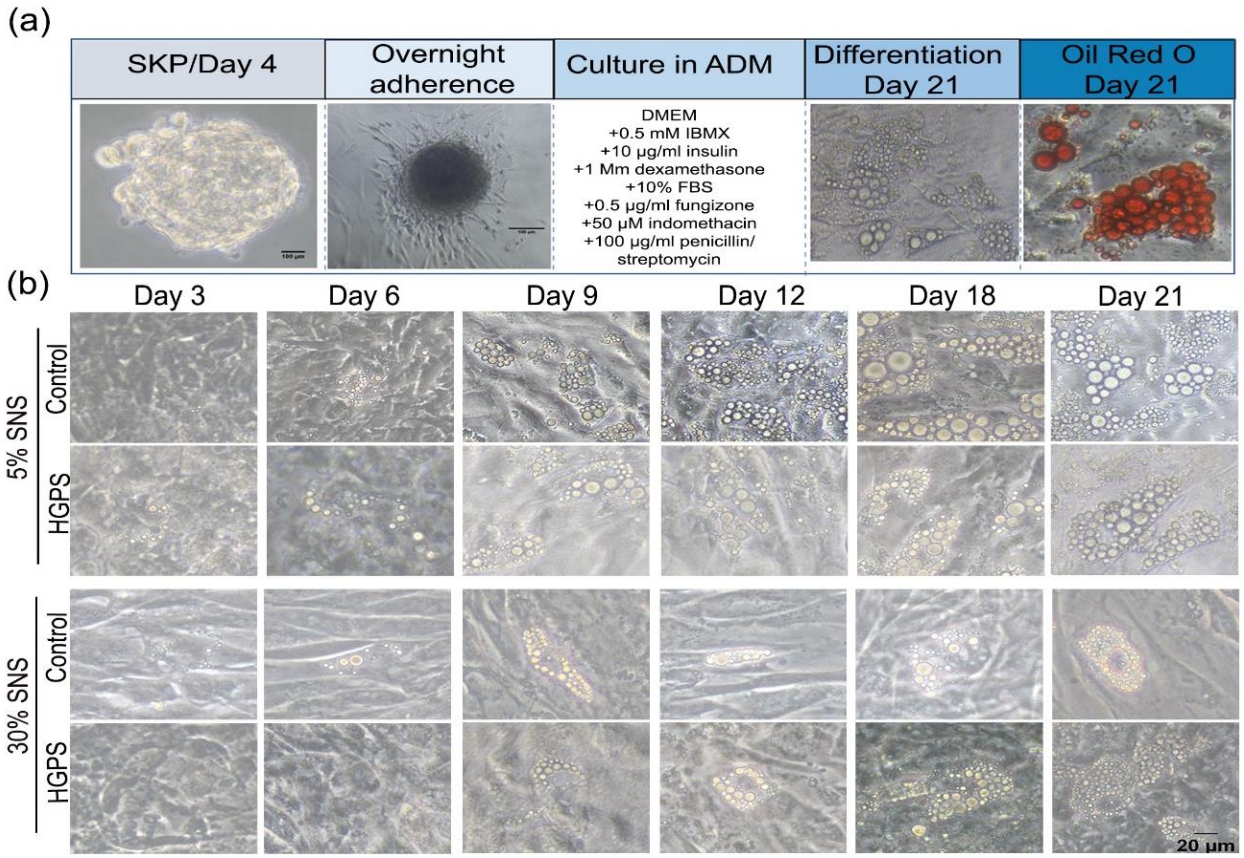

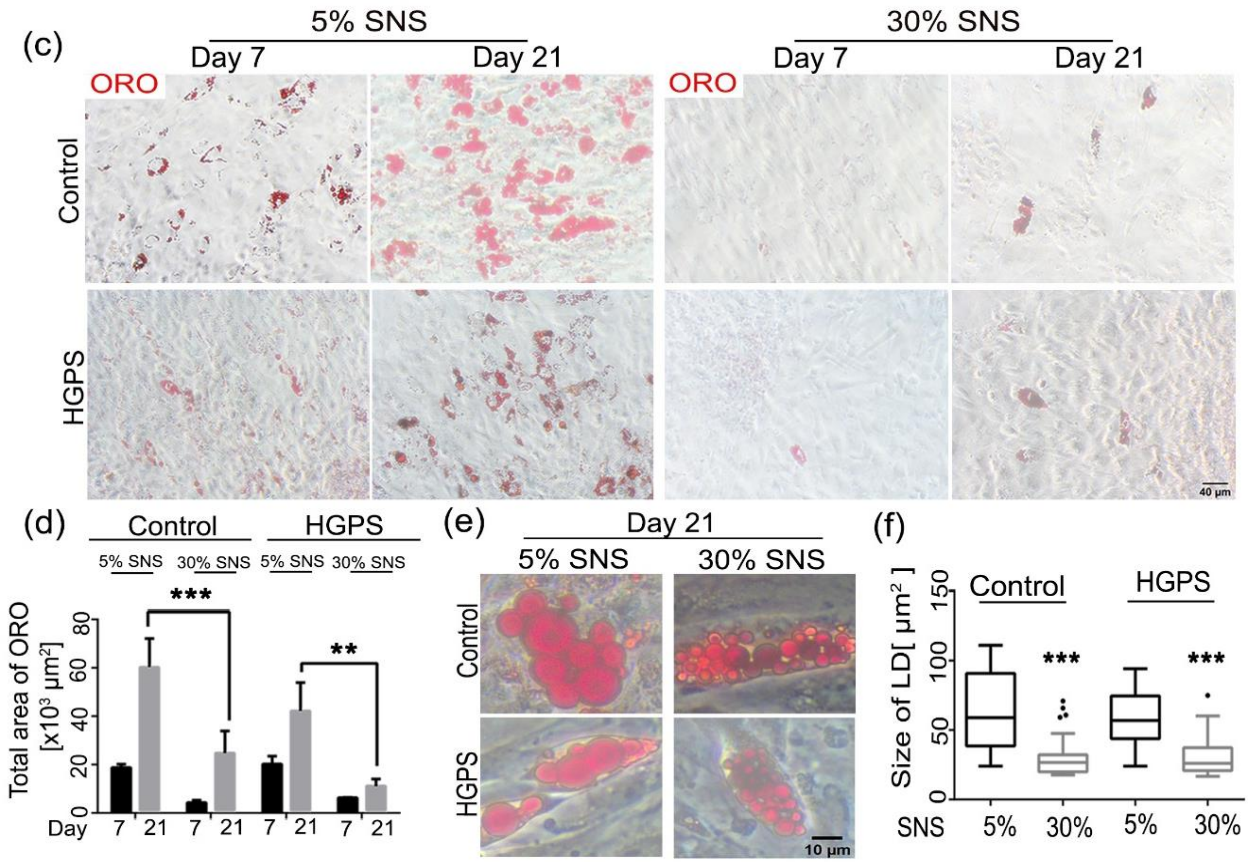

Figure 4. Differentiation of control and HGPS SKPs into adipocytes.

(**a**) Panel showing the protocol of SKPs adherence and differentiation. SKPs were collected at day 4 and allowed to adhere overnight in the presence of SKP adherence media. Next, the media was replaced with ADM supplemented with insulin, IBMX, and dexamethasone. Differentiation occurred for 21 days, and the differentiated adipocytes were stained with Oil Red O (ORO) at day 21. (**b**) Bright-field imaging of the differentiation of control and HGPS SKPs with 5% and 30% SNS into adipocytes at different time points. (**c**) ORO staining for differentiated control and HGPS SKPs originating from 5%- and 30%-senescence fibroblast cultures at day 7 and 21 of adipogenesis. (**d**) Quantification of total ORO-stained area using Image J. **(e, f**) Quantification of the size of lipid droplets in control and HGPS groups with 5% and 30% SNS at day 21 of differentiation. (**d**) Values are presented as mean ± SD (n=3), (**f**) In the Box and Whisker plot, the horizontal line crossing the box is the median, the bottom and top of the box are the lower and upper quartiles, the whiskers are the minimum and maximum values and the dots represent the outliers, * $p < 0.05$, ** $p < 0.01$, *** $p < 0.001$, (**d**) two-way ANOVA with Tukey's multiple comparisons test (**f**) unpaired t-test. FBS: fetal bovine serum, IBMX: Isobutylmethylxanthine.

The differentiation of the SKP spheroids isolated from control and HGPS fibroblasts from both young (5% SNS) and old (30% SNS) cultures was followed and observed at different time points (Image 4b).

For the SKPs obtained from young control and HGPS fibroblasts (Image 4b, first and second panel), small lipid droplets started to appear at day 3 of adipocyte differentiation. These lipid droplets from both cultures increased in number and size till day 21. For the control SKPs obtained from old fibroblast cultures (30% SNS), we could also observe the appearance of small lipid droplets at day 3 of differentiation (Image 4b, third panel). This was not the case with HGPS SKPs obtained from fibroblast cultures with 30% SNS, since the appearance of small lipid droplets was only visible at day 6 of differentiation (Image 4b, fourth panel). From day 9 to 21, few cells showed the presence of lipid versicles in both cell types, and their size at day 21 remained small.

The next step was to evaluate the total differentiation potentials of these spheroids obtained from both control and HGPS fibroblasts with the two senescence indexes 5% and 30%. Therefore, we stained the lipid droplets with a colorimetric dye Oil Red O at two time points: day 7 of differentiation (corresponding to early adipogenesis) and day 21 of differentiation (corresponding to mature adipocytes) (Image 4c). Images of the highly stained areas were taken from each condition and the quantification was performed using Fiji (Schindelin et al., 2012). Starting with 5% SNS cultures, the total area of ORO expression was relatively similar in control and HGPS differentiated adipocytes at the two time points: day 7 and day 21 (Image 4c, d). Following quantification, the average area of ORO expression at day 7 was 18750 μm^2 for control compared to 20254 μm^2 for HGPS (Image 4d). This value increased at day 21 due to the increase of number and size of

these lipid droplets, reaching a total ORO area of 60220 μm^2 for control compared to 42142 μm^2 for HGPS differentiated adipocytes (Image 4d). However, the total area of lipid droplet expression significantly decreased when working with SKPs collected from old fibroblast cultures (30% SNS) in both control and HGPS. The area of ORO expression decreased to a value of 4333 μm^2 in differentiated adipocytes obtained from old control SKPs (compared to 18750 μm^2 for the differentiated adipocytes obtained from young control SKPs) at day 7 of differentiation and to a value 24798 μm^2 at day 21 (compared to 60220 μm^2 for the differentiated adipocytes obtained from young control SKPs (Image 4d). The differentiated adipocytes from old HGPS SKPs also showed a decrease in the value of total ORO expression; at day 7 the value of ORO expression decreased to 5972 μm^2 (compared to 20254 for their young counterparts) and at day 21 the value decreased to 11180 μm^2 (compared to 42142 μm^2 for the differentiated adipocytes obtained from young HGPS SKPs) (Image 4d).

In addition, the average size of the lipid droplets obtained at day 21 of differentiation was smaller in adipocytes obtained from old fibroblast cultures compared to the ones obtained from 5% SNS cultures (Image 4e, f). The average size of the lipid droplet at day 21 decreased from 58.4 μm^2 (in 5% SNS cultures) to 26.4 μm^2 (in 30% SNS cultures) in control, and from 56.4 μm^2 (in 5% SNS cultures) to 25.4 μm^2 (in 30% SNS cultures) in HGPS differentiated adipocytes (Image 4f).

Altogether, these data show that the isolated SKPs from young HGPS fibroblasts could be differentiated into adipocytes, which accumulate lipid droplets with similar sizes to that in their control counterparts on day 21 of differentiation. We also show that an increase

in the senescence index of the original fibroblast culture hindered proper adipogenic differentiation in both control and HGPS.

3.3. Detection of the senescence level of SKP spheroids

In the first two result images, Figure 3 and 4, we showed that the senescence index of the initial fibroblast cultures affected the isolation and the differentiation of the SKPs. With higher senescence, the number of collected SKPs was lower and the adipogenic differentiation capacity of these SKPs was hindered, in both control and HGPS. On the opposite, working with low senescence cultures increased the SKP yield and showed proper adipocyte differentiation capabilities.

In order to detect if a number of cells entered into senescence after performing the SKP isolation technique, we measured the level of senescence of the initial fibroblast cultures and in the SKP preparation at day 4.

First, we tried to perform the SA-β-gal staining directly on the SKP spheroids from both control and HGPS cultures (Figure 5). However, this technique was not a success since it was hard to detect the positive stained spheroids form the ones that are not stained. The dye remained trapped in the spheroids and most of the spheroids were stained although we tried to optimize the protocol by trying different incubation time with the SA-β-gal staining solution (Figure 5).

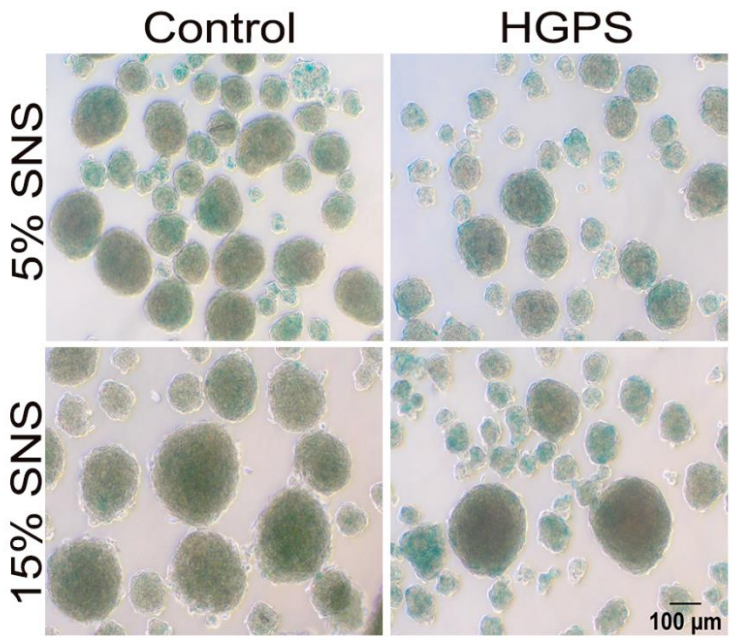

Figure 5. Senescence index of the SKPs: SA-β-gal staining from on spheroids from original control and HGPS fibroblast cultures.

SA-β-gal test performed directly on the SKPs from control and HGPS SKPs starting from 5% and 15% senescence.

To circumvent this problem, we decided to trypsinize the spheroids at day 4, leave them to adhere overnight in SKP adherence media and then perform the SA-β-gal staining. In parallel, we also performed the SA-β-gal staining on the starting fibroblast cultures and on their corresponding dissociated spheroids (Figure 6). Starting from young control fibroblast cultures (5% SNS), the percentage of senescence increased 4% (From 5% SNS in the initial control cultures to 9% SNS in the dissociated spheroids at day 4) (Figure 6). Whereas when starting from young HGPS fibroblast cultures, the percentage of senescence increased 12% (From 5% SNS in the original HGPS cultures to 17% in the corresponding dissociated SKPs) (Figure 6). Same analysis was performed when starting from older fibroblast cultures with a 15% senescence percentage. In the initial control fibroblast cultures, the percentage of senescence increased from 15% SNS to 20% SNS (5% increase) (Figure 6). For the initial HGPS fibroblast cultures, the percentage of senescence increased from 15% SNS to 24% SNS (9% increase) (Figure 6).

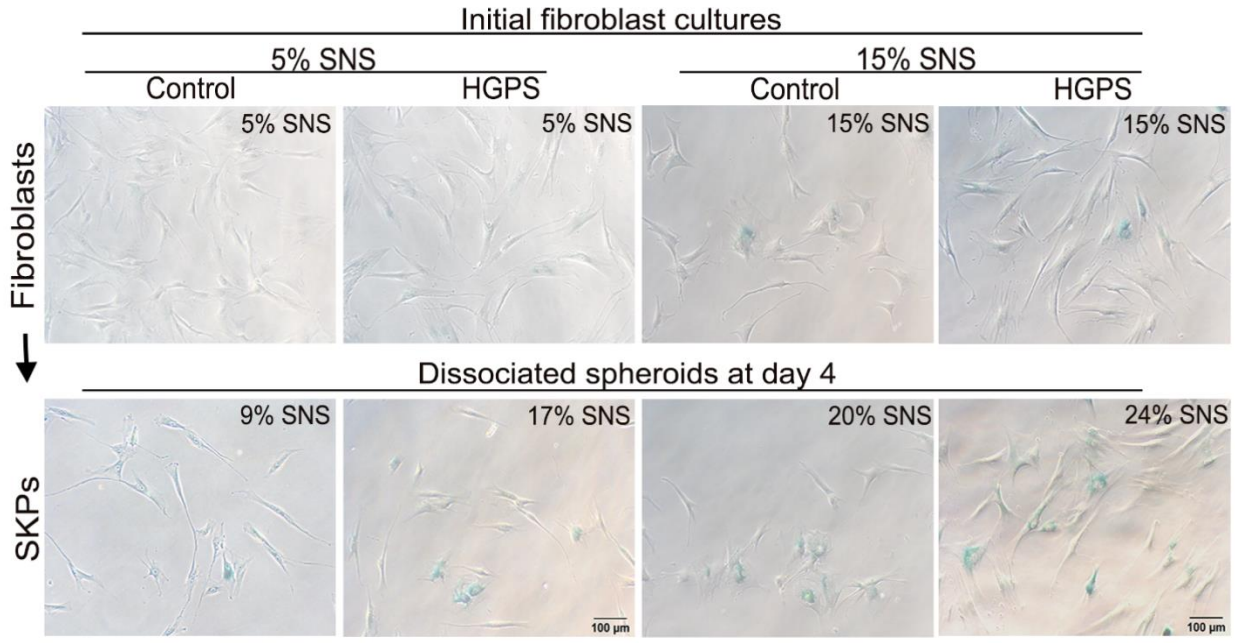

Figure 6. Senescence index of SKPs: SA-β-gal staining of original fibroblasts and dissociated SKPs at day 4.

SA-β-gal test performed using initial fibroblast cultures and on dissociated spheroids at day 4 for both control and HGPS groups starting from 5% and 15% SNS.

In order to validate these data, we performed immunofluorescence staining on three additional senescence markers: p21 (Figure 7), p16INK4A (p16) (Figure 8) and IL-8 (Figure 9) (Hotamisligil & Bernlohr, 2015; Rosen et al., 1999; Sharpless & Sherr, 2015). We started by the immunofluorescence with p21 (Figure 7) and the staining was performed on the original fibroblast cultures (Figure 7a) and on the dissociated spheroids (Figure 7b) for both control and HGPS with either 5% or 15% SNS. For all the conditions, the percentage of p21 expression increased in the dissociated spheroids compared to the original fibroblast cultures (Figure 7c). In addition, a significant increase was observed in the percentage of p21 expression between the HGPS dissociated SKPs compared to their control counterparts in both 5% and 15% SNS cultures. The HGPS dissociated SKPs

at day 4 showed 14.25% p21 expression compared to 8.16% in the control dissociated SKPs, when starting with young cultures. With 15% SNS cultures, the percentage of p21 expression in HGPS dissociated SKPs was 26.8% compared to 17.6% in control dissociated SKPs at day 4 (Figure 7c).

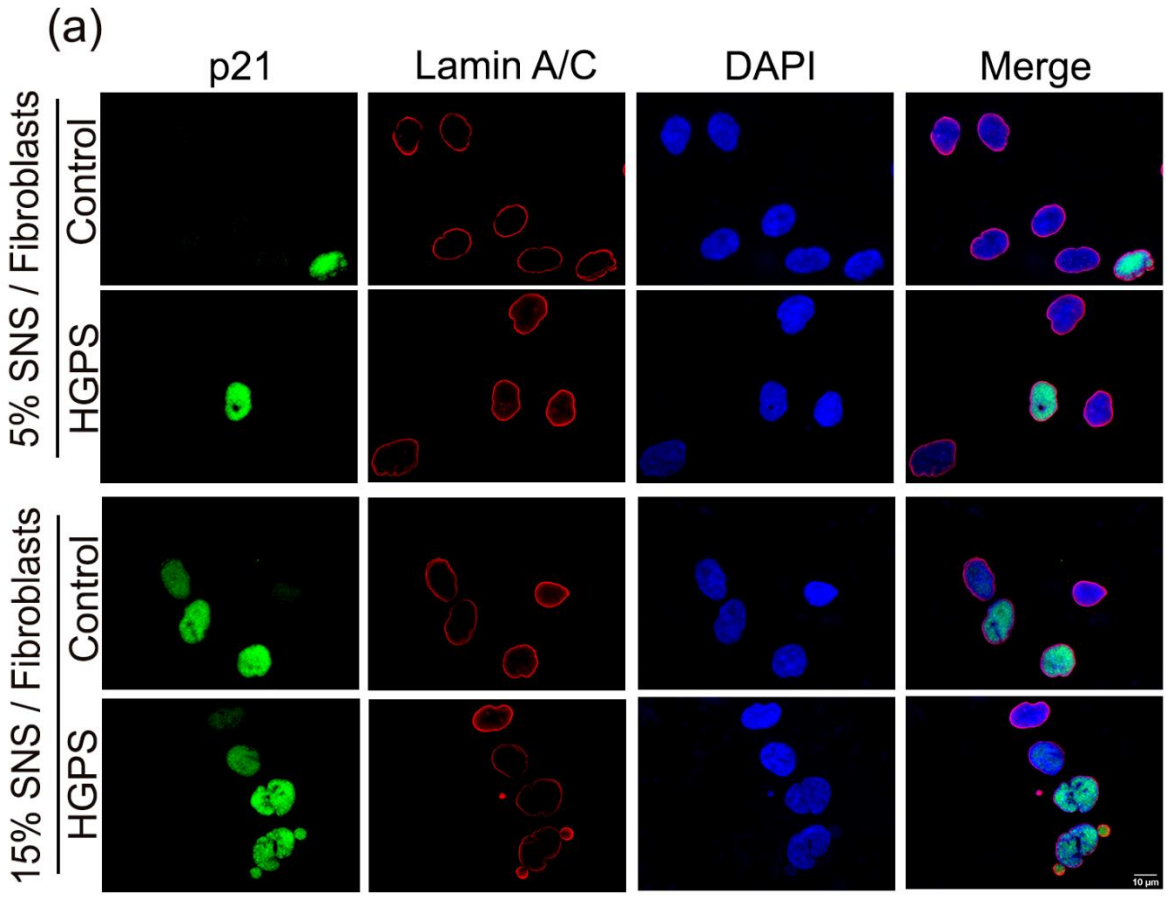

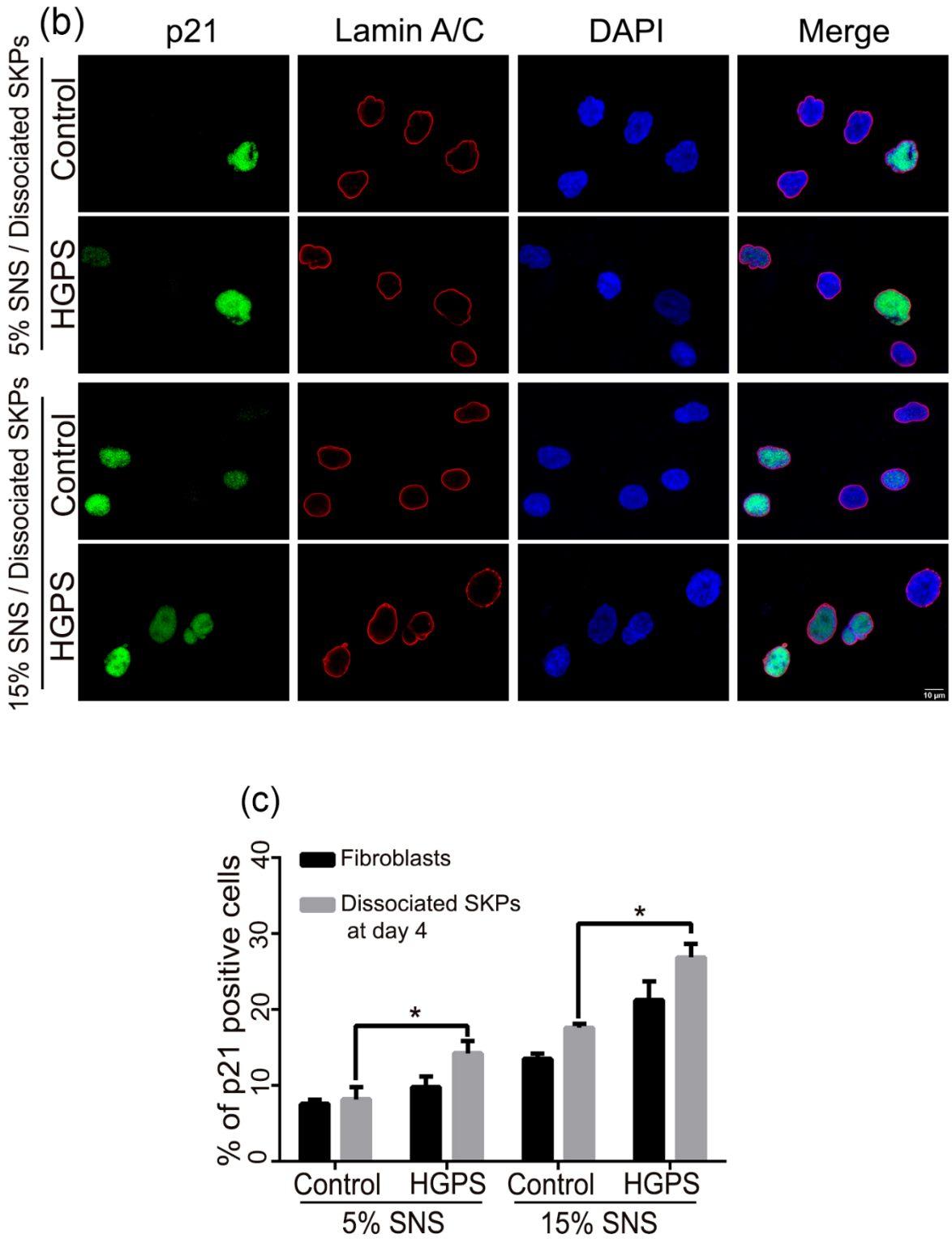

Figure 7. p21 staining of original fibroblasts and dissociated SKPs at day 4.

(**a**) Immunofluorescence staining against p21 and Lamin A/C of the initial control and HGPS fibroblast cultures with 5% and 15% senescence. (**b**) Immunofluorescence staining for p21 and

Lamin A/C in dissociated spheroids at day 4, from control and HGPS SKPs with 5% and 15% SNS. Cells were counterstained with DAPI. (**c**) Quantification of the percentage of p21-positive nuclei in the initial fibroblast cultures and in dissociated SKPs at day 4 in both control and HGPS groups. Values are presented as mean ± SD (n=3), * $p < 0.05$, ** $p < 0.01$, *** $p < 0.001$, (c) two-way ANOVA with Tukey's multiple comparisons test.

Next, we investigated the expression of p16INK4A (p16) (Figure 8) and IL-8 (Figure 9) again in the original fibroblast cultures and in their corresponding dissociated spheroids in control and HGPS from either 5% and 15% SNS cultures.

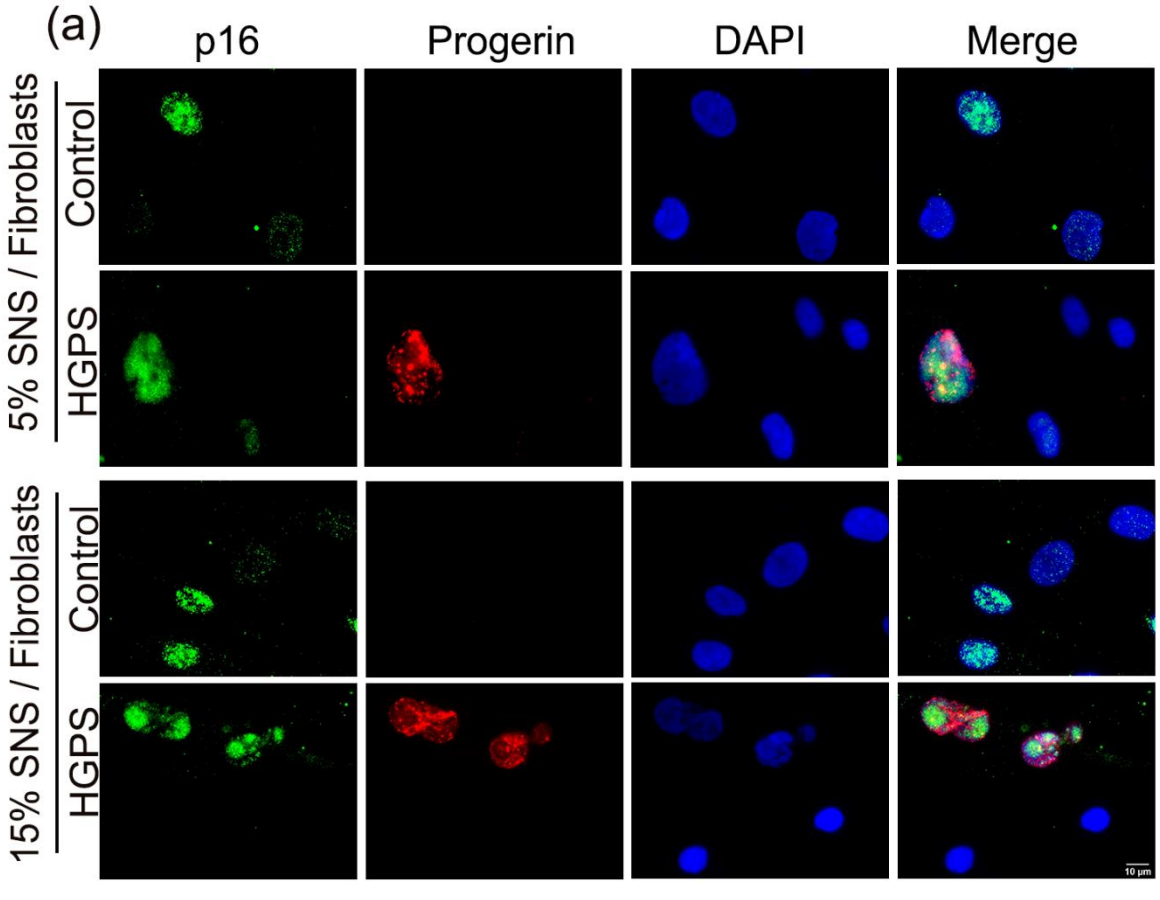

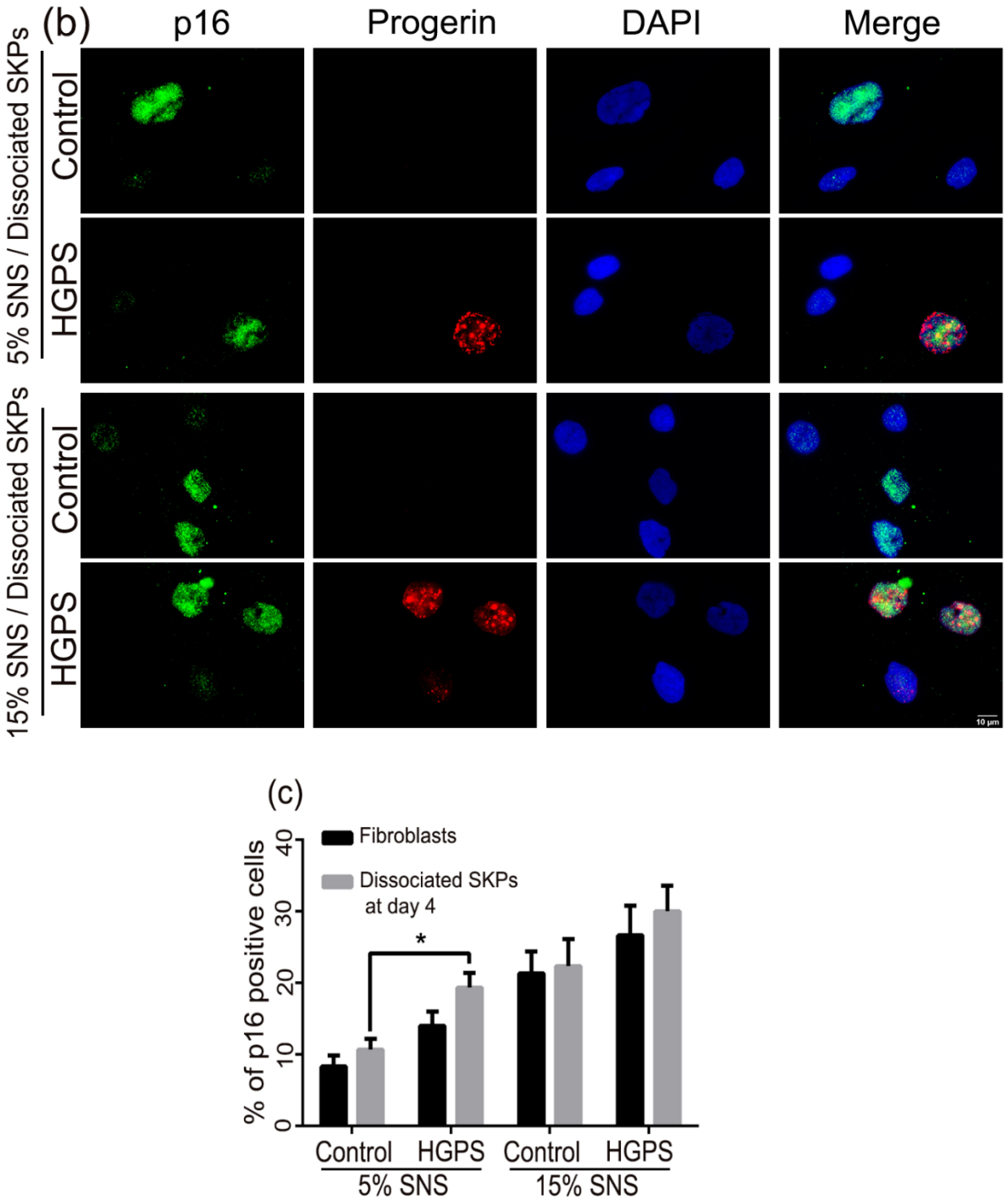

Figure 8. Immunofluorescence staining for p16 in the initial fibroblasts and in the dissociated control and HGPS SKPs at day 4.

(**a**) Immunofluorescence staining against p16 and progerin of the initial fibroblast cultures from control and HGPS with 5% and 15% senescence. (**b)** Immunofluorescence staining for p16 and progerin at day 4 in dissociated spheroids from control and HGPS SKPs with 5% and 15% SNS.

(**c**) Quantification of the percentage of p16-positive nuclei in the initial fibroblast cultures and in dissociated SKPs at day 4 from both control and HGPS cultures. Cells were counterstained with DAPI. Values are presented as mean ± SD (n=3), * $p < 0.05$, ** $p < 0.01$, *** $p < 0.001$, (**c**) two-way ANOVA with Tukey's multiple comparisons test.

The expression of p16 and IL-8 increased in the dissociated spheroids at day 4 compared to the original fibroblast cultures in all the conditions (In control and HGPS cultures also with 5% and 15% SNS). In addition, the expression of p16 and IL-8 significantly increased in HGPS dissociated SKPs compared to their expression in the original fibroblast, when working with 5% SNS cultures. For p16, the expression was 19.3% in young HGPS dissociated SKPs compared to 10.6% in the young control dissociated SKPs at day 4 (Figure 8c). For the IL-8, the expression was 14.3% in the young HGPS dissociated SKPs compared to 6.3% in the young control dissociated SKPs (Figure 9c).

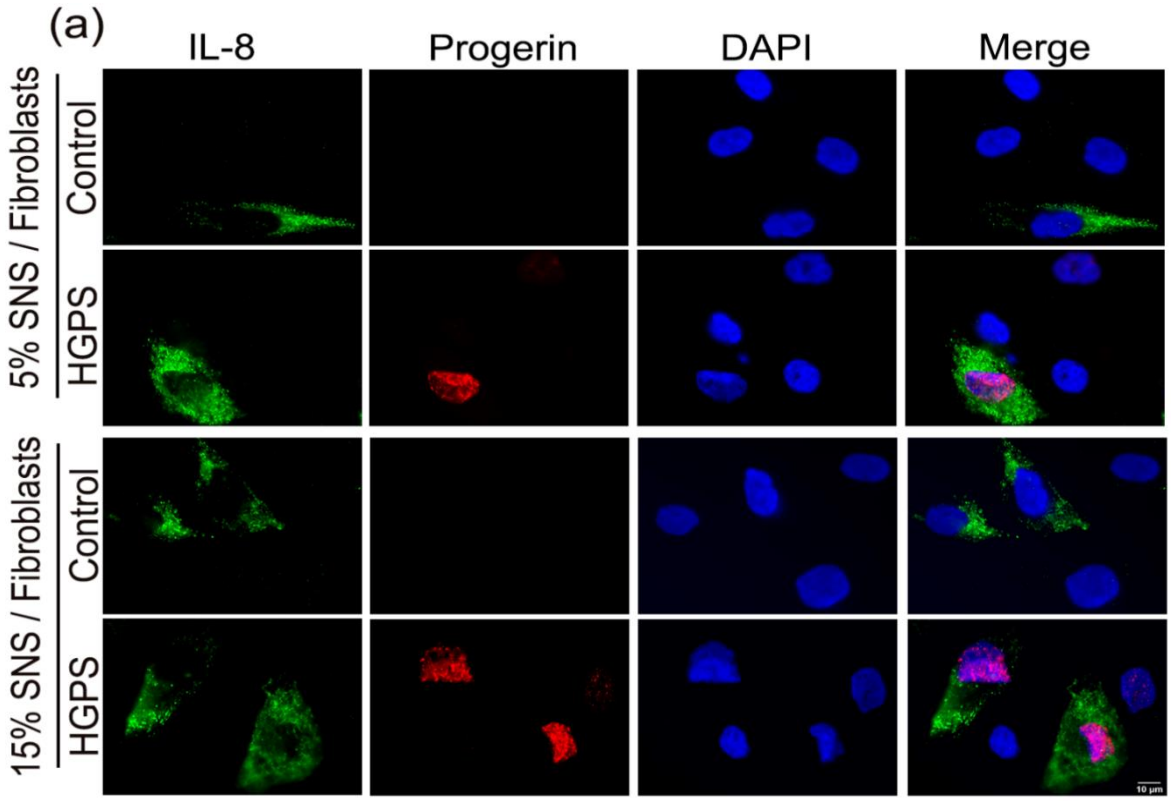

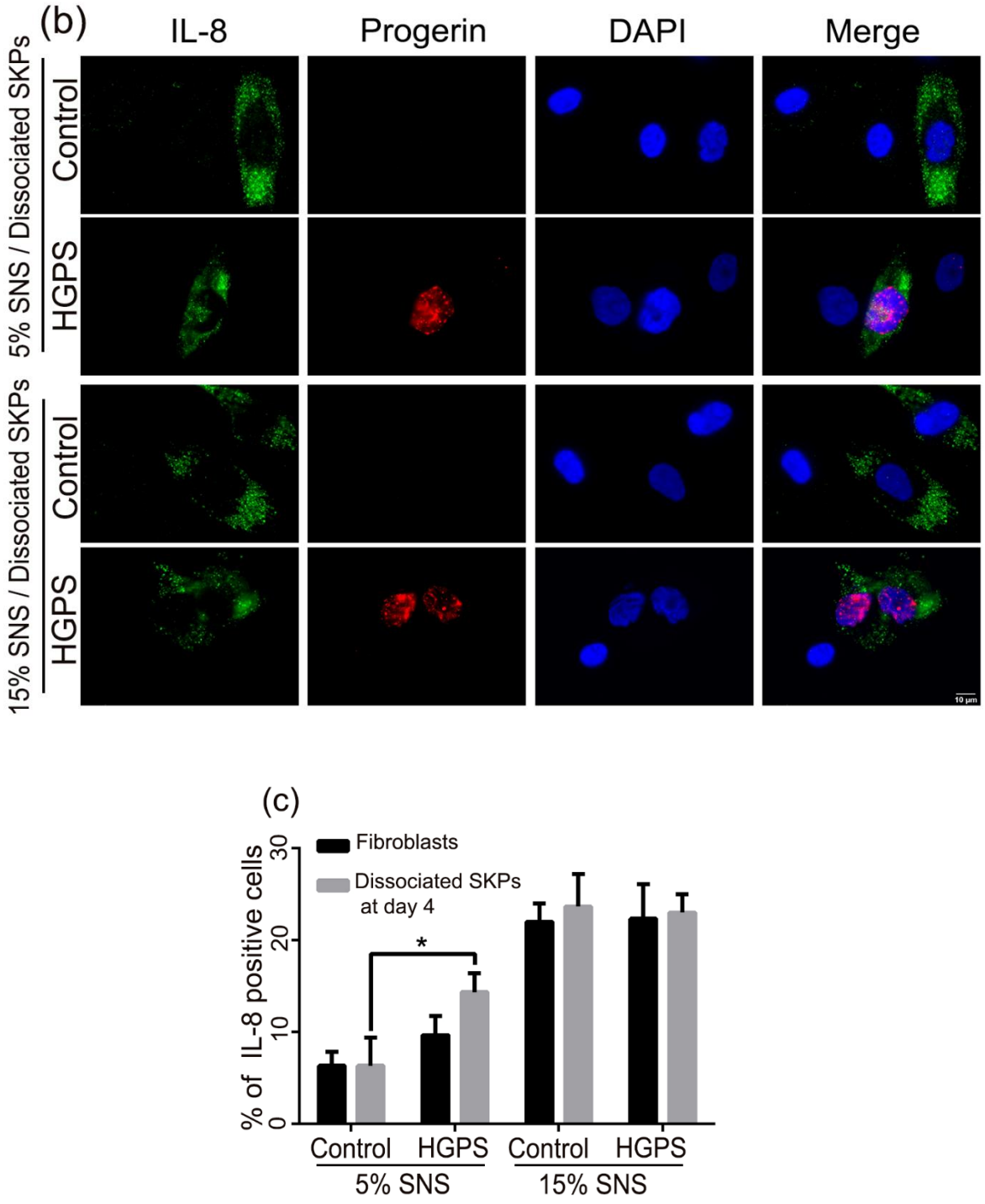

Figure 9. Immunofluorescence staining for IL-8 in the initial fibroblasts and in the dissociated control and HGPS SKPs at day 4.

(**a)** Immunofluorescence staining against IL-8 and progerin of the initial fibroblast cultures from control and HGPS with 5% and 15% senescence. (**b**) Immunofluorescence staining for IL-8 and progerin at day 4 in dissociated spheroids from control and HGPS SKPs with 5% and 15% SNS.

Cells were counterstained with DAPI. (**c**) Quantification of the percentage of IL-8-positive cells at day 4 in the initial fibroblast cultures and in dissociated SKPs from both control and HGPS cultures. Values are presented as mean ± SD (n=3), * $p < 0.05$, ** $p < 0.01$, *** $p < 0.001$, (**c**) two-way ANOVA with Tukey's multiple comparisons test.

Altogether, these findings indicate that the pH-SKP protocol induces cellular stress and increases the level of senescence in the cultures particularly in the case of the HGPS SKPs. This increased stress and senescence could affect the differentiation capabilities of the HGPS SKPs into adipocytes.

3.4. Differentiation of SKP spheroids derived from low senescence fibroblast cultures

The previously described differentiation protocol (Methodology 2.2.1.3.1); that consists on collecting the whole spheroids at day 4 and let them to adhere overnight in the presence of adipocyte adherence media (Table 13) and then culture them in adipocyte differentiation media (Table 15), let to proper adipocyte differentiation. Unfortunately, this protocol had one limitation, the whole spheroids were left to adhere, meaning that the number of spheroids added in each well was hard to monitor between all the conditions. In this case, if we see higher differentiation in one well compared to another, we will not be able to know if this is due to a higher potential of the cells to differentiated into adipocytes, or this is due to the presence of a higher number of spheroids in the first place.

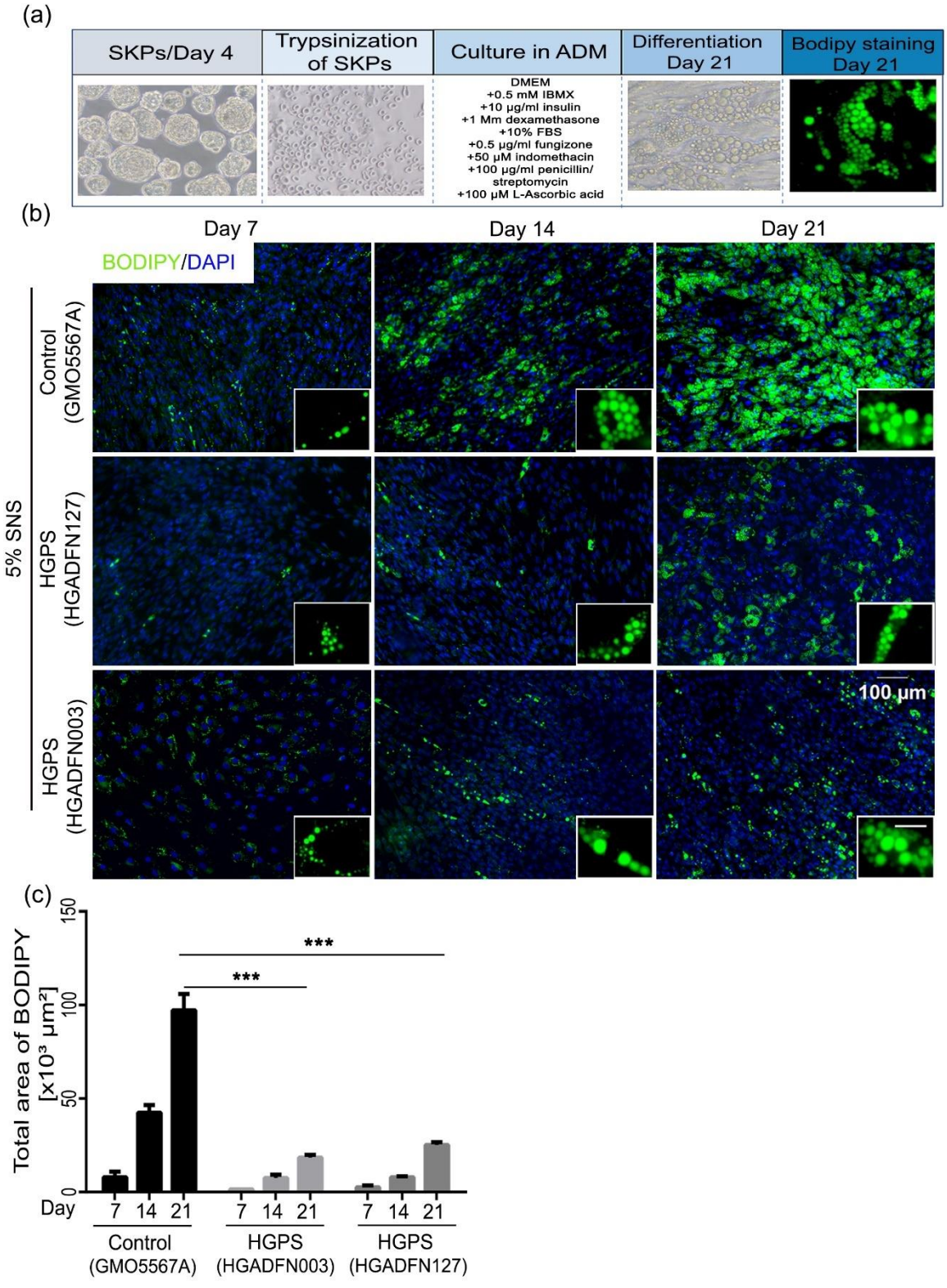

Figure 10. Differentiation of trypsinized SKPs into adipocytes.

(**a**) Panel showing the optimized protocol for SKPs trypsinization at day 4 and differentiation into adipocytes. The spheroids were trypsinized at day 4 and cultured directly in ADM. The differentiated cells were observed for 21 days and then stained with ORO and Bodipy at day 21. (**b**) Bodipy staining of lipid vesicles for control (GMO5567A) and HGPS (HGADFN127 and HGADFN003) cells, starting from 5% SNS fibroblast cultures. Staining was performed at days 7, 14, and 21 of differentiation. Cells were counterstained with DAPI. Scale bar: 100 µm / for the magnified images, scale bar: 20 µm. (**c**) Quantification of area with Bodipy signals at the three time points for both control and HGPS adipocytes. Values are presented as mean ±S D (n=3), * $p < 0.05$, ** $p < 0.01$, *** $p < 0.001$, (c) two-way ANOVA with Tukey's multiple comparisons test.

In order to optimize the protocol, we decided to trypsinize the spheroids at day 4 of SKP culture and then seed a specific number of cells in each well. After several optimization trials, we determined the following seeding conditions; for HGPS, we seeded 100.000 cells from the dissociated spheroids (in a 24-well plate) and for control, 80.000 cells from the dissociated spheroids were seeded. The dissociated adipocytes were cultured in adipocyte differentiation media (ADM) (Table 15) for a period of 21 days (Figure 10a).

We followed the differentiation of the dissociated young SKPs (5% SNS) for one control (GMO5567A) and two HGPS cell lines (HGADFN127 and HGADFN003). Two different dyes were used to stain the lipid droplets, Oil Red O (ORO) as a colorimetric dye and Bodipy as a fluorescent dye. The differentiation of the dissociated SKPs was followed and monitored every day and the staining with the previously mentioned dyes was performed on the following time points: day 7, 14 and 21 of differentiation. In this experiment, the dissociated SKPs were cultures on glass coated cover slips and seeded in a 24 well-plate. For each condition and each time point, a minimum of 8 cover slips were performed; 4 cover slips were used for Bodipy staining and 4 were used for ORO staining. At day 7

of adipocyte differentiation, the number of lipid droplets was relatively low, this was reflected by the low expression of ORO and Bodipy (Figure 10b and 11) for both control and HGPS adipocytes. For the differentiated adipocytes obtained from control (GMO5567A), the total area of Bodipy expression at day 7 was 7951 μm^2 compared to 1982 μm^2 for HGPS HGADFN003 and 2598 μm^2 for HGPS HGADFN127.

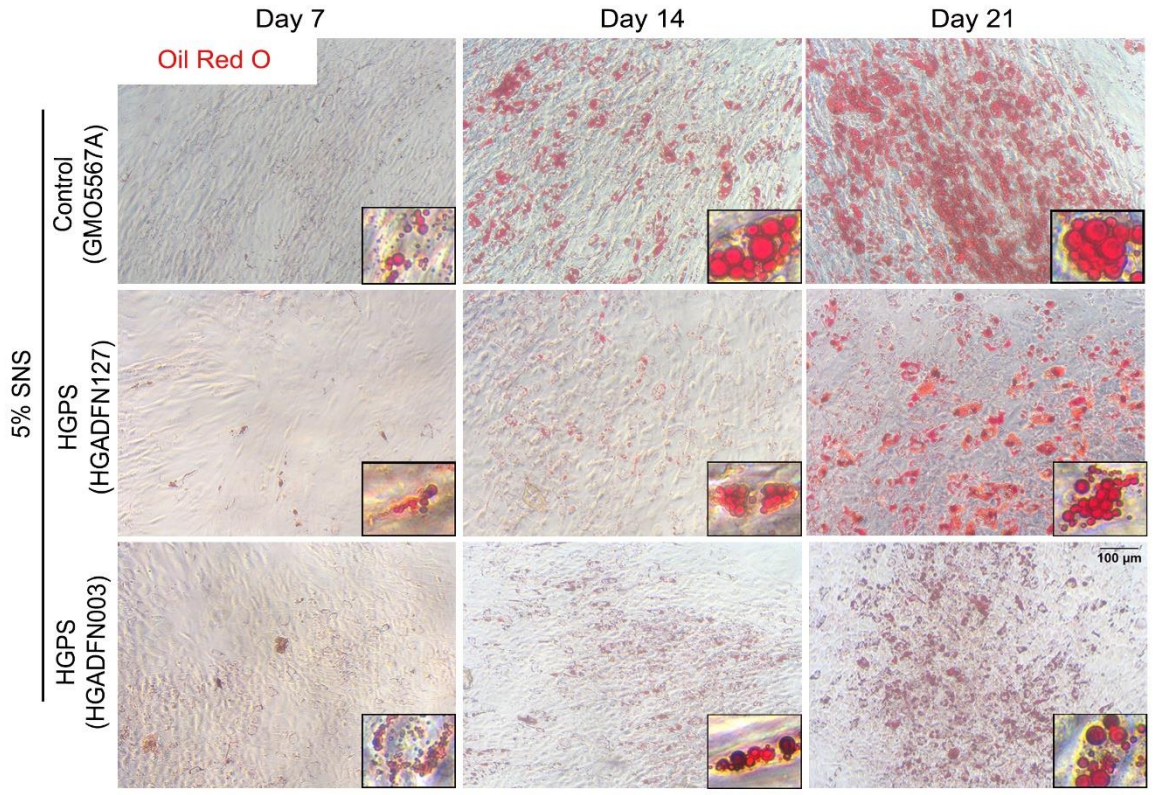

Figure 11. ORO staining of differentiated control and HGPS SKPs.

Oil Red O staining for control (GMO5567A) and HGPS (HGADFN127 and HGADFN003) differentiated adipocytes at days 7, 14 and 21 of adipogenesis, starting from 5% SNS fibroblast cultures.

This difference in the Bodipy expression profile between the control and the two HGPS cell lines was not significant at day 7. The number and size of the lipid droplets increased

from day 7 till day 14 until reaching a total area of Bodipy expression almost 5 times higher (42462 μm^2) at day 14 compared to day 7 in control differentiated adipocytes. For the two HGPS cell lines, this value was lower, with an increase of almost 3 times from day 7 to day 14. The total area of Bodipy expression reached a value of 7569 μm^2 for the HGADFN003 adipocytes at day 14 (increased form 1982 μm^2 at day 7) and a value of 7912 μm^2 for the HGADFN127 (increased from 2598 μm^2 at day 7) (Figure 10c). The difference of Bodipy expression at day 14 between the control adipocytes and the two HGPS differentiated adipocytes was significant with a *p* value < 0.01 (**). At day 21 of differentiation, the total area of Bodipy expression significantly increased in control differentiated adipocytes compared to day 14 (increase from 42462 μm^2 at day 14 to 97150 μm^2 at day 21 with a *p* value < 0.001) (Figure 10c). This is also reflected by the intense green (For Bodipy) (Figure 10b) or red (For ORO) (Figure 11) coloration observed in the differentiated adipocytes in the control group at day 21. For the HGADFN003, the total area of Bodipy expression did not significantly increase between day 14 and day 21 of differentiation. The area of Bodipy expression increased from 7569 μm^2 at day 14 to 18441 μm^2 at day 21 (Figure 10c). Same was observed for the HGADFN127 differentiated adipocytes, as the total area of Bodipy expression did not show any significant increase between day 14 and day 21. The value increased from 7912 μm^2 to 25170 μm^2 with a *p* value > 0.05 indicating no significance (Figure 10c).

Nevertheless, the total area of Bodipy expression in GMO5567A differentiated adipocytes at day 21 was significantly higher (5 times higher) compared to the value obtained from HGADFN003 adipocytes at the same time point, with 97150 μm^2 for control adipocytes compared 18441 μm^2 for HGADFN003 adipocytes at day 21 (*p* value < 0.001) (Figure

10c). The value obtained for GMO5567A differentiated adipocytes at day 21 was also significantly higher compared to the one obtained from the HGADFN127 adipocytes, with a total area of 25170 μm^2 in HGADFN127 compared to 97150 μm^2 in control adipocytes (almost 4 times higher in control with a *p* value < 0.001) (Figure 10c).

Collectively, the optimized adipocyte differentiation protocol showed impaired adipogenic capabilities of the HGPS SKPs from two different HGPS cell lines (HGADFN127 and HGADFN003) compared to control SKPs. This could be caused by a higher number of senescent cells found in the HGPS SKP cultures compared to their control counterparts.

3.5. Characterization of SKP formation and differentiation after treatment with Baricitinib

Previous studies from our lab showed that treating HGPS fibroblasts with Baricitinib, a JAK 1/2 inhibitor, delayed senescence, reduced the level of proinflammatory markers and restored cellular homeostasis (C. Liu et al., 2019). Based on that, we wanted to test if treatment with Baricitinib could also improve adipogenesis in HGPS spheroids. The previously used concentration of 1 µm of Baricitinib showed no cytotoxicity during long-term treatments *in vitro*, therefor we used this concentration in all our further experiments. First, we wanted to study the effect of Baricitinib treatment on the spheroid formation. Two groups were made for each control and HGPS SKPs with or without Baricitinib treatment. First, the SKP protocol (Method 2.2.1.2) was performed for all the groups in the same manner, and then 1 µm of Baricitinib was added to the SKP media (Table 10) for the treated groups (Figure 11a).

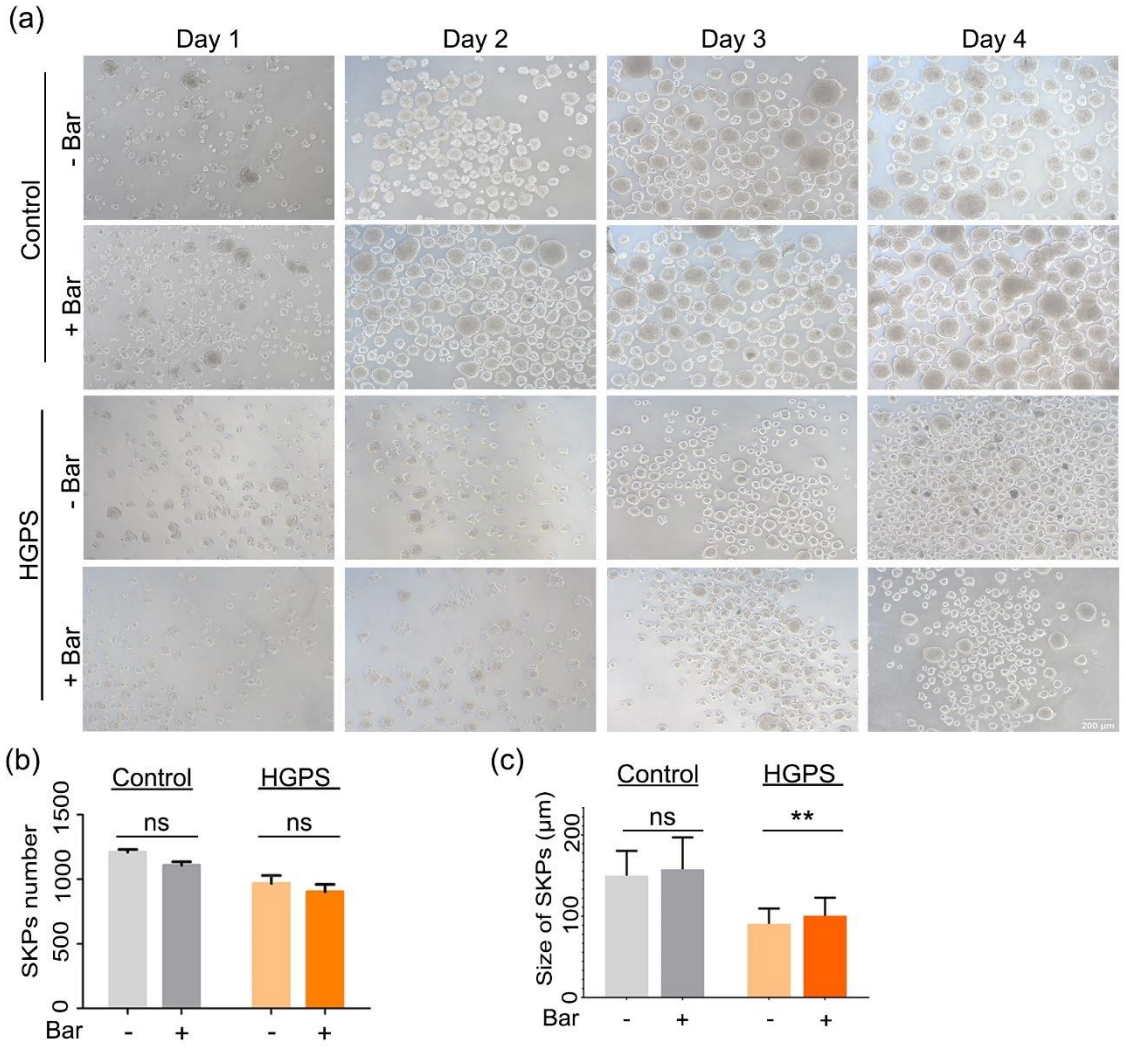

Figure 12. SKPs characterization after treatment with Baricitinib.

(**a**) SKPs isolation from control (GMO5567A) and HGPS (HGADFN127) fibroblasts after treatment with baricitinib (Bar). (**b**, **c**) Quantification of the number and average size of SKPs in control and HGPS groups with or without baricitinib treatment. Values are presented as mean ±SD (n=3), not significant (ns), * $p < 0.05$, ** $p < 0.01$, *** $p < 0.001$, (b, c) unpaired t-test.

The growth of the spheroids was monitored and the SKPs were then counted and analyzed at day 4. The spheroids from all the groups grew in number and size from day 1 till day 4 (Figure 12a). For control SKP, the average number of the spheroids decreased

from 1209 per flask in control without treatment (Control/-Bar) to 1108 spheroids per flask after treatment with Baricitinib for a period of 4 days (Figure 12b). Nevertheless, this decrease was not statistically significant. For the HGPS SKPs, the number of spheroids also decreased from 966 spheroids per flask in non-treated HGPS SKP to 903 spheroids per flask after treatment with Baricitinib (Figure 12b). Like control, this decrease was statistically insignificant.

The average size of the spheroids was obtained by quantifying at least the biggest 50 spheroids from each flask, from 3 different flasks and from 3 different experiments. The size of the control spheroids increased from 150 µm in the non-treated group to 158 µm in the Baricitinib treated group at day 4 of SKP formation (Figure 12c). This slight increase was not significant. Whereas for the HGPS SKPs, the size of the spheroids increased significantly from 91 µm in the non-treated groups to 101 µm in the treated ones (p value <0.01) (Figure 12c).

These findings indicate that the used 1 µm concentration of Baricitinib did not induce any cytotoxicity, nor significant changes in the formation of the SKPs during the 4 days of culture.

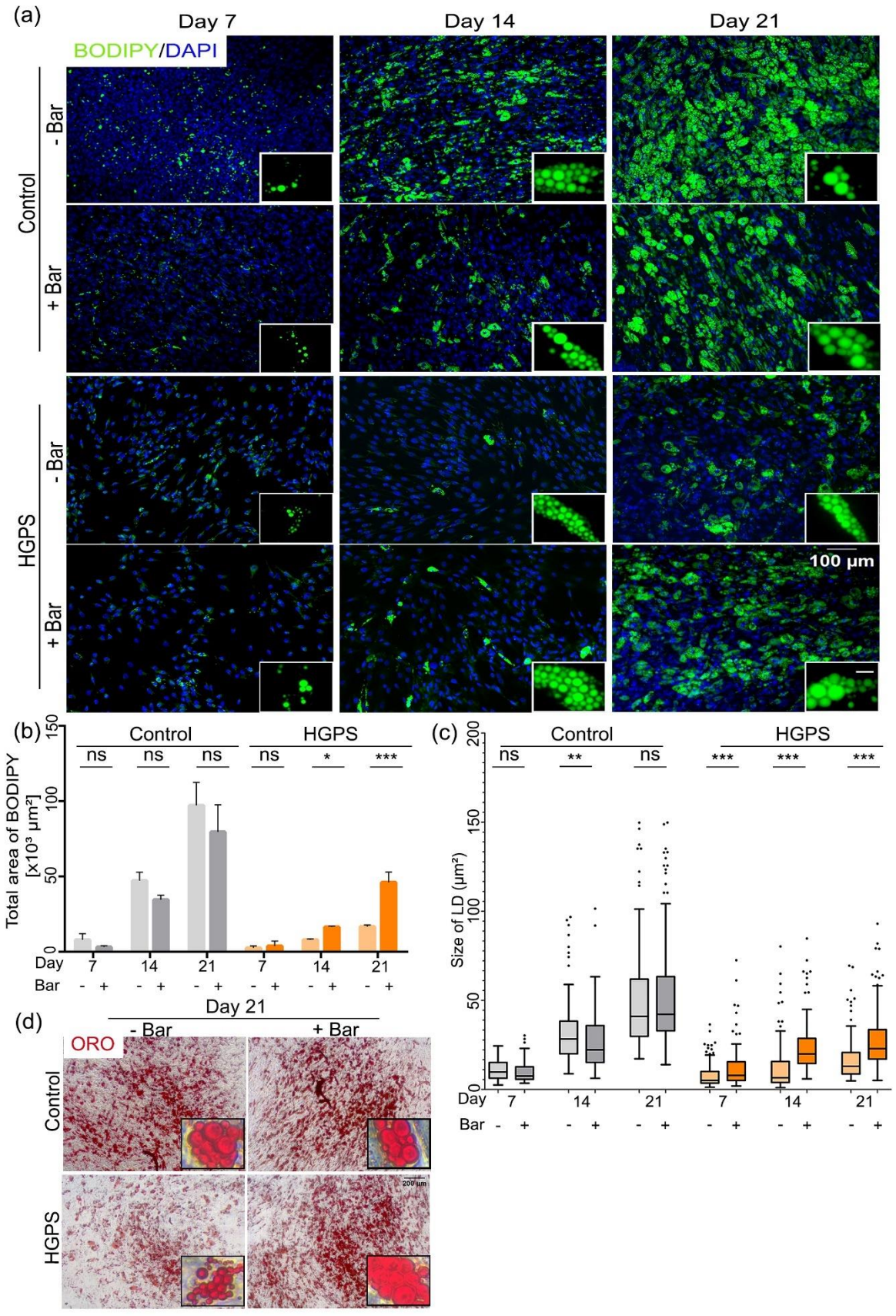
(a)
Day 7
Day 14
Day 21
BODIPY/DAPI
Control
- Bar
+ Bar
HGPS
- Bar
+ Bar
100 µm
(b)
Control
HGPS
ns
ns
ns
ns
*
***
Total area of BODIPY [x10³ µm²]
0
50
100
150
Day
7
14
21
7
14
21
Bar
- + - + - + - + - + - +
(c)
Control
HGPS
ns
**
ns
***
***
***
Size of LD (µm²)
0
50
100
150
200
Day
7
14
21
7
14
21
Bar
- + - + - + - + - + - +
(d)
Day 21
- Bar
+ Bar
ORO
Control
HGPS
200 µm

Figure 13. Improved differentiation of HGPS SKPs after treatment with Baricitinib.

(**a**) Bodipy staining of control (GMO5567A) and HGPS (HGADFN127) differentiated adipocytes after treatment with baricitinib. Scale bar: 100 µm / for the magnified images, scale bar: 20 µm. Cells were counterstained with DAPI. **(b, c**) Quantification of total area showing Bodipy signal and average size of lipid droplets (LD) at days 7, 14 and 21 of differentiation for both control and HGPS adipocytes. (**d**) ORO images at day 21 of differentiation for control and HGPS adipocytes. (**b**) Values are presented as mean ±SD (n=3), (**c**) In the Box and Whisker plot, the horizontal line crossing the box is the median, the bottom and top of the box are the lower and upper quartiles, the whiskers are the minimum and maximum values and the dots represent the outliers, not significant (ns), * $p < 0.05$, ** $p < 0.01$, *** $p < 0.001$, (b) two-way ANOVA with Tukey's multiple comparisons test, (**c**) unpaired t-test.

Second, we wanted to test the effect of Baricitinib treatment on the formation of adipocytes in control and HGPS SKPs (Figure 13). Here, we collected the spheroids at day 4 of SKP formation and the SKPs already treated with Baricitinib were also cultured in adipocyte differentiation media containing the drug. The formation of the lipid droplets was followed as usual for a period of 21 days and the vesicles were stained with Bodipy at 3 different time points: day 7,14 and 21 of differentiation (Figure 13a). The total area of Bodipy expression and the size of the lipid droplets were quantified at the previously mentioned time points (Figure 13b, c). The total area of Bodipy expression increased in control without Baricitinib treatment from 7951 μm^2 at day 7, to 47129 μm^2 at day 14, until reaching a value of 97150 μm^2 at day 21 of differentiation (Figure 13b). After treating the control group with Baricitinib, the total area of Bodipy expression decreased but in a non-significant way (Figure 13b). At day 7 of differentiation, Bodipy expression decreased from 7951 μm^2 in control without Baricitinib to 3125 μm^2 in control group with Baricitinib treatment (Figure 13b). The total area of Bodipy expression increased in the treated and

non-treated groups at day 14 due to the increase of the number and size of the lipid droplets (Figure 13b). At day 14 of differentiation, the average area of Bodipy expression decreased to 34523 μm^2 in control treated with Baricitinib, in a non-significant manner (Figure 13b). This value decreased also in a non-significant way in control treated with Baricitinib at day 21 of differentiation reaching 79563 μm^2 (Figure 13b). Next, we wanted to investigate the effect of Baricitinib treatment in HGPS SKPs. At day 7 of differentiation, the total area of Bodipy expression slightly increased from 2598 μm^2 to 3864 μm^2 in the Baricitinib treated HGPS SKPs (Figure 13b). This value of Bodipy expression significantly increased at day 14 of differentiation after Baricitinib treatment (*p* value <0.05), varying from 7912 μm^2 in the non-treated group to 16379 μm^2 in the treated one (2 times higher in the Baricitinib treated HGPS SKPs) (Figure 13b). At day 21 of differentiation, the total area of Bodipy expression significantly increased (*p* value <0.001) from 16748 μm^2 in the HGPS SKP not treated with Baricitinib compared to 42750 μm^2 in the treated group (Figure 13b). This increase was clearly visible after staining the samples with Bodipy (Figure 13a). The HGPS SKPs treated with Baricitinib clearly showed an increase in the levels of Bodipy expression in all the repetitions.

The size of the lipid droplets was also investigated again after staining with Bodipy at the 3 different time points: day 7, 14 and 21 of differentiation. In the control group, the average size of lipid droplets decreased from 9.7 μm^2 to 7.2 μm^2 after treatment with Baricitinib at day 7 of differentiation (Figure 13c). This decrease was also observed at day 14 of differentiation, with an average size ranging from 28.3 μm^2 in the non-treated control compared to 22 μm^2 in the Baricitinib treated group (Figure13). This decrease was significant with a *p* value < 0.01. At day 21 of differentiation, the average size of the lipid

droplets barely changed between the treated and non-treated control, reaching 40.7 μm^2 in the non-treated group compared to 42 μm^2 in the Baricitinib treated group (Figure 13c). Nevertheless, in HGPS differentiated SKPs, treatment with Baricitinib significantly increased the size of the lipid droplets at the 3 different time points (Figure 13c). At day 7 of differentiation, the size of the lipid droplets increased from 4.8 μm^2 in the non-treated HGPS differentiated adipocytes, to 7.83 μm^2 in the Baricitinib treated HGPS differentiated SKPs (*p* value < 0.001) (Figure 13c). A 3-time increase was observed at day 14 of differentiation in the Baricitinib treated HGPS SKPs, the size of the lipid droplets increased from 6.4 μm^2 in the non-treated group to 19.6 μm^2 after Baricitinib treatment (*p* value < 0.001) (Figure 13c). At day 21 of differentiation, the average size of the lipid droplets was also higher in the Baricitinib treated HGPS differentiated SKPs (22.7 μm^2) compared to the non-treated counterpart with a value of 12.8 μm^2 (*p* value < 0.001) (Figure 13c).

Finally, in order to double prove the effect of Baricitinib on the HGPS differentiated SKPs, we stained the lipid droplets at day 21 with another lipid dye, Oil Red O (Figure 13d). The differentiated adipocytes obtained from control SKPs did not show significant increase after treatment with Baricitinib as indicated by the red coloration (Figure 13d, Panel Control). Interestingly, Baricitinib treated HGPS SKPs showed a clear significant increase in the Oil Red O expression at day 21 of differentiation compared to the non-treated group (Figure 13d, Panel HGPS).

Altogether, these data indicates that Baricitinib treatment improved the adipogenic differentiation potential of the HGPS SKPs that started to be significant starting day 14 of

differentiation. This indicates that Baricitinib could be considered as a potential drug to improve adipogenesis in HGPS.

3.6. Expression of PPARγ and FABP4 in 3T3-L1 preadipocytes

To prove the presence of adipocytes in our cultures, we used two different adipocytes marker: peroxisome proliferator-activated receptor gamma (PPARγ) and fatty-acid-binding protein 4 (FABP4). First, we assessed the expression of these two markers in a well-established model of adipogenesis: 3T3-L1 preadipocytes. We chose this model since it was heavily studied in the literature in the field of adipogenesis (Green & Meuth, 1974).

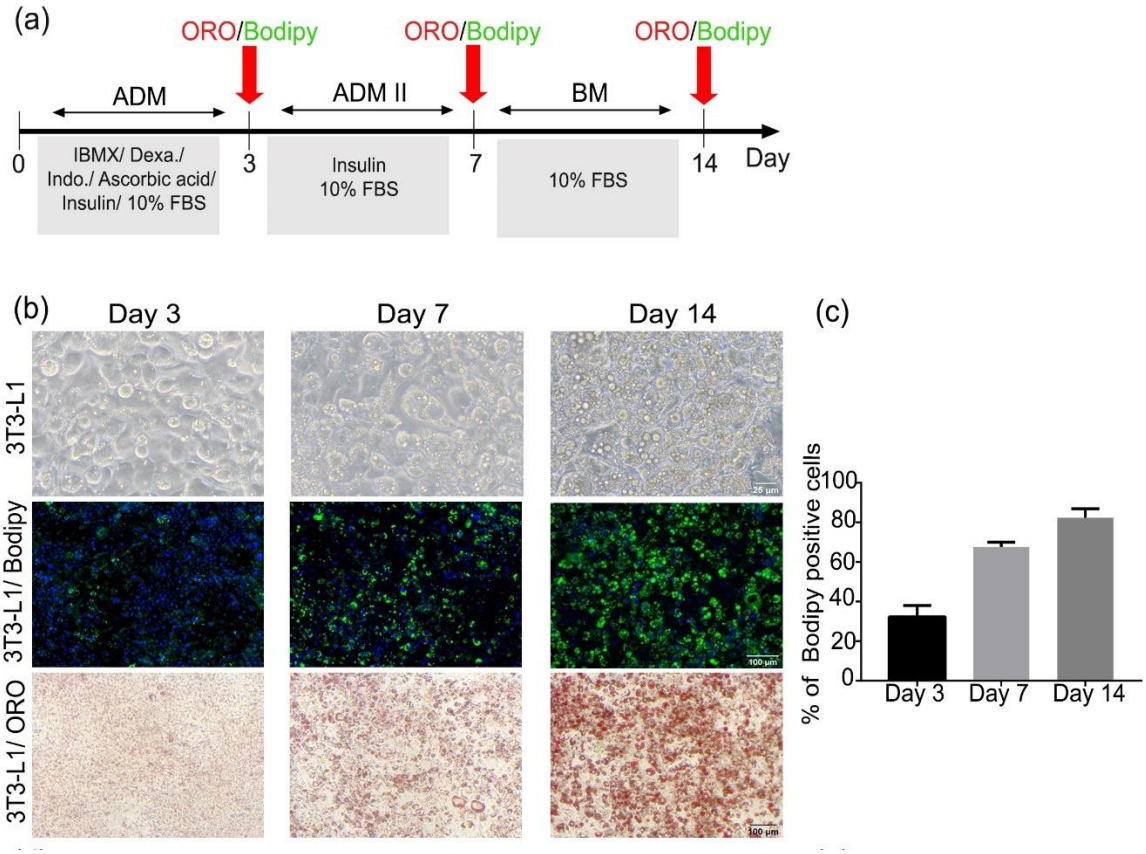

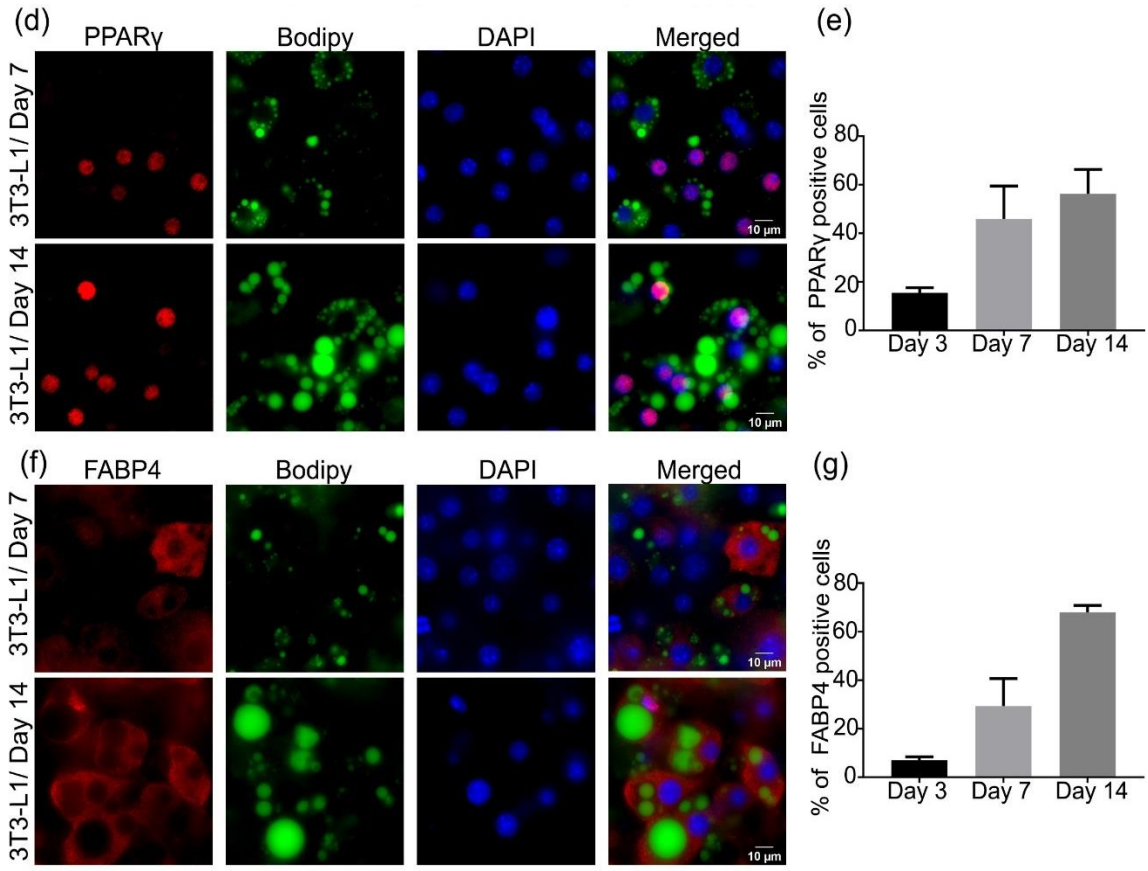

Figure 14. 3T3-L1 differentiation and expression of adipogenic markers.

(**a**) Panel showing the protocol for 3T3-L1 differentiation. After reaching confluency, 3T3-L1 cells were cultured for 3 days in adipocyte differentiation media (ADM) then switched to adipocyte differentiation media II (ADM II) containing only DMEM, insulin and 10% FBS. At day 7, the media was switched to basal media (BM) containing only DMEM and 10% FBS. BM was kept till day 14 of differentiation. At the three time points: day 3, day 7 and day 14, differentiated 3T3-L1 were fixed and stained with ORO and Bodipy. (**b**) First panel showing bright field microscopy images at day 3, 7 and 14 of 3T3-L1 adipogenic differentiation, scale bar: 25 µm. Second panel showing the differentiated 3T3-L1 after Bodipy 493/503 staining, scale bar: 100 µm and last panel after Oil red O (ORO) staining, scale bar: 100 µm. (**c**) Quantification of percentage of Bodipy expression in the 3T3-L1 differentiated cells. (**d**) Immunofluorescence showing co-expression of PPARγ and Bodipy 493/503 in 3T3-L1 at day 7 and 14 of differentiation. (**e**) Quantification of the percentage of PPARγ expression at day 7 and 14 of differentiation in 3T3-L1 cell line. (**f**) Immunofluorescence showing co-expression of FABP4 and Bodipy 493/503 in 3T3-L1 at day 7 and 14 of differentiation. Cells were counterstained with DAPI. (**g**) Quantification of percentage of FABP4 expression at

day 7 and 14 of adipogenic differentiation in 3T3-L1 cell line. IBMX: Isobutylmethylxanthine, Dexa: Dexamethasone, Indo.: Indomethacine, FBS: Fetal Bovine Serum.

We started first by optimizing the differentiation of the 3T3-L1 preadipocytes (Figure 14a, b). Briefly, the cells were collected and cultured in a 6-well plate on glass cover slips at a density of $2x10^5$ cells per well. After reaching confluency (Day 0), the normal media (Table 7) was switched to adipocyte differentiation media (ADM) (Table 15) containing DMEM, IBMX, dexamethasone, indomethacin, ascorbic acid, insulin, penicillin/streptomycin and 10% FBS. At day 3 of differentiation, the media was again switched to adipocyte differentiation media II containing only DMEM, insulin, penicillin/streptomycin and 10% FBS. The cells were kept in ADM II for a period of 4 days. At day 7 of differentiation, media was again switched to basal media containing DMEM, penicillin/streptomycin and 10% FBS, and this media was left till day 14 and was refreshed every second day. Staining with Bodipy and Oil Red O was performed at 3 different time points during the 14 days period of 3T3-L1 differentiation: day 3, 7 and 14 (Figure 14a, b). We first started by imaging the cells using an optic microscope at the 3 previously mentioned time points (Figure 14b / Panel 3T3-L1). Small lipid droplets started to appear at day 3 of differentiation and these vesicles grew in number and size till day 7, until becoming clearly visible and covering most of the area at day 21 (Figure 14b / Panel 3T3-L1). Staining with Bodipy and ORO was also performed at the three time points: day 3, 7 and 14 of differentiation (Figure 14b). To have an idea on the differentiation potential of the 3T3-L1, we quantified the expression of Bodipy by calculating the percentage of Bodipy positive cells. We counted a total of 1000 cells with the 40x objective from different areas within each cover slip and from a minimum of three different repetitions. The cells were

counterstained with DAPI, so first the whole number of cells from each area was counted manually and then we counted the cells with a positive Bodipy expression. At day 3 of differentiation, 32% of the 3T3-L1 showed positive Bodipy expression. This percentage increased to 68% at day 14 of differentiation, until reaching 82% at day 21 (Figure 14c). The increase in the lipid droplet accumulation was also double proven by Oil Red O staining (Figure 14b / Panel 3T3-L1/ORO). The intensity of the dye increased significantly from day 3 till day 14 of differentiation, showing high levels of differentiation at day 14 (Figure 14b / Panel 3T3-L1/ORO). These results are compatible with the results observed after Bodipy staining (Figure 14).

Next, we wanted to study the expression of two adipogenic markers, PPARγ and FABP4 in this model of 3T3-L1 preadipocytes. For that we performed immunofluorescence staining for each of these markers at day 7 and 14 of differentiation and we scored the levels of expression by calculating the percentage of positive cells compared to the total DAPI count (Figure 14d, e, f, g). FABP4 is a marker of mature adipocytes (Hotamisligil & Bernlohr, 2015), whereas PPARγ is an early marker of adipogenesis (Chawla, Schwarz, Dimaculangan, & Lazar, 1994; Tontonoz, Hu, Graves, Budavari, & Spiegelman, 1994). The expression of PPARγ increased from day 3 (15.5%) till day 7 (46%), while remaining high at day 14 (56%) (Figure 14d, e). For FABP4, the expression increased from 7% at day 3 to 30% at day 7 of differentiation (Figure 14f, g). At day 14, 68% of the cells were positive for FABP4 expression (Figure 14f, g).

3.7. PPARγ and FABP4 expression in control and HGPS differentiated adipocytes

After establishing the specificity and the expression of the two markers: PPARγ and FABP4 in the 3T3-L1 preadipocytes, we performed immunofluorescence staining of the two previously mentioned markers on the differentiated control and HGPS SKPs. We started with the immunofluorescence staining of PPARγ at day 7 and 14 of differentiation in both control (Figure 15a) and HGPS (Figure 15b) differentiated SKPs. The percentage of PPARγ was calculated by scoring the number of positive nuclei for PPARγ compared to the total DAPI count. At day 7 of differentiation, the percentage of PPARγ positive cells was 62.4% in control differentiated SKPs compared to 41% in HGPS differentiated SKPs at the same time point. This decrease in the percentage of PPARγ positive cells in HGPS differentiated SKPs is statistically significant with a p value < 0.01. At day 14 of differentiation, the value of PPARγ decreased in both conditions, reaching a value of 19.6% in control and 11.6% in HGPS differentiated adipocytes. This decrease at day 14 of differentiation in the percentage of PPARγ expression between control and HGPS differentiated adipocytes is however not significant (Figure 15c). Next, we studied the expression of FABP4, again at day 7 and 14 of differentiation in control and HGPS differentiated adipocytes (Figure 15d, e, f). The percentage of FABP4 positive cells increased significantly at day 14 in both control and HGPS differentiated SKPs (Figure 15f). Interestingly, the percentage of FABP4 expression at day 14 remained higher in control differentiated SKPs compared to their HGPS counterparts (Figure 15f).

Altogether, these results indicates that HGPS SKPs are capable of differentiating into mature adipocytes, as indicated by the positive FABP4 expression. Nevertheless, the

adipogenic differentiation of the HGPS SKPs remained lower compared to the control SKPs as shown by the lower expression of FABP4 at day 14 and PPARγ at day 7 in HGPS adipocytes.

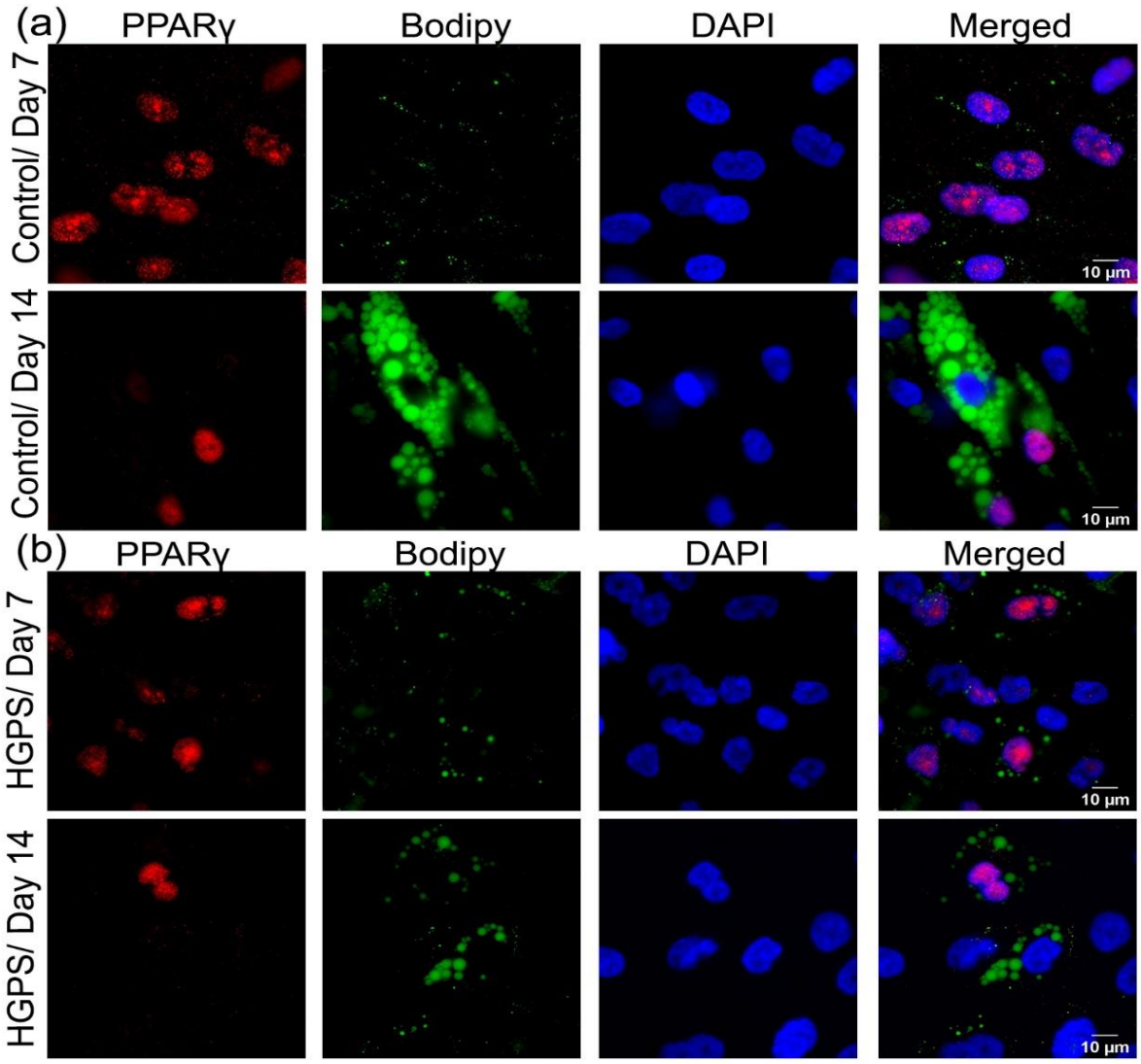

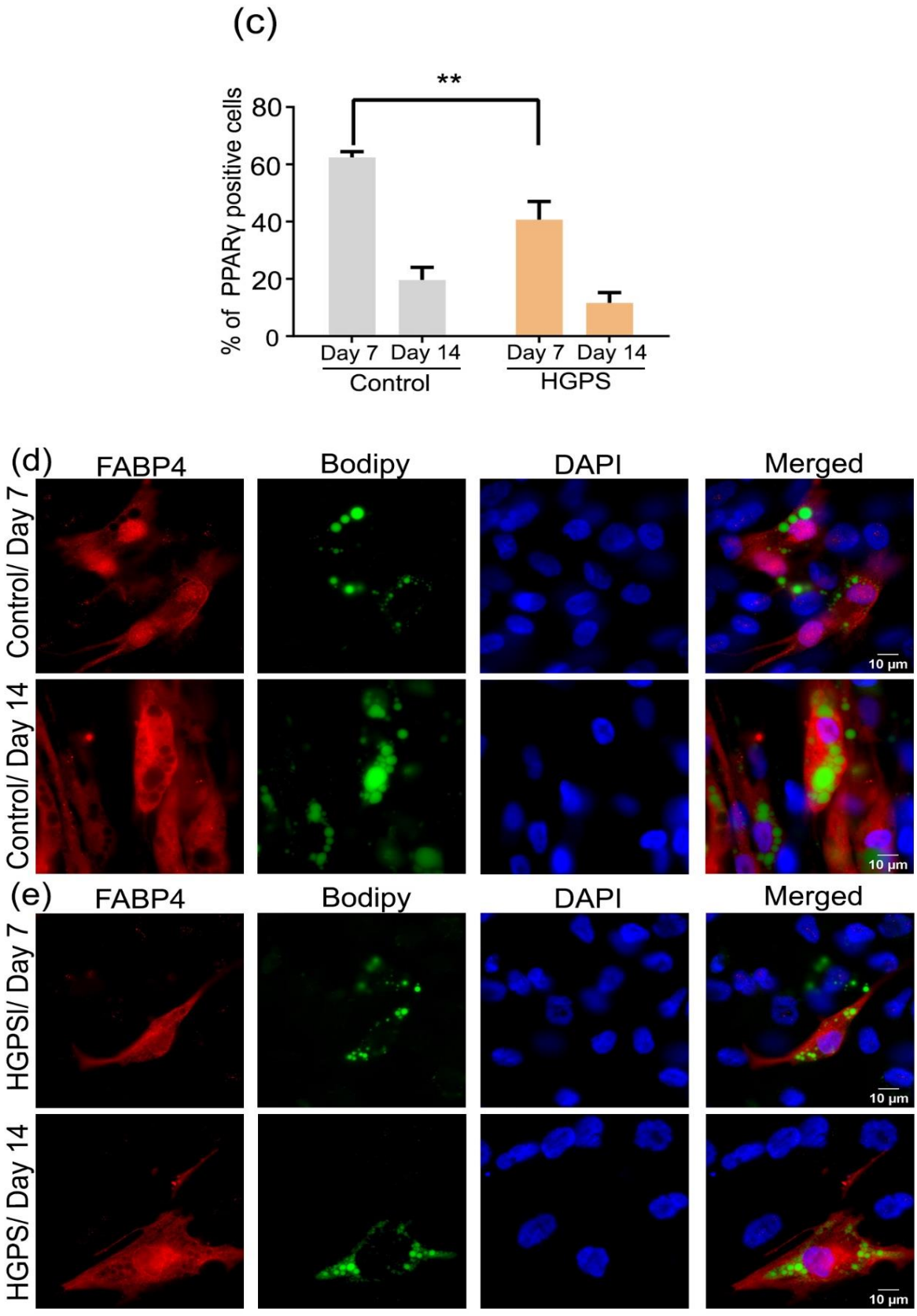
(c)
**
% of PPARγ positive cells
80
60
40
20
0
Day 7
Day 14
Day 7
Day 14
Control
HGPS
(d)
FABP4
Bodipy
DAPI
Merged
Control/ Day 7
Control/ Day 14
10 µm
(e)
FABP4
Bodipy
DAPI
Merged
HGPSI/ Day 7
HGPS/ Day 14
10 µm

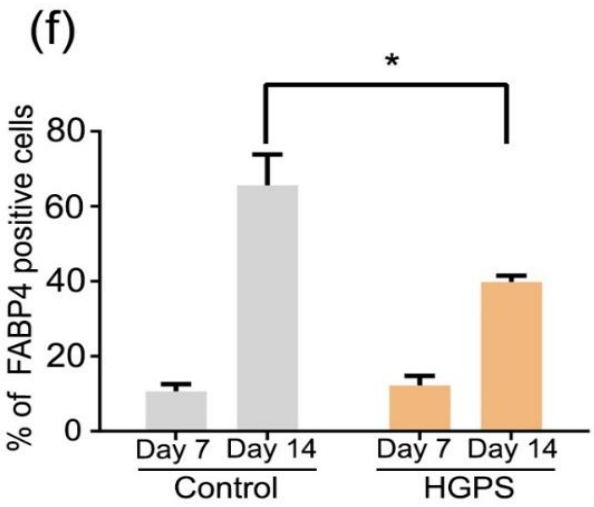

Figure 15. Expression of adipogenic markers in control and HGPS differentiated adipocytes.

(**a, b**) Immunofluorescence showing the dual PPARγ and Bodipy staining in control (GMO5567A) and HGPS (HGADFN127) adipocytes at days 7 and 14 of differentiation. (**c**) Quantification of the percentage of PPARγ positive cells at days 7 and 14 of differentiation in both control and HGPS differentiated SKPs (**d, e**) FABP4 and Bodipy staining in control (GMO5567A) and HGPS (HGADFN127) differentiated adipocytes at days 7 and 14. Scale bar: 10 µm. Cells were counterstained with DAPI. Values are presented as mean ± SD (n=3), * $p < 0.05$, ** $p < 0.01$, (c, f) two-way ANOVA with Tukey's multiple comparisons test.

3.8. Progerin accumulation and high senescence underlined defective adipogenesis in HGPS

To investigate whether senescence is the reason behind the reduced differentiation capacity observed in HGPS SKPs, we performed several immunofluorescences staining for progerin, Bodipy and IL-8 (Figure 16).

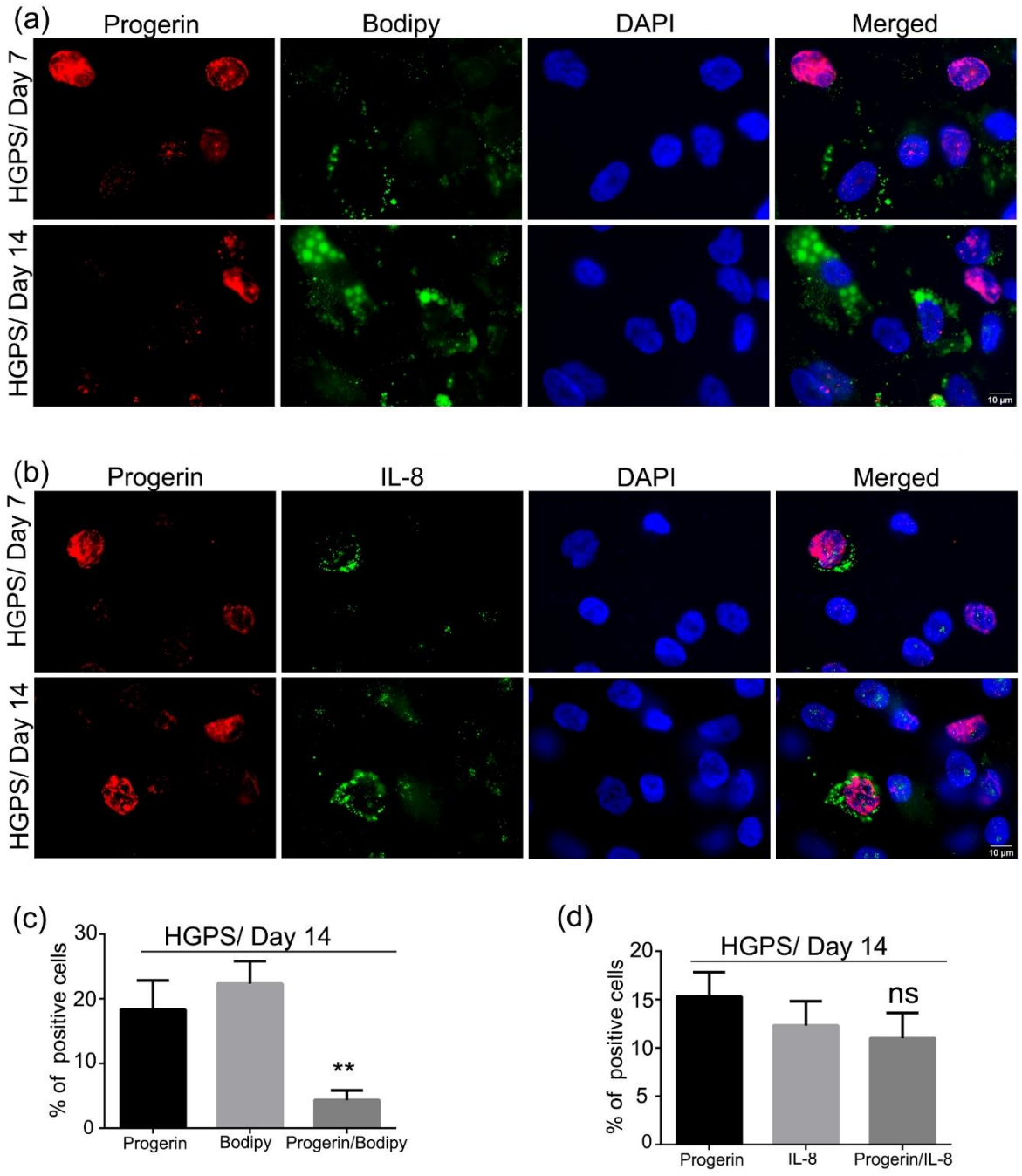

Figure 16. Co-expression of progerin with Bodipy and IL-8 in HGPS differentiated SKPs.

(**a**) Immunofluorescence staining for progerin and Bodipy at days 7 and 14 of adipogenesis in HGPS (HGADFN127). (**b**) Immunofluorescence staining for progerin and IL-8 at days 7 and 14 of adipogenesis in HGPS. Cells were counterstained with DAPI. (**c**) Percentage of positive nuclei expressing either progerin, Bodipy or both (progerin / Bodipy 493/503). (**d**) Percentage of

progerin-positive nuclei, IL-8-positive or progerin / IL-8-positive cells. Values are presented as mean ± SD (n=3), not significant (ns), * $p < 0.05$, ** $p < 0.01$, *** $p < 0.001$, (**c, d**) unpaired t-test.

We started with the co-staining of progerin and Bodipy at day 7 and 14 of differentiation in HGPS differentiated adipocytes (Figure 16a). We then scored the number of cells expressing either progerin alone, Bodipy alone or both markers at the same time (Figure 16c). We noticed that the cells with high progerin expression are negative for the Bodipy marker. The opposite is also true, cells with Bodipy expression barely or do not express progerin (Figure 16a, c). At day 14 of differentiation, almost 18% of the differentiated HGPS SKPs expressed high progerin levels, 22% were positive for Bodipy expression and the percentage of cells expressing both markers at the same time was 4.3% (Figure 16a, c). The low level of cell with double expression (progerin and Bodipy) means that the cells with progerin signal have negative or low Bodipy signal indicating that these cells are not capable of accumulating proper lipid droplets. Interestingly, cells who expressed both markers at the same time, showed low progerin signal. With high progerin expression, almost no cells were capable of expressing Bodipy at the same time.

Next, we performed a co-staining of progerin and the senescence marker: IL-8, again at day 7 and 14 of differentiation in HGPS adipocytes (Figure 16b). We noticed that the cells expressing progerin, also express IL-8 (Figure 16b). Following counting and quantification, we show that 15.3% of the differentiated HGPS adipocytes expressed high progerin levels at day 14 (Figure 16c). At the same time point, 12.3% of the differentiated adipocytes were positive for IL-8 (Figure 16c). The percentage of the cells expressing

both progerin and IL-8 at the same time was 11%, this indicates that majority of the cells with IL-8 expression were also positive for progerin (Figure 16c).

These data show that most of the cells expressing progerin also expressed the senescence marker IL-8 and therefor were senescent. Cells with high progerin levels, and consequently with IL-8 expression, could not differentiate into adipocytes and therefor were not capable of accumulating lipid droplets and expressing Bodipy signal. Altogether, we show that the impaired adipogenesis observed in HGPS SKPs could be linked to the increased accumulation of progerin, inducing premature senescence entry in these cells.

4. Discussion

Lipodystrophy is a major physiological feature in which HGPS patients suffer from. To date, how mutation in the *LMNA* gene is causing loss of fat in these patients is still unknown. This study highlights the effect of increased level of senescent cells on adipose tissue depletion observed in HGPS.

4.1 SKP spheroids from HGPS fibroblasts

The first goal we wanted to achieve in this study, was the collection of SKPs from HGPS fibroblasts. HGPS is a very rare disease, with a prevalence of approximately 1 in 20 million (Gordon et al., 1993), meaning that at any given time the number of children living with progeria worldwide does not exceed 350 patients. This low number of HGPS children made the collection of adipose tissue from the patients almost impossible. Not to mention, that the children suffer from lipodystrophy, so from the beginning they have very low or no adipose tissue.

Our group showed the possibility of collecting skin derived precursor stem cells (SKPs) from normal fibroblast cultures (collected from healthy individuals) and proved their ability to differentiate into adipocytes (Budel & Djabali, 2017). Here, we show that the collection of SKPs is also possible from fibroblasts obtained from HGPS patients, and that they are also capable of differentiating into adipocytes (Najdi, Kruger, & Djabali, 2021).

In this study, we used the senescence percentage to divide our HGPS and control fibroblast cultures instead of using the passage number. HGPS fibroblasts have shown to enter senescence faster than their control counterparts (C. Liu et al., 2019), therefor

using control and HGPS fibroblasts with the same passage number will not necessarily mean that they express the same senescence percentage. Control and HGPS fibroblast cultures were divided into young cultures expressing 5% senescence (using the SA-β-gal test) and old cultures with a senescence index of 30%.

Senescence and the chronic inflammatory milieu that it creates have shown to be implicated in stem cell depletion (Freund et al., 2010). Our data are in accordance with this finding, since in high senescence cultures, the number of SKPs collected was significantly lower compared to low senescence cultures in both control and HGPS fibroblasts (Figure 3).

Another parameter we quantified was the size of the obtained spheroids. Interestingly, SKPs collected from 30% senescent fibroblasts were bigger in size compared to the spheroids obtained from 5% senescent fibroblast cultures (Figure 3). Studies have shown that the diameter of a multicellular spheroid can be used as a parameter to examine hypoxia or necrosis (Barisam, Saidi, Kashaninejad, & Nguyen, 2018). In very large spheroids, the inner regions become necrotic due to the difficulty of oxygen and glucose diffusion to the core (Barisam et al., 2018). With an increased spheroid diameter, the hypoxic and necrotic zones in these spheroids become larger (Curcio et al., 2007). This explains the larger spheroid size obtained when collecting the SKPs from old fibroblast cultures, and can also explain the hindered differentiation capability in these spheroids.

4.2 Differentiation of SKPs into adipocytes

Next, we followed the differentiation of these SKPs from both control and HGPS fibroblasts with 5% and 30% senescence. We used the same protocol established by our

group (Budel & Djabali, 2017), consisting on letting the spheroids adhere overnight in adipocyte adherence media followed by adipocyte differentiation media for a period of 21 days. Here, we showed a delay in the initiation of adipogenesis and the appearance of lipid droplets in 30% senescence HGPS SKPs (Figure 4). The differentiation potential was significantly reduced in SKPs obtained from old fibroblast cultures in both control and HGPS compared to the SKPs obtained from young fibroblasts (Figure 4).

Although this technique led to proper adipocyte differentiation, it had one limitation. The complete spheroids were led to adhere and differentiate, therefor the exact number of spheroids added in each well will be hard to control. Meaning that, when we observe increased differentiation in a well, this could not necessarily reflect the differentiation potential of the spheroids, and could mean that we added a high number of spheroids in the first place.

In order to circumvent this problem, the spheroids were dissociated and the cell number was determined. Several optimization techniques were performed to identify the optimal seeding conditions for control and HGPS SKPs. In order to differentiate into adipocytes, it was mandatory that the dissociated SKPs are close to each other, forcing us to add a high number of cells in each well. Following this protocol, we show a hindered differentiation capability of HGPS SKPs compared to control also at 5% senescence (Figure 10 and 11).

Other studies using induced pluripotent stem cells (iPSCs) obtained from HGPS fibroblasts also showed lipid storage defect in HGPS compared to control (Xiong et al., 2013). The impaired differentiation observed was due to the suppression of late

adipogenic marker PPARγ2 and C/EBPα (Xiong et al., 2013). How progerin is interfering with the previously mentioned late adipogenic regulators is still unknown. Two possible explanations are suggested. One possibility is the direct interaction of progerin with an essential adipogenic gene causing perturbation in the transcription of downstream effectors. Another possibility is the interaction of progerin with an intermediate transcription factor such as, FOXQ1 (Candelario, Chen, Marjoram, Reddy, & Comai, 2012). Expression of FOXQ1 is activated in fibroblasts with accumulated progerin (Candelario et al., 2012). In addition, overactivation of FOXQ1 in normal fibroblasts showed the appearance of features similar to that observed in cells with progerin expression, suggesting a link between FOXQ1 and the cellular dysfunction caused by the truncated Lamin A (Candelario et al., 2012).

Induction of progerin in human mesenchymal stem cells (hMSCs) also showed a reduction in their adipogenic differentiation potentials (Scaffidi & Misteli, 2008). Several downstream effectors of the Notch pathway -implicated in the regulation of stem cell differentiation (Chiba, 2006)- are activated due to progerin expression (Scaffidi & Misteli, 2008). Activation of the Notch pathway in hMSCs reproduced the cellular abnormalities observed in progerin-expressing hMSCs, in particular impaired adipogenesis. On the other hand, inhibiting this pathway (by the Notch pathway inhibitor DAPT) in progerin-expressing hMSCs reversed the effect of progerin and induced adipocyte differentiation (Scaffidi & Misteli, 2008).

4.3 Senescence and adipogenesis

In the first part of this thesis, the collection of the SKPs from low and high senescence fibroblasts and their differentiation into adipocytes, we highlighted the negative effect that

senescence has on the spheroids´ collection and their differentiation. In this part, we wanted to determine whether during the SKP preparation, the cells entered into senescence faster and if this could further affect the differentiation process.

To determine the senescence level of the spheroids, we performed the SA-β-gal test directly on the SKPs. This technique did not show any success, since the dye remained trapped within the spheroids and it was not possible to quantify the SKPs with positive SA-β-gal expression (Figure 5). To circumvent this issue, the spheroids were dissociated and the SA-β-gal test was then performed (Figure 6). We also performed the senescence test on the initial fibroblast cultures on the day of SKP collection, in order to compare the change in the senescence percentage following the SKP protocol and the use of the slightly acidic buffer (HBSS). We proved that the pH-SKP protocol used to collect the spheroids increased the senescence rate of the SKPs, particularly in the case of HGPS (Figure 6).

The SKPs collected from HGPS fibroblasts showed increase in the senescence percentage compared to the SKPs collected from normal fibroblasts, as proven by the SA-β-gal test and the use of three different senescence markers: p21, p16INK4A (p16) and IL-8 (Figure 7, 8 and 9). This high accumulation of senescent cells, in the case of HGPS SKPs, could be the cause of the poor differentiation potential observed.

Treating the adipocytes obtained from HGPS SKPs with baricitinib, a JAK1/2 inhibitor, showed significant increase in adipogenesis and lipid vesicles formation (Figure 13). The JAK-STAT pathway plays important roles in several cellular functions including proliferation, differentiation and immune cell development (Harrison, 2012). It was shown

that this pathway is overactivated in replicative senescence (C. Liu et al., 2019). This overactivation creates a pro-inflammatory milieu due to the alteration of the cytokine balance (Fulop, Witkowski, Olivieri, & Larbi, 2018). Accumulation of senescent cells with aging and the secretion of the SASPs induce chronic inflammation, causing loss of function in the affected tissue (Campisi, 2013). Here, we show that the inflammation caused by the high number of senescent cells could be the reason behind the hindered differentiation observed in HGPS. Baricitinib is an FDA approved JAK 1/2 inhibitor used to treat rheumatoid arthritis (Al-Salama & Scott, 2018). A previous study from our group showed that the use of baricitinib could delay senescence in HGPS fibroblasts and reduce the expression of pro-inflammatory markers in these cells (C. Liu et al., 2019). Treating the SKPs with baricitinib did not show any cytotoxicity on sphere formation (Figure 12). The significant improve in adipogenesis observed in HGPS SKPs after treatment with baricitinib could be caused by the reduction of inflammation and the proinflammatory markers.

Aging is characterized by an increase in the expression of fat tissue inflammatory cytokines (Cartwright et al., 2010; Starr, Evers, & Saito, 2009) and the levels of circulating pro-inflammatory cytokines such as IL-6 and TNFα (Morin, Pagliassotti, Windmiller, & Eckel, 1997). It was shown that preadipocytes from old rats secret higher levels of TNFα compared to young rats (Tchkonia et al., 2007). In addition, the expression levels of IL-6 are higher in old compared to young rats (Cartwright et al., 2010). The impaired adipogenesis observed in these old rats, is due to the preadipocytes and the cytokines they secrete. Potentially causing age related lipodystrophy and metabolic dysfunction (Tchkonia et al., 2007).

Mice that are hypomorphic for the gene *BubR1*- gene implicated in the mitotic checkpoint- have shown symptoms of accelerated aging (Baker et al., 2004). In these hypomorphic BubR1 mice, the adipose tissue showed increased SA-β-gal activity and $p16^{Ink4a}$ expression (Baker et al., 2006). Inactivating $p16^{Ink4a}$ in the previously mentioned mice, reduced senescence and premature aging (Baker et al., 2008).

In addition, eliminating $p16^{Ink4a}$ positive senescent cells in INK-ATTAC mouse model prevented lipodystrophy (Baker et al., 2011). Xu et al. showed that activin A secreted by human senescent fat progenitors acts on inhibiting adipogenesis in healthy progenitors (Xu et al., 2015). Blocking activin A expression improved adipogenesis and lipid accumulation in progenitors exposed to senescent cells (Xu et al., 2015). Treatment with Ruxolitinib, an FDA-approved JAK1/2 inhibitor, significantly reduced the level of activin A, rescued adipogenesis and improved metabolic function in old mice (Xu et al., 2015).

4.4 Adipogenic markers' expression in HGPS

With aging, several changes occur to preadipocyte function including reduced adipogenesis (Karagiannides et al., 2001; Karagiannides et al., 2006; Kirkland, Hollenberg, & Gillon, 1990) and increase in the level of pro-inflammatory cytokines and chemokines (Cartwright et al., 2010; Tchkonia et al., 2007). Interestingly, the expression of adipogenic markers PPARγ and C/EBPα was lower in preadipocytes obtained from old individuals (Karagiannides et al., 2001; Schipper, Marra, Zhang, Donnenberg, & Rubin, 2008). In HGPS, studies on iPSCs showed that the presence of progerin inhibited the activation of PPARγ and C/EBPα (Xiong et al., 2013). This is in accordance with our data, where we show a higher expression of PPARγ in adipocytes differentiated from control SKPs compared to the ones obtained from HGPS SKPs (Figure 14).

Inducing C/EBPα overexpression, improved lipid accumulation in preadipocytes in elderly people (Karagiannides et al., 2006; Tchkonia et al., 2007). In addition, reduction in the level of these master regulators of adipogenesis causes a decline in insulin responsiveness (El-Jack, Hamm, Pilch, & Farmer, 1999), a feature that can be observed in HGPS patients (Rosenbloom, Karacan, & DeBusk, 1970; Villee, Nichols, & Talbot, 1969).

Therapeutical interventions targeting the expression of these adipogenic markers can be an important insight in rescuing fat loss in HGPS patients.

4.5 Ectopic fat deposition and alteration of endocrine proteins in HGPS

In elderly, the storage of fat in subcutaneous depots starts to decrease and the fat starts to accumulate in ectopic sites including liver, bone marrow and muscle (Garg & Agarwal, 2009). Similar to that in aging, in lipodystrophic syndrome, dysfunction of the white adipose tissue also induces accumulation of fat in ectopic regions. This ectopic accumulation, also observed in HGPS (Olive et al., 2010) causes metabolic syndromes associated with cardiovascular diseases, inflammation and mortality (Koster et al., 2010; Morley, 2004).

Loss of adipose tissue observed in HGPS causes the alteration of several signaling markers and endocrine proteins (Kreienkamp & Gonzalo, 2020). Patients with HGPS express low levels of leptin (Gordon et al., 2018), a hormone secreted by the adipose tissue. Low levels of leptin are associated with reduced immunity and can also be linked to cardiovascular diseases (Koh et al., 2008; Piemonti et al., 2003). Another endocrine

protein altered in HGPS is adiponectin. Adiponectin plays several important roles in lipid metabolism and insulin sensitivity (Nguyen, 2020). Reduced levels of adiponectin may contribute to the accelerated atherosclerosis in patients with HGPS (Gordon, Harten, Patti, & Lichtenstein, 2005). Gordon et al. showed that the expression levels of some of these endocrine proteins can be corrected after treatment with FTI (Gordon et al., 2018). Nevertheless, many endocrine proteins remained altered even after treatment with FTI, suggesting the importance of testing combination therapies.

5. Conclusion

Loss of fat in HGPS children causes several systemic effects on the macroscopic and the microscopic levels. This study highlights the role of senescence on the impaired adipogenic capabilities observed in HGPS. Accumulation of senescent cells before and during adipogenesis decreased the differentiation potentials of HGPS SKPs. With aging, accumulation of senescent cells in the adipose tissue can contribute to fat tissue inflammation and metabolic dysfunction. The SASPs produced by the senescent cells are capable of spreading cellular senescence locally and systematically. Therefore, senescent cells and the SASPs they secret constitute a logical target for therapeutical intervention in normal and accelerated aging. Treatment with Baricitinib reduced the chronic inflammation caused by the increased number of senescent cells and improved adipogenesis in HGPS SKPs. Further research should be performed to study the effect of this drug on fat in HGPS mouse models.

Moreover, in our study we were able to optimize a disease model allowing the study of adipogenesis in HGPS *in vitro* using fibroblasts. This model can be used for further analysis on adipogenesis and the loss of fat in HGPS, alongside testing other possible therapeutical interventions.

The implication of senescence in age-related adipose tissue inflammation and metabolic dysfunction, makes it an interesting target for intervention in both normal aging and HGPS.

6. Appendix

6.1. List of Abbreviations

ADM	adipocyte differentiation medium
AFC	N-acetyl-S-farnesyl-cysteine
AP2	APETALA2
ATP	Adenosine triphosphate
ATRA	all-trans retinoic acid
Bar	Baricitinib
BAT	Brown adipose tissue
bFGF	basis fibroblast growth factor
BM	basal medium
BMP2	bone morphogenetic protein 2
BMP4	bone morphogenetic protein 4
BubR1	budding uninhibited by benzimidazole-related 1
C/EBP	CCAAT-enhancer-binding proteins
CAAX	Cysteine, Aliphatic Amino acid, any amino acid (X)
CGL	congenital generalized lipodystrophies
CRISPR/Cas	Clustered Regularly Interspaced Short Palindromic Repeats/Cas protein
CSIM	cysteine, serine, isoleucine, and methionine
DAPI	4,6-diamidino-2-phenylindole
Dexa	Dexamethasone
DMEM	Dulbecco's Modified Eagle Medium
DMSO	Dimethyl sulfoxide

DNA	deoxyribonucleic acid
DSBs	double strand breaks
ECG	Electrocardiogram
EDTA	ethylenediaminetetraacetic acid
EGF	epidermal growth factor
EtOH	Ethanol absolute
FABP4	fatty acid binding protein 4
FBS	Fetal Bovine Serum
FDA	Food and Drug Administration
FOXQ1	Forkhead box Q1
FPLD	familial partial lipodystrophies
FTI	farnesyltransferase inhibitor
FTI	farnesyltransferase inhibitor
HBSS	Hank's balanced salt solution
HGPS	Hutchinson-Gilford progeria syndrome
hMSCs	Human mesenchymal stem cells
IBMX	3-Isobutyl-1-methylxanthin
ICMT	Isoprenylcysteine carboxyl methyltransferase
IgG	Immunoglobulin G
IL-8	Interleukin 8
Indo	Indomethacin
iPSCs	induced pluripotent stem cells
JAK-STAT	Janus kinase-signal transducer and activator of transcription
kDa	kilo Dalton
LD	lipid droplets
LMNA	gene expressing Lamin A and Lamin C
LMNB	gene expressing Lamin Lamin B1 and B2
MG132	
min	minute

mRNA	messenger ribonucleic acid
MSCs	mesenchymal stem cells
mTOR	mammalian target of rapamycin
NAC	N-acetyl cysteine
NF-κB	nuclear factor kappa-light-chain-enhancer of activated B cells
NG2	nerve/glial antigen 2
ns	not significant
ORO	Oil Red O
p16INK4A	cyclin-dependent kinase inhibitor 2A
p21	cyclin-dependent kinase inhibitor 1
PBS	phosphate-buffered saline
Pen/Strep	Penicillin/streptomycin
PFA	Paraformaldehyde
pH-SKP	low pH isolated skin-derived precursor cells
PPARγ	Peroxisome proliferator- activated receptor gamma
Rac1b	Ras-related C3 botulinum toxin substrate 1
RNA	Ribonucleic acid
ROCK	rho-associated protein kinase
ROS	Reactive Oxygen Species
RT	room temperature
SASPs	Senescence-associated secretory phenotypes
SA-β-gal	Senescence-associated Beta-galactosidase
SD	standard deviation
SFN	Sulforaphane
sh	short hairpin

SIM	serine, isoleucine, and methionine
SKP	skin-derived Precursor
SMAD1	Suppressor of Mothers against Decapentaplegic
SNS	senescence
SRSF-1	Serine/Arginine-Rich Splicing Factor 1
TNF alpha	Tumor Necrosis Factor alpha
WAT	white adipose tissue
ZMPSTE24	zinc metallopeptidase STE24 homolog

6.2. List of Tables

6.3. List of Images

7. References

Acosta, J. C., Banito, A., Wuestefeld, T., Georgilis, A., Janich, P., Morton, J. P., . . . Gil, J. (2013). A complex secretory program orchestrated by the inflammasome controls paracrine senescence. *Nat Cell Biol, 15*(8), 978-990. doi:10.1038/ncb2784

Acosta, J. C., O'Loghlen, A., Banito, A., Guijarro, M. V., Augert, A., Raguz, S., . . . Gil, J. (2008). Chemokine signaling via the CXCR2 receptor reinforces senescence. *Cell, 133*(6), 1006-1018. doi:10.1016/j.cell.2008.03.038

Adler, A. S., Sinha, S., Kawahara, T. L., Zhang, J. Y., Segal, E., & Chang, H. Y. (2007). Motif module map reveals enforcement of aging by continual NF-kappaB activity. *Genes Dev, 21*(24), 3244-3257. doi:10.1101/gad.1588507

Agarwal, A. K., & Garg, A. (2006). Genetic disorders of adipose tissue development, differentiation, and death. *Annu Rev Genomics Hum Genet, 7*, 175-199. doi:10.1146/annurev.genom.7.080505.115715

Al-Salama, Z. T., & Scott, L. J. (2018). Baricitinib: A Review in Rheumatoid Arthritis. *Drugs, 78*(7), 761-772. doi:10.1007/s40265-018-0908-4

Avilion, A. A., Nicolis, S. K., Pevny, L. H., Perez, L., Vivian, N., & Lovell-Badge, R. (2003). Multipotent cell lineages in early mouse development depend on SOX2 function. *Genes Dev, 17*(1), 126-140. doi:10.1101/gad.224503

Baker, D. J., Jeganathan, K. B., Cameron, J. D., Thompson, M., Juneja, S., Kopecka, A., . . . van Deursen, J. M. (2004). BubR1 insufficiency causes early onset of aging-associated phenotypes and infertility in mice. *Nat Genet, 36*(7), 744-749. doi:10.1038/ng1382

Baker, D. J., Jeganathan, K. B., Malureanu, L., Perez-Terzic, C., Terzic, A., & van Deursen, J. M. (2006). Early aging-associated phenotypes in Bub3/Rae1 haploinsufficient mice. *J Cell Biol, 172*(4), 529-540. doi:10.1083/jcb.200507081

Baker, D. J., Perez-Terzic, C., Jin, F., Pitel, K. S., Niederlander, N. J., Jeganathan, K., . . . van Deursen, J. M. (2008). Opposing roles for p16Ink4a and p19Arf in senescence and ageing caused by BubR1 insufficiency. *Nat Cell Biol, 10*(7), 825-836. doi:10.1038/ncb1744

Baker, D. J., Wijshake, T., Tchkonia, T., LeBrasseur, N. K., Childs, B. G., van de Sluis, B., . . . van Deursen, J. M. (2011). Clearance of p16Ink4a-positive senescent cells delays ageing-associated disorders. *Nature, 479*(7372), 232-236. doi:10.1038/nature10600

Barisam, M., Saidi, M. S., Kashaninejad, N., & Nguyen, N. T. (2018). Prediction of Necrotic Core and Hypoxic Zone of Multicellular Spheroids in a Microbioreactor with a U-Shaped Barrier. *Micromachines (Basel), 9*(3). doi:10.3390/mi9030094

Barrowman, J., Hamblet, C., George, C. M., & Michaelis, S. (2008). Analysis of prelamin A biogenesis reveals the nucleus to be a CaaX processing compartment. *Mol Biol Cell, 19*(12), 5398-5408. doi:10.1091/mbc.E08-07-0704

Basso, A. D., Kirschmeier, P., & Bishop, W. R. (2006). Lipid posttranslational modifications. Farnesyl transferase inhibitors. *J Lipid Res, 47*(1), 15-31. doi:10.1194/jlr.R500012-JLR200

Beausejour, C. M., Krtolica, A., Galimi, F., Narita, M., Lowe, S. W., Yaswen, P., & Campisi, J. (2003). Reversal of human cellular senescence: roles of the p53 and p16 pathways. *EMBO J, 22*(16), 4212-4222. doi:10.1093/emboj/cdg417

Beck, L. A., Hosick, T. J., & Sinensky, M. (1990). Isoprenylation is required for the processing of the lamin A precursor. *J Cell Biol, 110*(5), 1489-1499. doi:10.1083/jcb.110.5.1489

Bergo, M. O., Gavino, B., Ross, J., Schmidt, W. K., Hong, C., Kendall, L. V., . . . Young, S. G. (2002). Zmpste24 deficiency in mice causes spontaneous bone fractures, muscle weakness, and a prelamin A processing defect. *Proc Natl Acad Sci U S A, 99*(20), 13049-13054. doi:10.1073/pnas.192460799

Beyret, E., Liao, H. K., Yamamoto, M., Hernandez-Benitez, R., Fu, Y., Erikson, G., . . . Izpisua Belmonte, J. C. (2019). Single-dose CRISPR-Cas9 therapy extends lifespan of mice with Hutchinson-Gilford progeria syndrome. *Nat Med, 25*(3), 419-422. doi:10.1038/s41591-019-0343-4

Bowers, R. R., Kim, J. W., Otto, T. C., & Lane, M. D. (2006). Stable stem cell commitment to the adipocyte lineage by inhibition of DNA methylation: role of the BMP-4 gene. *Proc Natl Acad Sci U S A, 103*(35), 13022-13027. doi:10.1073/pnas.0605789103

Boyartchuk, V. L., Ashby, M. N., & Rine, J. (1997). Modulation of Ras and a-factor function by carboxyl-terminal proteolysis. *Science, 275*(5307), 1796-1800. doi:10.1126/science.275.5307.1796

Budel, L., & Djabali, K. (2017). Rapid isolation and expansion of skin-derived precursor cells from human primary fibroblast cultures. *Biol Open, 6*(11), 1745-1755. doi:10.1242/bio.025130

Campisi, J. (2013). Aging, cellular senescence, and cancer. *Annu Rev Physiol, 75*, 685-705. doi:10.1146/annurev-physiol-030212-183653

Candelario, J., Chen, L. Y., Marjoram, P., Reddy, S., & Comai, L. (2012). A filtering strategy identifies FOXQ1 as a potential effector of lamin A dysfunction. *Aging (Albany NY), 4*(8), 567-577. doi:10.18632/aging.100483

Cao, H., & Hegele, R. A. (2000). Nuclear lamin A/C R482Q mutation in canadian kindreds with Dunnigan-type familial partial lipodystrophy. *Hum Mol Genet, 9*(1), 109-112. doi:10.1093/hmg/9.1.109

Cao, H., & Hegele, R. A. (2003). LMNA is mutated in Hutchinson-Gilford progeria (MIM 176670) but not in Wiedemann-Rautenstrauch progeroid syndrome (MIM 264090). *J Hum Genet, 48*(5), 271-274. doi:10.1007/s10038-003-0025-3

Cao, K., Graziotto, J. J., Blair, C. D., Mazzulli, J. R., Erdos, M. R., Krainc, D., & Collins, F. S. (2011). Rapamycin reverses cellular phenotypes and enhances mutant protein clearance in Hutchinson-Gilford progeria syndrome cells. *Sci Transl Med, 3*(89), 89ra58. doi:10.1126/scitranslmed.3002346

Capell, B. C., Erdos, M. R., Madigan, J. P., Fiordalisi, J. J., Varga, R., Conneely, K. N., . . . Collins, F. S. (2005). Inhibiting farnesylation of progerin prevents the characteristic nuclear blebbing of Hutchinson-Gilford progeria syndrome. *Proc Natl Acad Sci U S A, 102*(36), 12879-12884. doi:10.1073/pnas.0506001102

Capell, B. C., Olive, M., Erdos, M. R., Cao, K., Faddah, D. A., Tavarez, U. L., . . . Collins, F. S. (2008). A farnesyltransferase inhibitor prevents both the onset and late progression of cardiovascular disease in a progeria mouse model. *Proc Natl Acad Sci U S A, 105*(41), 15902-15907. doi:10.1073/pnas.0807840105

Cartwright, M. J., Schlauch, K., Lenburg, M. E., Tchkonia, T., Pirtskhalava, T., Cartwright, A., . . . Kirkland, J. L. (2010). Aging, depot origin, and preadipocyte gene expression. *J Gerontol A Biol Sci Med Sci, 65*(3), 242-251. doi:10.1093/gerona/glp213

Charlesworth, C. T., Deshpande, P. S., Dever, D. P., Camarena, J., Lemgart, V. T., Cromer, M. K., . . . Porteus, M. H. (2019). Identification of preexisting adaptive immunity to Cas9 proteins in humans. *Nat Med, 25*(2), 249-254. doi:10.1038/s41591-018-0326-x

Chawla, A., Schwarz, E. J., Dimaculangan, D. D., & Lazar, M. A. (1994). Peroxisome proliferator-activated receptor (PPAR) gamma: adipose-predominant expression and induction early in adipocyte differentiation. *Endocrinology, 135*(2), 798-800. doi:10.1210/endo.135.2.8033830

Chiba, S. (2006). Notch signaling in stem cell systems. *Stem Cells, 24*(11), 2437-2447. doi:10.1634/stemcells.2005-0661

Cho, H. J., Park, J., Lee, H. W., Lee, Y. S., & Kim, J. B. (2004). Regulation of adipocyte differentiation and insulin action with rapamycin. *Biochem Biophys Res Commun, 321*(4), 942-948. doi:10.1016/j.bbrc.2004.07.050

Chueh, S. C., & Kahan, B. D. (2005). Clinical application of sirolimus in renal transplantation: an update. *Transpl Int, 18*(3), 261-277. doi:10.1111/j.1432-2277.2004.00039.x

Cinti, S. (2005). The adipose organ. *Prostaglandins Leukot Essent Fatty Acids, 73*(1), 9-15. doi:10.1016/j.plefa.2005.04.010

Constantinescu, D., Csoka, A. B., Navara, C. S., & Schatten, G. P. (2010). Defective DSB repair correlates with abnormal nuclear morphology and is improved with FTI treatment in Hutchinson-Gilford progeria syndrome fibroblasts. *Exp Cell Res, 316*(17), 2747-2759. doi:10.1016/j.yexcr.2010.05.015

Coppe, J. P., Patil, C. K., Rodier, F., Sun, Y., Munoz, D. P., Goldstein, J., . . . Campisi, J. (2008). Senescence-associated secretory phenotypes reveal cell-nonautonomous functions of oncogenic RAS and the p53 tumor suppressor. *PLoS Biol, 6*(12), 2853-2868. doi:10.1371/journal.pbio.0060301

Crane, G. M., Jeffery, E., & Morrison, S. J. (2017). Adult haematopoietic stem cell niches. *Nat Rev Immunol, 17*(9), 573-590. doi:10.1038/nri.2017.53

Cristancho, A. G., & Lazar, M. A. (2011). Forming functional fat: a growing understanding of adipocyte differentiation. *Nat Rev Mol Cell Biol, 12*(11), 722-734. doi:10.1038/nrm3198

Csoka, A. B., English, S. B., Simkevich, C. P., Ginzinger, D. G., Butte, A. J., Schatten, G. P., . . . Sedivy, J. M. (2004). Genome-scale expression profiling of Hutchinson-Gilford progeria syndrome reveals widespread transcriptional misregulation leading to mesodermal/mesenchymal defects and accelerated atherosclerosis. *Aging Cell, 3*(4), 235-243. doi:10.1111/j.1474-9728.2004.00105.x

Curcio, E., Salerno, S., Barbieri, G., De Bartolo, L., Drioli, E., & Bader, A. (2007). Mass transfer and metabolic reactions in hepatocyte spheroids cultured in rotating wall gas-permeable membrane system. *Biomaterials, 28*(36), 5487-5497. doi:10.1016/j.biomaterials.2007.08.033

Dai, Q., Choy, E., Chiu, V., Romano, J., Slivka, S. R., Steitz, S. A., . . . Philips, M. R. (1998). Mammalian prenylcysteine carboxyl methyltransferase is in the endoplasmic reticulum. *J Biol Chem, 273*(24), 15030-15034. doi:10.1074/jbc.273.24.15030

De Kock, J., Vanhaecke, T., Biernaskie, J., Rogiers, V., & Snykers, S. (2009). Characterization and hepatic differentiation of skin-derived precursors from adult foreskin by sequential

exposure to hepatogenic cytokines and growth factors reflecting liver development. *Toxicol In Vitro, 23*(8), 1522-1527. doi:10.1016/j.tiv.2009.08.014

De Sandre-Giovannoli, A., Bernard, R., Cau, P., Navarro, C., Amiel, J., Boccaccio, I., . . . Levy, N. (2003). Lamin a truncation in Hutchinson-Gilford progeria. *Science, 300*(5628), 2055. doi:10.1126/science.1084125

DeBusk, F. L. (1972). The Hutchinson-Gilford progeria syndrome. Report of 4 cases and review of the literature. *J Pediatr, 80*(4), 697-724. doi:10.1016/s0022-3476(72)80229-4

Delbarre, E., Tramier, M., Coppey-Moisan, M., Gaillard, C., Courvalin, J. C., & Buendia, B. (2006). The truncated prelamin A in Hutchinson-Gilford progeria syndrome alters segregation of A-type and B-type lamin homopolymers. *Hum Mol Genet, 15*(7), 1113-1122. doi:10.1093/hmg/ddl026

Dimri, G. P., Lee, X., Basile, G., Acosta, M., Scott, G., Roskelley, C., . . . et al. (1995). A biomarker that identifies senescent human cells in culture and in aging skin in vivo. *Proc Natl Acad Sci U S A, 92*(20), 9363-9367. doi:10.1073/pnas.92.20.9363

Doudna, J. A., & Charpentier, E. (2014). Genome editing. The new frontier of genome engineering with CRISPR-Cas9. *Science, 346*(6213), 1258096. doi:10.1126/science.1258096

Egesipe, A. L., Blondel, S., Lo Cicero, A., Jaskowiak, A. L., Navarro, C., Sandre-Giovannoli, A., . . . Nissan, X. (2016). Metformin decreases progerin expression and alleviates pathological defects of Hutchinson-Gilford progeria syndrome cells. *NPJ Aging Mech Dis, 2*, 16026. doi:10.1038/npjamd.2016.26

El-Jack, A. K., Hamm, J. K., Pilch, P. F., & Farmer, S. R. (1999). Reconstitution of insulin-sensitive glucose transport in fibroblasts requires expression of both PPARgamma and C/EBPalpha. *J Biol Chem, 274*(12), 7946-7951. doi:10.1074/jbc.274.12.7946

Eriksson, M., Brown, W. T., Gordon, L. B., Glynn, M. W., Singer, J., Scott, L., . . . Collins, F. S. (2003). Recurrent de novo point mutations in lamin A cause Hutchinson-Gilford progeria syndrome. *Nature, 423*(6937), 293-298. doi:10.1038/nature01629

Evan, G. I., & d'Adda di Fagagna, F. (2009). Cellular senescence: hot or what? *Curr Opin Genet Dev, 19*(1), 25-31. doi:10.1016/j.gde.2008.11.009

Fernandes, K. J., McKenzie, I. A., Mill, P., Smith, K. M., Akhavan, M., Barnabe-Heider, F., . . . Miller, F. D. (2004). A dermal niche for multipotent adult skin-derived precursor cells. *Nat Cell Biol, 6*(11), 1082-1093. doi:10.1038/ncb1181

Freund, A., Orjalo, A. V., Desprez, P. Y., & Campisi, J. (2010). Inflammatory networks during cellular senescence: causes and consequences. *Trends Mol Med, 16*(5), 238-246. doi:10.1016/j.molmed.2010.03.003

Frontini, A., & Cinti, S. (2010). Distribution and development of brown adipocytes in the murine and human adipose organ. *Cell Metab, 11*(4), 253-256. doi:10.1016/j.cmet.2010.03.004

Fuchs, E., & Segre, J. A. (2000). Stem cells: a new lease on life. *Cell, 100*(1), 143-155. doi:10.1016/s0092-8674(00)81691-8

Fulop, T., Witkowski, J. M., Olivieri, F., & Larbi, A. (2018). The integration of inflammaging in age-related diseases. *Semin Immunol, 40*, 17-35. doi:10.1016/j.smim.2018.09.003

Gabriel, D., Roedl, D., Gordon, L. B., & Djabali, K. (2015). Sulforaphane enhances progerin clearance in Hutchinson-Gilford progeria fibroblasts. *Aging Cell, 14*(1), 78-91. doi:10.1111/acel.12300

Gabriel, D., Shafry, D. D., Gordon, L. B., & Djabali, K. (2017). Intermittent treatment with farnesyltransferase inhibitor and sulforaphane improves cellular homeostasis in Hutchinson-Gilford progeria fibroblasts. *Oncotarget, 8*(39), 64809-64826. doi:10.18632/oncotarget.19363

Galic, S., Oakhill, J. S., & Steinberg, G. R. (2010). Adipose tissue as an endocrine organ. *Mol Cell Endocrinol, 316*(2), 129-139. doi:10.1016/j.mce.2009.08.018

Garg, A., & Agarwal, A. K. (2009). Lipodystrophies: disorders of adipose tissue biology. *Biochim Biophys Acta, 1791*(6), 507-513. doi:10.1016/j.bbalip.2008.12.014

Gesta, S., Tseng, Y. H., & Kahn, C. R. (2007). Developmental origin of fat: tracking obesity to its source. *Cell, 131*(2), 242-256. doi:10.1016/j.cell.2007.10.004

Ghaben, A. L., & Scherer, P. E. (2019). Adipogenesis and metabolic health. *Nat Rev Mol Cell Biol, 20*(4), 242-258. doi:10.1038/s41580-018-0093-z

Glynn, M. W., & Glover, T. W. (2005). Incomplete processing of mutant lamin A in Hutchinson-Gilford progeria leads to nuclear abnormalities, which are reversed by farnesyltransferase inhibition. *Hum Mol Genet, 14*(20), 2959-2969. doi:10.1093/hmg/ddi326

Goldman, R. D., Shumaker, D. K., Erdos, M. R., Eriksson, M., Goldman, A. E., Gordon, L. B., . . . Collins, F. S. (2004). Accumulation of mutant lamin A causes progressive changes in nuclear architecture in Hutchinson-Gilford progeria syndrome. *Proc Natl Acad Sci U S A, 101*(24), 8963-8968. doi:10.1073/pnas.0402943101

Gordon, L. B. (2019). The progeria handbook: a guide for families & health care providers of children with progeria. *Progeria Research Foundation, Peabody, MA*.

Gordon, L. B., Brown, W. T., & Collins, F. S. (1993). Hutchinson-Gilford Progeria Syndrome. In M. P. Adam, H. H. Ardinger, R. A. Pagon, S. E. Wallace, L. J. H. Bean, G. Mirzaa, & A. Amemiya (Eds.), *GeneReviews((R))*. Seattle (WA).

Gordon, L. B., Campbell, S. E., Massaro, J. M., D'Agostino, R. B., Sr., Kleinman, M. E., Kieran, M. W., & Moses, M. A. (2018). Survey of plasma proteins in children with progeria pre-therapy and on-therapy with lonafarnib. *Pediatr Res, 83*(5), 982-992. doi:10.1038/pr.2018.9

Gordon, L. B., Harten, I. A., Patti, M. E., & Lichtenstein, A. H. (2005). Reduced adiponectin and HDL cholesterol without elevated C-reactive protein: clues to the biology of premature atherosclerosis in Hutchinson-Gilford Progeria Syndrome. *J Pediatr, 146*(3), 336-341. doi:10.1016/j.jpeds.2004.10.064

Graziotto, J. J., Cao, K., Collins, F. S., & Krainc, D. (2012). Rapamycin activates autophagy in Hutchinson-Gilford progeria syndrome: implications for normal aging and age-dependent neurodegenerative disorders. *Autophagy, 8*(1), 147-151. doi:10.4161/auto.8.1.18331

Green, H., & Meuth, M. (1974). An established pre-adipose cell line and its differentiation in culture. *Cell, 3*(2), 127-133. doi:10.1016/0092-8674(74)90116-0

Gruenbaum, Y., Margalit, A., Goldman, R. D., Shumaker, D. K., & Wilson, K. L. (2005). The nuclear lamina comes of age. *Nat Rev Mol Cell Biol, 6*(1), 21-31. doi:10.1038/nrm1550

Hansen, M., Rubinsztein, D. C., & Walker, D. W. (2018). Autophagy as a promoter of longevity: insights from model organisms. *Nat Rev Mol Cell Biol, 19*(9), 579-593. doi:10.1038/s41580-018-0033-y

Harhouri, K., Navarro, C., Depetris, D., Mattei, M. G., Nissan, X., Cau, P., . . . Levy, N. (2017). MG132-induced progerin clearance is mediated by autophagy activation and splicing regulation. *EMBO Mol Med, 9*(9), 1294-1313. doi:10.15252/emmm.201607315

Harrison, D. A. (2012). The Jak/STAT pathway. *Cold Spring Harb Perspect Biol, 4*(3). doi:10.1101/cshperspect.a011205

Hegele, R. A., Anderson, C. M., Wang, J., Jones, D. C., & Cao, H. (2000). Association between nuclear lamin A/C R482Q mutation and partial lipodystrophy with hyperinsulinemia, dyslipidemia, hypertension, and diabetes. *Genome Res, 10*(5), 652-658. doi:10.1101/gr.10.5.652

Hegele, R. A., Cao, H., Anderson, C. M., & Hramiak, I. M. (2000). Heterogeneity of nuclear lamin A mutations in Dunnigan-type familial partial lipodystrophy. *J Clin Endocrinol Metab, 85*(9), 3431-3435. doi:10.1210/jcem.85.9.6822

Hegele, R. A., Joy, T. R., Al-Attar, S. A., & Rutt, B. K. (2007). Thematic review series: Adipocyte Biology. Lipodystrophies: windows on adipose biology and metabolism. *J Lipid Res, 48*(7), 1433-1444. doi:10.1194/jlr.R700004-JLR200

Hennekam, R. C. (2006). Hutchinson-Gilford progeria syndrome: review of the phenotype. *Am J Med Genet A, 140*(23), 2603-2624. doi:10.1002/ajmg.a.31346

Hennekes, H., & Nigg, E. A. (1994). The role of isoprenylation in membrane attachment of nuclear lamins. A single point mutation prevents proteolytic cleavage of the lamin A precursor and confers membrane binding properties. *J Cell Sci, 107 (Pt 4)*, 1019-1029.

Hernandez-Segura, A., de Jong, T. V., Melov, S., Guryev, V., Campisi, J., & Demaria, M. (2017). Unmasking Transcriptional Heterogeneity in Senescent Cells. *Curr Biol, 27*(17), 2652-2660 e2654. doi:10.1016/j.cub.2017.07.033

Hernandez-Segura, A., Nehme, J., & Demaria, M. (2018). Hallmarks of Cellular Senescence. *Trends Cell Biol, 28*(6), 436-453. doi:10.1016/j.tcb.2018.02.001

Hill, R. P., Gledhill, K., Gardner, A., Higgins, C. A., Crawford, H., Lawrence, C., . . . Jahoda, C. A. (2012). Generation and characterization of multipotent stem cells from established dermal cultures. *PLoS One, 7*(11), e50742. doi:10.1371/journal.pone.0050742

Hotamisligil, G. S., & Bernlohr, D. A. (2015). Metabolic functions of FABPs--mechanisms and therapeutic implications. *Nat Rev Endocrinol, 11*(10), 592-605. doi:10.1038/nrendo.2015.122

Hsu, P. D., Lander, E. S., & Zhang, F. (2014). Development and applications of CRISPR-Cas9 for genome engineering. *Cell, 157*(6), 1262-1278. doi:10.1016/j.cell.2014.05.010

Huang, H., Song, T. J., Li, X., Hu, L., He, Q., Liu, M., . . . Tang, Q. Q. (2009). BMP signaling pathway is required for commitment of C3H10T1/2 pluripotent stem cells to the adipocyte lineage. *Proc Natl Acad Sci U S A, 106*(31), 12670-12675. doi:10.1073/pnas.0906266106

Ibrahim, M. X., Sayin, V. I., Akula, M. K., Liu, M., Fong, L. G., Young, S. G., & Bergo, M. O. (2013). Targeting isoprenylcysteine methylation ameliorates disease in a mouse model of progeria. *Science, 340*(6138), 1330-1333. doi:10.1126/science.1238880

International Stem Cell, I., Adewumi, O., Aflatoonian, B., Ahrlund-Richter, L., Amit, M., Andrews, P. W., . . . Zhang, W. (2007). Characterization of human embryonic stem cell lines by the International Stem Cell Initiative. *Nat Biotechnol, 25*(7), 803-816. doi:10.1038/nbt1318

Kang, H. T., Park, J. T., Choi, K., Choi, H. J. C., Jung, C. W., Kim, G. R., . . . Park, S. C. (2017). Chemical screening identifies ROCK as a target for recovering mitochondrial function in Hutchinson-Gilford progeria syndrome. *Aging Cell, 16*(3), 541-550. doi:10.1111/acel.12584

Karagiannides, I., Tchkonia, T., Dobson, D. E., Steppan, C. M., Cummins, P., Chan, G., . . . Kirkland, J. L. (2001). Altered expression of C/EBP family members results in decreased

adipogenesis with aging. *Am J Physiol Regul Integr Comp Physiol, 280*(6), R1772-1780. doi:10.1152/ajpregu.2001.280.6.R1772

Karagiannides, I., Thomou, T., Tchkonia, T., Pirtskhalava, T., Kypreos, K. E., Cartwright, A., . . . Kirkland, J. L. (2006). Increased CUG triplet repeat-binding protein-1 predisposes to impaired adipogenesis with aging. *J Biol Chem, 281*(32), 23025-23033. doi:10.1074/jbc.M513187200

Keep off-target effects in focus. (2018). *Nat Med, 24*(8), 1081. doi:10.1038/s41591-018-0150-3

Kim, Y. C., & Guan, K. L. (2015). mTOR: a pharmacologic target for autophagy regulation. *J Clin Invest, 125*(1), 25-32. doi:10.1172/JCI73939

Kirkland, J. L., Hollenberg, C. H., & Gillon, W. S. (1990). Age, anatomic site, and the replication and differentiation of adipocyte precursors. *Am J Physiol, 258*(2 Pt 1), C206-210. doi:10.1152/ajpcell.1990.258.2.C206

Koh, K. K., Park, S. M., & Quon, M. J. (2008). Leptin and cardiovascular disease: response to therapeutic interventions. *Circulation, 117*(25), 3238-3249. doi:10.1161/CIRCULATIONAHA.107.741645

Koster, A., Stenholm, S., Alley, D. E., Kim, L. J., Simonsick, E. M., Kanaya, A. M., . . . Health, A. B. C. S. (2010). Body fat distribution and inflammation among obese older adults with and without metabolic syndrome. *Obesity (Silver Spring), 18*(12), 2354-2361. doi:10.1038/oby.2010.86

Kreienkamp, R., & Gonzalo, S. (2020). Metabolic Dysfunction in Hutchinson-Gilford Progeria Syndrome. *Cells, 9*(2). doi:10.3390/cells9020395

Kubben, N., Brimacombe, K. R., Donegan, M., Li, Z., & Misteli, T. (2016). A high-content imaging-based screening pipeline for the systematic identification of anti-progeroid compounds. *Methods, 96*, 46-58. doi:10.1016/j.ymeth.2015.08.024

Kubben, N., Zhang, W., Wang, L., Voss, T. C., Yang, J., Qu, J., . . . Misteli, T. (2016). Repression of the Antioxidant NRF2 Pathway in Premature Aging. *Cell, 165*(6), 1361-1374. doi:10.1016/j.cell.2016.05.017

Kuilman, T., Michaloglou, C., Vredeveld, L. C., Douma, S., van Doorn, R., Desmet, C. J., . . . Peeper, D. S. (2008). Oncogene-induced senescence relayed by an interleukin-dependent inflammatory network. *Cell, 133*(6), 1019-1031. doi:10.1016/j.cell.2008.03.039

Kuilman, T., & Peeper, D. S. (2009). Senescence-messaging secretome: SMS-ing cellular stress. *Nat Rev Cancer, 9*(2), 81-94. doi:10.1038/nrc2560

Kumar, R., Sinha, S., Hagner, A., Stykel, M., Raharjo, E., Singh, K. K., . . . Biernaskie, J. (2016). Adult skin-derived precursor Schwann cells exhibit superior myelination and regeneration

supportive properties compared to chronically denervated nerve-derived Schwann cells. *Exp Neurol, 278*, 127-142. doi:10.1016/j.expneurol.2016.02.006

Kurz, D. J., Decary, S., Hong, Y., & Erusalimsky, J. D. (2000). Senescence-associated (beta)-galactosidase reflects an increase in lysosomal mass during replicative ageing of human endothelial cells. *J Cell Sci, 113 (Pt 20)*, 3613-3622. doi:10.1242/jcs.113.20.3613

Lau, D. C., Dhillon, B., Yan, H., Szmitko, P. E., & Verma, S. (2005). Adipokines: molecular links between obesity and atheroslcerosis. *Am J Physiol Heart Circ Physiol, 288*(5), H2031-2041. doi:10.1152/ajpheart.01058.2004

Lecot, P., Alimirah, F., Desprez, P. Y., Campisi, J., & Wiley, C. (2016). Context-dependent effects of cellular senescence in cancer development. *Br J Cancer, 114*(11), 1180-1184. doi:10.1038/bjc.2016.115

Lee, B. Y., Han, J. A., Im, J. S., Morrone, A., Johung, K., Goodwin, E. C., . . . Hwang, E. S. (2006). Senescence-associated beta-galactosidase is lysosomal beta-galactosidase. *Aging Cell, 5*(2), 187-195. doi:10.1111/j.1474-9726.2006.00199.x

Lefterova, M. I., Zhang, Y., Steger, D. J., Schupp, M., Schug, J., Cristancho, A., . . . Lazar, M. A. (2008). PPARgamma and C/EBP factors orchestrate adipocyte biology via adjacent binding on a genome-wide scale. *Genes Dev, 22*(21), 2941-2952. doi:10.1101/gad.1709008

Legg, J., Jensen, U. B., Broad, S., Leigh, I., & Watt, F. M. (2003). Role of melanoma chondroitin sulphate proteoglycan in patterning stem cells in human interfollicular epidermis. *Development, 130*(24), 6049-6063. doi:10.1242/dev.00837

Lendahl, U., Zimmerman, L. B., & McKay, R. D. (1990). CNS stem cells express a new class of intermediate filament protein. *Cell, 60*(4), 585-595. doi:10.1016/0092-8674(90)90662-x

Lin, F. T., & Lane, M. D. (1994). CCAAT/enhancer binding protein alpha is sufficient to initiate the 3T3-L1 adipocyte differentiation program. *Proc Natl Acad Sci U S A, 91*(19), 8757-8761. doi:10.1073/pnas.91.19.8757

Liu, C., Arnold, R., Henriques, G., & Djabali, K. (2019). Inhibition of JAK-STAT Signaling with Baricitinib Reduces Inflammation and Improves Cellular Homeostasis in Progeria Cells. *Cells, 8*(10). doi:10.3390/cells8101276

Liu, S., Dontu, G., & Wicha, M. S. (2005). Mammary stem cells, self-renewal pathways, and carcinogenesis. *Breast Cancer Res, 7*(3), 86-95. doi:10.1186/bcr1021

Lopez-Mejia, I. C., Vautrot, V., De Toledo, M., Behm-Ansmant, I., Bourgeois, C. F., Navarro, C. L., . . . Tazi, J. (2011). A conserved splicing mechanism of the LMNA gene controls premature aging. *Hum Mol Genet, 20*(23), 4540-4555. doi:10.1093/hmg/ddr385

Lowe, C. E., O'Rahilly, S., & Rochford, J. J. (2011). Adipogenesis at a glance. *J Cell Sci, 124*(Pt 16), 2681-2686. doi:10.1242/jcs.079699

MacDougald, O. A., & Mandrup, S. (2002). Adipogenesis: forces that tip the scales. *Trends Endocrinol Metab, 13*(1), 5-11. doi:10.1016/s1043-2760(01)00517-3

Mallampalli, M. P., Huyer, G., Bendale, P., Gelb, M. H., & Michaelis, S. (2005). Inhibiting farnesylation reverses the nuclear morphology defect in a HeLa cell model for Hutchinson-Gilford progeria syndrome. *Proc Natl Acad Sci U S A, 102*(40), 14416-14421. doi:10.1073/pnas.0503712102

Marji, J., O'Donoghue, S. I., McClintock, D., Satagopam, V. P., Schneider, R., Ratner, D., . . . Djabali, K. (2010). Defective lamin A-Rb signaling in Hutchinson-Gilford Progeria Syndrome and reversal by farnesyltransferase inhibition. *PLoS One, 5*(6), e11132. doi:10.1371/journal.pone.0011132

McConnell, B. B., Starborg, M., Brookes, S., & Peters, G. (1998). Inhibitors of cyclin-dependent kinases induce features of replicative senescence in early passage human diploid fibroblasts. *Curr Biol, 8*(6), 351-354. doi:10.1016/s0960-9822(98)70137-x

Mehrabi, M., Mansouri, K., Hosseinkhani, S., Yarani, R., Yari, K., Bakhtiari, M., & Mostafaie, A. (2015). Differentiation of human skin-derived precursor cells into functional islet-like insulin-producing cell clusters. *In Vitro Cell Dev Biol Anim, 51*(6), 595-603. doi:10.1007/s11626-015-9866-2

Merideth, M. A., Gordon, L. B., Clauss, S., Sachdev, V., Smith, A. C., Perry, M. B., . . . Introne, W. J. (2008). Phenotype and course of Hutchinson-Gilford progeria syndrome. *N Engl J Med, 358*(6), 592-604. doi:10.1056/NEJMoa0706898

Mitalipov, S., & Wolf, D. (2009). Totipotency, pluripotency and nuclear reprogramming. *Adv Biochem Eng Biotechnol, 114*, 185-199. doi:10.1007/10_2008_45

Mitsui, K., Tokuzawa, Y., Itoh, H., Segawa, K., Murakami, M., Takahashi, K., . . . Yamanaka, S. (2003). The homeoprotein Nanog is required for maintenance of pluripotency in mouse epiblast and ES cells. *Cell, 113*(5), 631-642. doi:10.1016/s0092-8674(03)00393-3

Morin, C. L., Pagliassotti, M. J., Windmiller, D., & Eckel, R. H. (1997). Adipose tissue-derived tumor necrosis factor-alpha activity is elevated in older rats. *J Gerontol A Biol Sci Med Sci, 52*(4), B190-195. doi:10.1093/gerona/52a.4.b190

Morley, J. E. (2004). The metabolic syndrome and aging. *J Gerontol A Biol Sci Med Sci, 59*(2), 139-142. doi:10.1093/gerona/59.2.m139

Mozafari, S., Laterza, C., Roussel, D., Bachelin, C., Marteyn, A., Deboux, C., . . . Baron-Van Evercooren, A. (2015). Skin-derived neural precursors competitively generate functional

myelin in adult demyelinated mice. *J Clin Invest, 125*(9), 3642-3656. doi:10.1172/JCI80437

Munoz-Espin, D., & Serrano, M. (2014). Cellular senescence: from physiology to pathology. *Nat Rev Mol Cell Biol, 15*(7), 482-496. doi:10.1038/nrm3823

Najdi, F., Kruger, P., & Djabali, K. (2021). Impact of Progerin Expression on Adipogenesis in Hutchinson-Gilford Progeria Skin-Derived Precursor Cells. *Cells, 10*(7). doi:10.3390/cells10071598

Nguyen, T. M. D. (2020). Adiponectin: Role in Physiology and Pathophysiology. *Int J Prev Med, 11*, 136. doi:10.4103/ijpvm.IJPVM_193_20

Olive, M., Harten, I., Mitchell, R., Beers, J. K., Djabali, K., Cao, K., . . . Gordon, L. B. (2010). Cardiovascular pathology in Hutchinson-Gilford progeria: correlation with the vascular pathology of aging. *Arterioscler Thromb Vasc Biol, 30*(11), 2301-2309. doi:10.1161/ATVBAHA.110.209460

Osorio, F. G., Barcena, C., Soria-Valles, C., Ramsay, A. J., de Carlos, F., Cobo, J., . . . Lopez-Otin, C. (2012). Nuclear lamina defects cause ATM-dependent NF-kappaB activation and link accelerated aging to a systemic inflammatory response. *Genes Dev, 26*(20), 2311-2324. doi:10.1101/gad.197954.112

Pacheco, L. M., Gomez, L. A., Dias, J., Ziebarth, N. M., Howard, G. A., & Schiller, P. C. (2014). Progerin expression disrupts critical adult stem cell functions involved in tissue repair. *Aging (Albany NY), 6*(12), 1049-1063. doi:10.18632/aging.100709

Pellegrini, C., Columbaro, M., Capanni, C., D'Apice, M. R., Cavallo, C., Murdocca, M., . . . Squarzoni, S. (2015). All-trans retinoic acid and rapamycin normalize Hutchinson Gilford progeria fibroblast phenotype. *Oncotarget, 6*(30), 29914-29928. doi:10.18632/oncotarget.4939

Pesce, M., & Scholer, H. R. (2001). Oct-4: gatekeeper in the beginnings of mammalian development. *Stem Cells, 19*(4), 271-278. doi:10.1634/stemcells.19-4-271

Petrova, N. V., Velichko, A. K., Razin, S. V., & Kantidze, O. L. (2016). Small molecule compounds that induce cellular senescence. *Aging Cell, 15*(6), 999-1017. doi:10.1111/acel.12518

Piemonti, L., Calori, G., Mercalli, A., Lattuada, G., Monti, P., Garancini, M. P., . . . Perseghin, G. (2003). Fasting plasma leptin, tumor necrosis factor-alpha receptor 2, and monocyte chemoattracting protein 1 concentration in a population of glucose-tolerant and glucose-intolerant women: impact on cardiovascular mortality. *Diabetes Care, 26*(10), 2883-2889. doi:10.2337/diacare.26.10.2883

Rajawat, Y., Hilioti, Z., & Bossis, I. (2010). Autophagy: a target for retinoic acids. *Autophagy, 6*(8), 1224-1226. doi:10.4161/auto.6.8.13793

Rajawat, Y., Hilioti, Z., & Bossis, I. (2011). Retinoic acid induces autophagosome maturation through redistribution of the cation-independent mannose-6-phosphate receptor. *Antioxid Redox Signal, 14*(11), 2165-2177. doi:10.1089/ars.2010.3491

Reddel, C. J., & Weiss, A. S. (2004). Lamin A expression levels are unperturbed at the normal and mutant alleles but display partial splice site selection in Hutchinson-Gilford progeria syndrome. *J Med Genet, 41*(9), 715-717. doi:10.1136/jmg.2004.019323

Revechon, G., Viceconte, N., McKenna, T., Sola Carvajal, A., Vrtacnik, P., Stenvinkel, P., . . . Eriksson, M. (2017). Rare progerin-expressing preadipocytes and adipocytes contribute to tissue depletion over time. *Sci Rep, 7*(1), 4405. doi:10.1038/s41598-017-04492-0

Richards, S. A., Muter, J., Ritchie, P., Lattanzi, G., & Hutchison, C. J. (2011). The accumulation of un-repairable DNA damage in laminopathy progeria fibroblasts is caused by ROS generation and is prevented by treatment with N-acetyl cysteine. *Hum Mol Genet, 20*(20), 3997-4004. doi:10.1093/hmg/ddr327

Rietze, R. L., & Reynolds, B. A. (2006). Neural stem cell isolation and characterization. *Methods Enzymol, 419*, 3-23. doi:10.1016/S0076-6879(06)19001-1

Robbins, A. L., & Savage, D. B. (2015). The genetics of lipid storage and human lipodystrophies. *Trends Mol Med, 21*(7), 433-438. doi:10.1016/j.molmed.2015.04.004

Rosen, E. D., Hsu, C. H., Wang, X., Sakai, S., Freeman, M. W., Gonzalez, F. J., & Spiegelman, B. M. (2002). C/EBPalpha induces adipogenesis through PPARgamma: a unified pathway. *Genes Dev, 16*(1), 22-26. doi:10.1101/gad.948702

Rosen, E. D., & MacDougald, O. A. (2006). Adipocyte differentiation from the inside out. *Nat Rev Mol Cell Biol, 7*(12), 885-896. doi:10.1038/nrm2066

Rosen, E. D., Sarraf, P., Troy, A. E., Bradwin, G., Moore, K., Milstone, D. S., . . . Mortensen, R. M. (1999). PPAR gamma is required for the differentiation of adipose tissue in vivo and in vitro. *Mol Cell, 4*(4), 611-617. doi:10.1016/s1097-2765(00)80211-7

Rosen, E. D., Walkey, C. J., Puigserver, P., & Spiegelman, B. M. (2000). Transcriptional regulation of adipogenesis. *Genes Dev, 14*(11), 1293-1307.

Rosenbloom, A. L., Karacan, I. J., & DeBusk, F. L. (1970). Sleep characteristics and endocrine response in progeria. *J Pediatr, 77*(4), 692-695. doi:10.1016/s0022-3476(70)80217-7

Samuel, V. T., & Shulman, G. I. (2012). Mechanisms for insulin resistance: common threads and missing links. *Cell, 148*(5), 852-871. doi:10.1016/j.cell.2012.02.017

Sander, J. D., & Joung, J. K. (2014). CRISPR-Cas systems for editing, regulating and targeting genomes. *Nat Biotechnol, 32*(4), 347-355. doi:10.1038/nbt.2842

Sarkar, P. K., & Shinton, R. A. (2001). Hutchinson-Guilford progeria syndrome. *Postgrad Med J, 77*(907), 312-317. doi:10.1136/pmj.77.907.312

Savage, D. B., Petersen, K. F., & Shulman, G. I. (2007). Disordered lipid metabolism and the pathogenesis of insulin resistance. *Physiol Rev, 87*(2), 507-520. doi:10.1152/physrev.00024.2006

Scaffidi, P., & Misteli, T. (2005). Reversal of the cellular phenotype in the premature aging disease Hutchinson-Gilford progeria syndrome. *Nat Med, 11*(4), 440-445. doi:10.1038/nm1204

Scaffidi, P., & Misteli, T. (2008). Lamin A-dependent misregulation of adult stem cells associated with accelerated ageing. *Nat Cell Biol, 10*(4), 452-459. doi:10.1038/ncb1708

Schindelin, J., Arganda-Carreras, I., Frise, E., Kaynig, V., Longair, M., Pietzsch, T., . . . Cardona, A. (2012). Fiji: an open-source platform for biological-image analysis. *Nat Methods, 9*(7), 676-682. doi:10.1038/nmeth.2019

Schipper, B. M., Marra, K. G., Zhang, W., Donnenberg, A. D., & Rubin, J. P. (2008). Regional anatomic and age effects on cell function of human adipose-derived stem cells. *Ann Plast Surg, 60*(5), 538-544. doi:10.1097/SAP.0b013e3181723bbe

Schneider, S., Unger, M., van Griensven, M., & Balmayor, E. R. (2017). Adipose-derived mesenchymal stem cells from liposuction and resected fat are feasible sources for regenerative medicine. *Eur J Med Res, 22*(1), 17. doi:10.1186/s40001-017-0258-9

Shackleton, S., Lloyd, D. J., Jackson, S. N., Evans, R., Niermeijer, M. F., Singh, B. M., . . . Trembath, R. C. (2000). LMNA, encoding lamin A/C, is mutated in partial lipodystrophy. *Nat Genet, 24*(2), 153-156. doi:10.1038/72807

Sharpless, N. E., & Sherr, C. J. (2015). Forging a signature of in vivo senescence. *Nat Rev Cancer, 15*(7), 397-408. doi:10.1038/nrc3960

Shin, H. S., Ko, J., Kim, D. A., Ryu, E. S., Ryu, H. M., Park, S. H., . . . Kang, D. H. (2017). Metformin ameliorates the Phenotype Transition of Peritoneal Mesothelial Cells and Peritoneal Fibrosis via a modulation of Oxidative Stress. *Sci Rep, 7*(1), 5690. doi:10.1038/s41598-017-05836-6

Sinensky, M., Fantle, K., Trujillo, M., McLain, T., Kupfer, A., & Dalton, M. (1994). The processing pathway of prelamin A. *J Cell Sci, 107 (Pt 1)*, 61-67.

Starr, M. E., Evers, B. M., & Saito, H. (2009). Age-associated increase in cytokine production during systemic inflammation: adipose tissue as a major source of IL-6. *J Gerontol A Biol Sci Med Sci, 64*(7), 723-730. doi:10.1093/gerona/glp046

Stuurman, N., Heins, S., & Aebi, U. (1998). Nuclear lamins: their structure, assembly, and interactions. *J Struct Biol, 122*(1-2), 42-66. doi:10.1006/jsbi.1998.3987

Tchkonia, T., Pirtskhalava, T., Thomou, T., Cartwright, M. J., Wise, B., Karagiannides, I., . . . Kirkland, J. L. (2007). Increased TNFalpha and CCAAT/enhancer-binding protein homologous protein with aging predispose preadipocytes to resist adipogenesis. *Am J Physiol Endocrinol Metab, 293*(6), E1810-1819. doi:10.1152/ajpendo.00295.2007

Tilstra, J. S., Clauson, C. L., Niedernhofer, L. J., & Robbins, P. D. (2011). NF-kappaB in Aging and Disease. *Aging Dis, 2*(6), 449-465.

Toma, J. G., Akhavan, M., Fernandes, K. J., Barnabe-Heider, F., Sadikot, A., Kaplan, D. R., & Miller, F. D. (2001). Isolation of multipotent adult stem cells from the dermis of mammalian skin. *Nat Cell Biol, 3*(9), 778-784. doi:10.1038/ncb0901-778

Toma, J. G., McKenzie, I. A., Bagli, D., & Miller, F. D. (2005). Isolation and characterization of multipotent skin-derived precursors from human skin. *Stem Cells, 23*(6), 727-737. doi:10.1634/stemcells.2004-0134

Tontonoz, P., Hu, E., Graves, R. A., Budavari, A. I., & Spiegelman, B. M. (1994). mPPAR gamma 2: tissue-specific regulator of an adipocyte enhancer. *Genes Dev, 8*(10), 1224-1234. doi:10.1101/gad.8.10.1224

Tontonoz, P., Hu, E., & Spiegelman, B. M. (1994). Stimulation of adipogenesis in fibroblasts by PPAR gamma 2, a lipid-activated transcription factor. *Cell, 79*(7), 1147-1156. doi:10.1016/0092-8674(94)90006-x

Toth, J. I., Yang, S. H., Qiao, X., Beigneux, A. P., Gelb, M. H., Moulson, C. L., . . . Fong, L. G. (2005). Blocking protein farnesyltransferase improves nuclear shape in fibroblasts from humans with progeroid syndromes. *Proc Natl Acad Sci U S A, 102*(36), 12873-12878. doi:10.1073/pnas.0505767102

Ullrich, N. J., & Gordon, L. B. (2015). Hutchinson-Gilford progeria syndrome. *Handb Clin Neurol, 132*, 249-264. doi:10.1016/B978-0-444-62702-5.00018-4

Unger, R. H. (2003). The physiology of cellular liporegulation. *Annu Rev Physiol, 65*, 333-347. doi:10.1146/annurev.physiol.65.092101.142622

Vasudeva, V. S., Abd-El-Barr, M. M., & Chi, J. H. (2015). Implantation of Neonatal Skin-Derived Precursor Schwann Cells Improves Outcomes After Incomplete Cervical Spinal Cord Injury in Rats. *Neurosurgery, 77*(2), N15-17. doi:10.1227/01.neu.0000467294.10763.69

Villee, D. B., Nichols, G., Jr., & Talbot, N. B. (1969). Metabolic studies in two boys with classical progeria. *Pediatrics, 43*(2), 207-216.

Virtue, S., & Vidal-Puig, A. (2010). Adipose tissue expandability, lipotoxicity and the Metabolic Syndrome--an allostatic perspective. *Biochim Biophys Acta, 1801*(3), 338-349. doi:10.1016/j.bbalip.2009.12.006

Walsh, T., Biernaskie, J., Midha, R., & Kallos, M. S. (2016). Bioreactor Expansion of Skin-Derived Precursor Schwann Cells. *Methods Mol Biol, 1502*, 103-110. doi:10.1007/7651_2016_355

Wang, E. A., Israel, D. I., Kelly, S., & Luxenberg, D. P. (1993). Bone morphogenetic protein-2 causes commitment and differentiation in C3H10T1/2 and 3T3 cells. *Growth Factors, 9*(1), 57-71. doi:10.3109/08977199308991582

Wenzel, V., Roedl, D., Gabriel, D., Gordon, L. B., Herlyn, M., Schneider, R., . . . Djabali, K. (2012). Naive adult stem cells from patients with Hutchinson-Gilford progeria syndrome express low levels of progerin in vivo. *Biol Open, 1*(6), 516-526. doi:10.1242/bio.20121149

Wiley, C. D., Flynn, J. M., Morrissey, C., Lebofsky, R., Shuga, J., Dong, X., . . . Campisi, J. (2017). Analysis of individual cells identifies cell-to-cell variability following induction of cellular senescence. *Aging Cell, 16*(5), 1043-1050. doi:10.1111/acel.12632

Wiley, C. D., Velarde, M. C., Lecot, P., Liu, S., Sarnoski, E. A., Freund, A., . . . Campisi, J. (2016). Mitochondrial Dysfunction Induces Senescence with a Distinct Secretory Phenotype. *Cell Metab, 23*(2), 303-314. doi:10.1016/j.cmet.2015.11.011

Willis, M. A., & Fox, R. J. (2016). Progressive Multiple Sclerosis. *Continuum (Minneap Minn), 22*(3), 785-798. doi:10.1212/CON.0000000000000323

Wozniak, S. E., Gee, L. L., Wachtel, M. S., & Frezza, E. E. (2009). Adipose tissue: the new endocrine organ? A review article. *Dig Dis Sci, 54*(9), 1847-1856. doi:10.1007/s10620-008-0585-3

Wu, Z., Rosen, E. D., Brun, R., Hauser, S., Adelmant, G., Troy, A. E., . . . Spiegelman, B. M. (1999). Cross-regulation of C/EBP alpha and PPAR gamma controls the transcriptional pathway of adipogenesis and insulin sensitivity. *Mol Cell, 3*(2), 151-158. doi:10.1016/s1097-2765(00)80306-8

Xiong, Z. M., LaDana, C., Wu, D., & Cao, K. (2013). An inhibitory role of progerin in the gene induction network of adipocyte differentiation from iPS cells. *Aging (Albany NY), 5*(4), 288-303. doi:10.18632/aging.100550

Xu, M., Palmer, A. K., Ding, H., Weivoda, M. M., Pirtskhalava, T., White, T. A., . . . Kirkland, J. L. (2015). Targeting senescent cells enhances adipogenesis and metabolic function in old age. *Elife, 4*, e12997. doi:10.7554/eLife.12997

Yang, L., Ge, Y., Tang, J., Yuan, J., Ge, D., Chen, H., . . . Cao, X. (2015). Schwann Cells Transplantation Improves Locomotor Recovery in Rat Models with Spinal Cord Injury: a

Systematic Review and Meta-Analysis. *Cell Physiol Biochem, 37*(6), 2171-2182. doi:10.1159/000438574

Yang, S. H., Andres, D. A., Spielmann, H. P., Young, S. G., & Fong, L. G. (2008). Progerin elicits disease phenotypes of progeria in mice whether or not it is farnesylated. *J Clin Invest, 118*(10), 3291-3300. doi:10.1172/JCI35876

Yang, S. H., Bergo, M. O., Toth, J. I., Qiao, X., Hu, Y., Sandoval, S., . . . Fong, L. G. (2005). Blocking protein farnesyltransferase improves nuclear blebbing in mouse fibroblasts with a targeted Hutchinson-Gilford progeria syndrome mutation. *Proc Natl Acad Sci U S A, 102*(29), 10291-10296. doi:10.1073/pnas.0504641102

Yang, S. H., Meta, M., Qiao, X., Frost, D., Bauch, J., Coffinier, C., . . . Fong, L. G. (2006). A farnesyltransferase inhibitor improves disease phenotypes in mice with a Hutchinson-Gilford progeria syndrome mutation. *J Clin Invest, 116*(8), 2115-2121. doi:10.1172/JCI28968

Yeh, W. C., Bierer, B. E., & McKnight, S. L. (1995). Rapamycin inhibits clonal expansion and adipogenic differentiation of 3T3-L1 cells. *Proc Natl Acad Sci U S A, 92*(24), 11086-11090. doi:10.1073/pnas.92.24.11086

Zhu, Y., Tchkonia, T., Pirtskhalava, T., Gower, A. C., Ding, H., Giorgadze, N., . . . Kirkland, J. L. (2015). The Achilles' heel of senescent cells: from transcriptome to senolytic drugs. *Aging Cell, 14*(4), 644-658. doi:10.1111/acel.12344

Acknowledgment

First of all, I would like to express my deepest gratitude to my supervisor Prof. Dr. Karima Djabali, for allowing me to join her team and for guiding me during the whole project. Without your insightful feedback and ideas this work would not be possible.

I would also like to thank my committee members: my second advisor Prof. Dr. Thomas Brück and my mentor Prof. Dr. Benjamin Schusser, for attending my committee meetings and for all the helpful advices and critical questions that helped push my research forward.

A huge thank you goes to the Progeria Research Foundation, the HGPS patients and their families. The progeria meeting that you organized allowed us to meet some of the magnificent patients, which incredibly increased our motivation to go further with our research.

I would like to thank my fellow lab mates: Elena Vehns, Jennifer Röhrl, Rouven Arnold, Chang Liu, Peter Krüger, Hannah Randl and Eva Lederer. Thank you for the good times inside and outside the lab, the support and the insightful conversations. Elena, thank you for the continuous support even in the hardest time. You were always ready to hear anything and offer solutions. You made this journey so much easier. Jenny, thank you for always having time to answer my non-ending questions! You are the best desk neighbor anyone could ask for. Rouven, thank you for the time you spent instructing me when I started in the lab and all the advices you gave me during my PhD. Chang, thank you for the help you offered when I started my project. I will always keep in mind our interesting conversations and topics during lunch! Peter, thank you for the help with the experiments and the paper. I will definitely miss your outstanding performances during karaoke nights! Hannah, you are definitely the most talented master student I have ever met. Thank you for making the long hours spent at the microscope bearable. Eva, thank you for the support and your patience when listening to me speaking German! Thank you all for everything!

In addition, I would like to thank my friends in Lebanon and in Germany for their support and encouragement.

Special thanks to Dr. Lara Hassan, who took the time to proofread this thesis. Thank you for your honest criticism and observations.

Last but not least, I want to thank my parents, my mother Zeinab and my father Abed. Everything I achieve in life; I owe it to you. I can never thank you enough. To my brothers Hadi and Hammoudi, thank you for believing in me and for always being next to me.

To Khaled and Emily, thank you for the love, the care and the unlimited support. This achievement would not have been possible without you. Thank you for always being there for me and for always encouraging me to do my best.